

**OECD MCCI Project**  
**2-D Core Concrete Interaction (CCI) Tests:**  
**CCI-4 Quick Look Data Report**

**Rev. 0 - FINAL**

**June, 2007**

**by:**

**M. T. Farmer, R. W. Aeschlimann, D. J. Kilsdonk, and, S. Lomperski**

**Nuclear Engineering Division**  
**Argonne National Laboratory**  
**9700 S. Cass Avenue**  
**Argonne, IL 60439**  
**USA**

## Table of Contents

<b>1.0 INTRODUCTION</b> .....	1
<b>2.0 FACILITY DESCRIPTION</b> .....	3
2.1 Test Apparatus .....	3
2.2 Instrumentation and Data Acquisition .....	9
2.3 Corium Composition and Concrete-Metal Inserts .....	11
2.4 Concrete Composition .....	15
<b>3.0 TEST PROCEDURES</b> .....	15
3.1 Pretest Preparations.....	15
3.2 Test Operations .....	18
<b>4.0 RESULTS</b> .....	23
4.1 Electric Power .....	23
4.2 Melt Temperatures .....	23
4.3 Concrete Basemat and Sidewall Ablation Rates.....	24
4.4 Corium Quench Rate.....	25
4.5 Posttest Cavity Erosion Profile .....	25
<b>5.0 REFERENCES</b> .....	29
<b>APPENDIX A: Data Acquisition System Channel Assignments</b> .....	30
<b>APPENDIX B: Test Data</b> .....	43

## List of Figures

<b><u>Figure</u></b>	<b><u>Page</u></b>
2-1 Schematic of CCI Test Facility.....	4
2-2 Top View of Lower Test Section.....	4
2-3 Side View of Lower Test Section Showing Inert MgO Sidewall Sections .....	5
2-4 Side View of Lower Test Section Showing Concrete Sidewall Section .....	6
2-5 Test Section Water Supply System.....	7
2-6 Illustration of CCI-4 Crust Lance Assembly Mounted in Test Section.....	8
2-7 Plan View of Basemat Instrumentation Layout (dimensions are in cm) .....	9
2-8 Elevation View of Basemat Type C Thermocouple Locations .....	10
2-9 CCI Data Acquisition and Control Systems .....	11
2-10 Illustration of Concrete-Metal Inserts in Place over the Concrete Basemat.....	12
3-1 Illustration of Thermite Sample Train Installed in Test Section .....	17
3-2 Voltage Reading Across Thermite Igniter Shunt.....	21
3-3 Bulk Melt Temperature Data Over the First 5 Minutes of the Interaction .....	21
3-4 Test Section Plenum Gas Temperatures During the Initial Interaction .....	22
3-5 Power Supply Current During the Initial Interaction.....	22
4-1 DEH Input Power .....	23
4-2 Melt Temperatures Measured During CCI-4.....	24
4-3 Basemat Axial Ablation Front Location.....	26
4-4 North Sidewall Lateral Ablation Front Location .....	26
4-5 South Sidewall Lateral Ablation Front Location.....	27
4-6 Melt-Water Heat Flux Based on Steam Formation Rate.....	27
4-7 Posttest Cavity Profile after Removal of West MgO Sidewall.....	28
B-1 Compensator Temperature, Channels B1-B50 and B51-B100.....	44
B-2 Basemat Type C “WCL” Array Data .....	44
B-3 Basemat Type C “WNW” Array Data .....	45
B-4 Basemat Type C “WNE” Array Data.....	45
B-5 Basemat Type C “WSE” Array Data .....	46
B-6 Basemat Type C “WSW” Array Data.....	46

**List of Figures (Contd.)**

<b><u>Figure</u></b>	<b><u>Page</u></b>
B-7 North Sidewall Type C “NW” Array Data.....	47
B-8 South Sidewall Type C “WS” Array Data .....	47
B-9 Basemat Type K “A” Array Data.....	48
B-10 Basemat Type K “B” Array Data .....	48
B-11 Basemat Type K “C” Array Data .....	49
B-12 Basemat Type K “D” Array Data.....	49
B-13 Basemat Type K “E” Array Data .....	50
B-14 North Sidewall Type K “SWA” Array Data .....	50
B-15 South Sidewall Type K “SWB” Array Data .....	51
B-16 North Sidewall Type K “SWC” Array Data .....	51
B-17 South Sidewall Type K “SWD” Array Data.....	52
B-18 North Sidewall Type K “SWE” Array Data.....	52
B-19 South Sidewall Type K “SWF” Array Data.....	53
B-20 North Sidewall Type K “SWG” Array Data .....	53
B-21 South Sidewall Type K “SWH” Array Data .....	54
B-22 North Sidewall Type K “SWI” Array Data.....	54
B-23 South Sidewall Type K “SWJ” Array Data .....	55
B-24 North Sidewall Type K “SWK” Array Data .....	55
B-25 South Sidewall Type K “SWL” Array Data.....	56
B-26 North Sidewall Type K “SWM” Array Data .....	56
B-27 South Sidewall Type K “SWN” Array Data .....	57
B-28 Thermocouple Compensator Data for Channels Q1-Q50 and Q51-Q100.....	57
B-29 Test Section Sidewall Heat Loss Data at -17.5 cm Elevation.....	58
B-30 Test Section Sidewall Heat Loss Data at -7.5 cm Elevation.....	58
B-31 Test Section Sidewall Heat Loss Data at +2.5 cm Elevation.....	59
B-32 Test Section Sidewall Heat Loss Data at +12.5 cm Elevation.....	59
B-33 Test Section Sidewall Heat Loss Data at +67.5 cm Elevation.....	60
B-34 Test Section Sidewall Heat Loss Data at +81.6 cm Elevation.....	60

## List of Figures (Contd.)

<b><u>Figure</u></b>	<b><u>Page</u></b>
B-35 Test Section Sidewall Heat Loss Data at +92.2 cm Elevation.....	61
B-36 Test Section Sidewall Heat Loss Data at +122.4 cm Elevation.....	61
B-37 Test Section Sidewall Heat Loss Data at +148.8 cm Elevation.....	62
B-38 Test Section Mainline Thermocouple Data .....	62
B-39 Test Section Plenum and Insertable Water Level Probe Thermocouple Data .....	63
B-40 Quench Tank Water Volume, Coil Inlet, and Coil Outlet Temperature Data.....	63
B-41 Miscellaneous Temperatures in Water Supply, Quench, and Off Gas Systems .....	64
B-42 Crust Lance Load Cell Data.....	64
B-43 Lance Position Indicator Data.....	65
B-44 Total Power Supply Power .....	65
B-45 Power Supply Voltage Data.....	66
B-46 Total Power Supply Current Data.....	66
B-47 Power Supply Current Transformer Data .....	67
B-48 Hall Effect Meter Data.....	67
B-49 Voltage across Igniter Shunt .....	68
B-50 Pressure Transducer Power Supply Voltages.....	68
B-51 Water Supply, Overflow, and Spray Tank Water Volume Data.....	69
B-52 Quench Tank Water Volume Data.....	69
B-53 Supply and Quench System Tank Head Data (Backup).....	70
B-54 Test Section Water Head Transducer Data.....	70
B-55 Calculated Water Depth in Test Section.....	71
B-56 Water Supply Tank Pressure.....	71
B-57 Test Section Pressure .....	72
B-58 Quench/Overflow and Spray Tank Plenum Differential Pressures.....	72
B-59 Water Flow Rates.....	73
B-60 Test Section Helium Cover Gas Flow Rates.....	73
B-61 Final Off Gas Flow Rate .....	74

## List of Tables

<b><u>Table</u></b>	<b><u>Page</u></b>
1-1 Specifications for CCI-4 .....	2
2-1 Bulk Composition of CCI-4 Melt at Start of Interaction with Inserts .....	13
2-2 Detailed Pre- and Post-Reaction Compositions for CCI-4 Thermite .....	13
2-3 Composition of CCI-4 Concrete/Metal Inserts .....	14
2-4 Bulk Melt Composition at Start of Basemat Ablation.....	14
2-5 Detailed Melt Composition at the Start of Basemat Ablation .....	14
2-6 Estimated Composition of CCI-4 Concrete (CCI-2 Basis [1])......	15
3-1 CCI-4 Event Sequence (times relative to onset of ablation of the basemat) .....	19
A-1 "Basemat" DAS Channel Assignments for CCI-4 .....	31
A-2 "Power" DAS Channel Assignments for CCI-4.....	35
A-3 "Quench" DAS Channel Assignments for CCI-4.....	39

## 1.0 INTRODUCTION

Ex-vessel debris coolability is an important light water reactor (LWR) safety issue. For existing plants, resolution of this issue will confirm the technical basis for severe accident management guidelines (SAMGs). For new reactors, understanding this issue will help confirm the effectiveness of the design and implementation of new accident mitigation features and severe accident management design alternatives (SAMDAs). The first OECD-MCCI program conducted reactor material experiments focused on achieving the following technical objectives: i) provide confirmatory evidence for various cooling mechanisms through separate effect tests and data for severe accident code model development, and ii) provide longer-term two-dimensional core-concrete interaction data for code assessment and improvement.

Debris cooling mechanisms investigated as part of the first MCCI program included: i) water ingress through cracks/fissures in the core debris, ii) melt eruption caused by gas sparging (volcanic-type event), and iii) large-scale crust mechanical failure leading to renewed bulk cooling. The results of this testing and associated analysis provided an envelope (principally determined by melt depth) for debris coolability. However, this envelope does not encompass the full range of melt depths that are calculated for all plant accident sequences. Cooling augmentation by additional means may be needed at the late stage to assure coolability for new reactor designs as well as for various accident sequences for existing reactors. In addition, the results of the CCI tests showed that lateral/axial power split is a function of concrete type. However, the first program produced limited data sets for code assessment. In light of significant differences in ablation behavior for different concrete types, additional data will be useful in reducing uncertainties and gaining confidence in code predictions.

Based on these findings, a workscope was defined for the follow-on MCCI program that can be divided into the following four categories:

1. Combined effect tests to investigate the interplay of different cooling mechanisms, and to provide data for model development and code assessment purposes.
2. Tests to investigate new design features to enhance coolability, applicable particularly to new reactor designs.
3. Tests to generate two-dimensional core-concrete interaction data.
4. Integral tests to validate severe accident codes.

Aside from these various testing categories, an analysis workscope was also defined to develop and validate debris coolability models to form the technical basis for extrapolating the experiment findings to plant conditions.

As one of the steps in satisfying these program objectives, the Management Board (MB) approved the conduct of a fourth longer-term 2-D Core-Concrete Interaction (CCI) experiment designed to provide information in several areas, including: i) lateral vs. axial power split during

dry core-concrete interaction, ii) integral debris coolability data following late phase flooding, and iii) data regarding the nature and extent of the cooling transient following breach of the crust formed at the melt-water interface. The first three tests [1] investigated the interaction of fully oxidized PWR core melt compositions with specially designed concrete test sections that were initially 50 cm x 50 cm in cross-sectional area. Both siliceous and limestone/common sand concrete types were addressed in the test matrix.

The fourth test that is addressed in this report, CCI-4, utilized a similar test apparatus and experiment boundary conditions, including a limestone/common sand concrete test section. However, instead of a fully oxidized PWR melt, CCI-4 utilized a partially oxidized BWR core melt containing ~ 8 wt % structural steel constituents. Thus, this test evaluated the effect of elevated melt metal content on two-dimensional cavity erosion and debris cooling behavior. The experiment was conducted on May 26, 2007. The objective of this quick look data report is to provide early thermalhydraulic results from this test so that the PRG will have sufficient information to begin formulating recommendations for the next experiment to be conducted in this test category. To this end, a summary description of the test apparatus is provided first, followed by descriptions of the test operating procedure and key experiment results. Overall specifications for CCI-4 are provided in Table 1-1. A full length data report that includes the results of posttest examinations will be provided when that phase of the work is completed.

**Table 1-1. Specifications for CCI-4.**

<b>Parameter</b>	<b>Specification</b>
Initial Corium Composition <sup>a</sup>	78 % oxidized BWR with 7.7 wt % stainless steel constituents and 10.0 wt % limestone/common sand concrete
Concrete type	Limestone/common sand concrete
Initial basemat dimension	50 cm x 40 cm
Initial melt mass (depth <sup>a</sup> )	300 kg (25 cm)
Test section sidewall construction	Nonelectrode walls: concrete Electrode walls: MgO protected by UO <sub>2</sub> pellet layer.
Lateral ablation limit	45.0 cm
Axial ablation limit	42.5 cm
System operating pressure	Atmospheric
Melt formation technique (timescale)	Chemical reaction (~30 seconds)
Initial melt temperature (estimate) <sup>a</sup>	2000 °C
Melt heating technique	Direct Electrical (Joule) Heating
Power supply operation before water addition	Constant power at 95 kW
Criteria for water addition	1) 7.0 hours of operation with DEH input, or 2) ablation reaches 5 cm of maximum permissible
Inlet water temperature	20 °C
Inlet water flow rate (2 MW/m <sup>2</sup> equivalent quench rate)	2 liters/second
Sustained water depth over melt	50 ± 5 cm
Power supply operation after water addition	Constant voltage
Test termination criteria	1) Melt temperature falls below concrete solidus, 2) concrete ablation is arrested, or 3) maximum ablation limit is reached.

<sup>a</sup>After erosion of concrete/metal inserts and at start of basemat ablation

## 2.0 FACILITY DESCRIPTION

The overall facility design and test operating procedures for CCI-4 were similar to those used in the previous three CCI tests [1]. However, at the first PRG meeting for MCCI-2, the MB made two specific design requests [2] for this test that are summarized as follows:

- 1) Increase the metal content of the melt to the highest practical level to more accurately mock up a prototypic BWR core melt composition at the time of vessel failure, and
- 2) modify the design to increase the duration of the dry core-concrete interaction phase.

The approach for satisfying the first requirement was to place a metal-bearing concrete insert on top of the concrete basemat that was ablated into the melt prior to onset of basemat ablation, thereby increasing the melt metal content to the target level. This technique was originally developed as part of the Advanced Containment Experiment Molten Core Concrete Interaction (ACE/MCCI) test series [3] that focused on quantifying fission product source term due to core-concrete interaction. The approach for satisfying the second request was to slightly reduce the initial inside dimension of the concrete crucible to provide more concrete for ablation, and also to let the ablation front proceed to a deeper depth relative to the limits utilized in the original test series [1]. Additional details regarding these modifications are provided in the balance of this section. Specifications for the experiment were shown previously in Table 1-1.

### 2.1 Test Apparatus

The CCI test facility consisted of a test apparatus, a power supply for Direct Electrical Heating (DEH) of the corium, a water supply system, two steam condensation (quench) tanks, a ventilation system to complete filtration and exhaust the off-gases, and a data acquisition system. A schematic illustration of the facility for CCI-4 is provided in Figure 2-1. The apparatus consisted of three rectilinear sidewall sections and a lid. The overall structure was 3.4 m tall. The two sidewall sections had a square internal cross sectional area of 50 cm x 50 cm. The concrete test section for containment of the core melt was located at the bottom of the apparatus. A top view of this component is shown in Figure 2-2, while cross-sectional views of the electrode and non-electrode sidewalls are provided in Figures 2-3 and 2-4, respectively. The cross-sectional area of the cavity was 50 cm x 40 cm. The distance between the tungsten electrodes was the same as that of previous tests (50 cm), while the distance between the concrete sidewalls was reduced by 10 cm to a width of 40 cm. This increase in sidewall thickness, combined with a 5 cm extension in allowable ablation, provided a total of ten extra centimeters of concrete for lateral ablation. The basemat thickness was increased by 2.5 cm to 57.5 cm to accommodate up to 42.5 cm of axial ablation. This design maintained a minimum concrete thickness of 15 cm in both the sidewalls and basemat for final melt containment.

As shown in Figures 2-2 and 2-3, the electrode sidewalls were fabricated from castable MgO refractory, while the non-electrode sidewalls were fabricated from concrete. The concrete and MgO were contained within a flanged steel form that was used to secure the lower section to

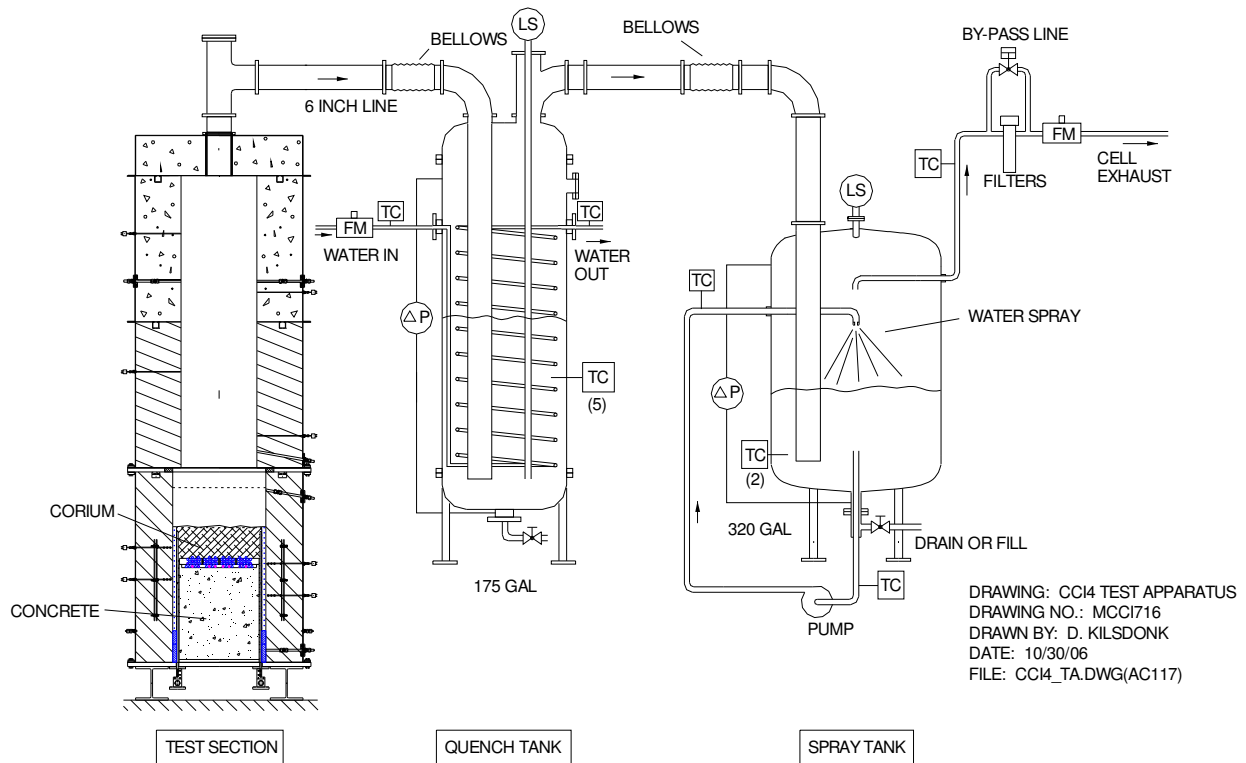


**Figure 2-1. Schematic of CCI Test Facility.**

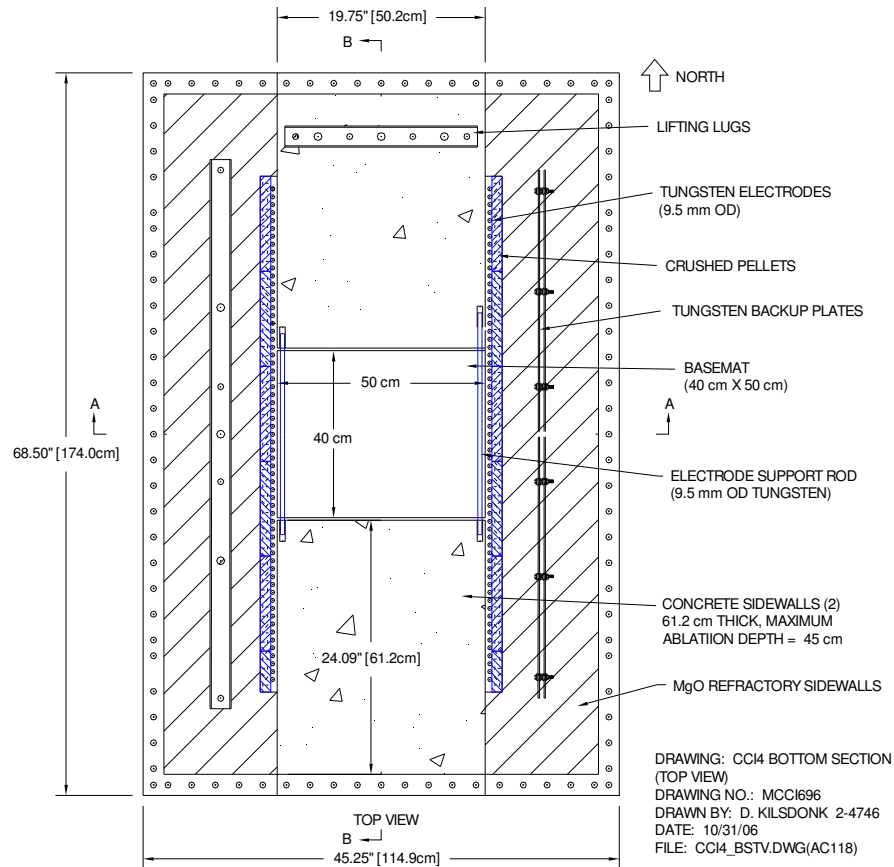


**Figure 2-2. Top View of Lower Test Section.**

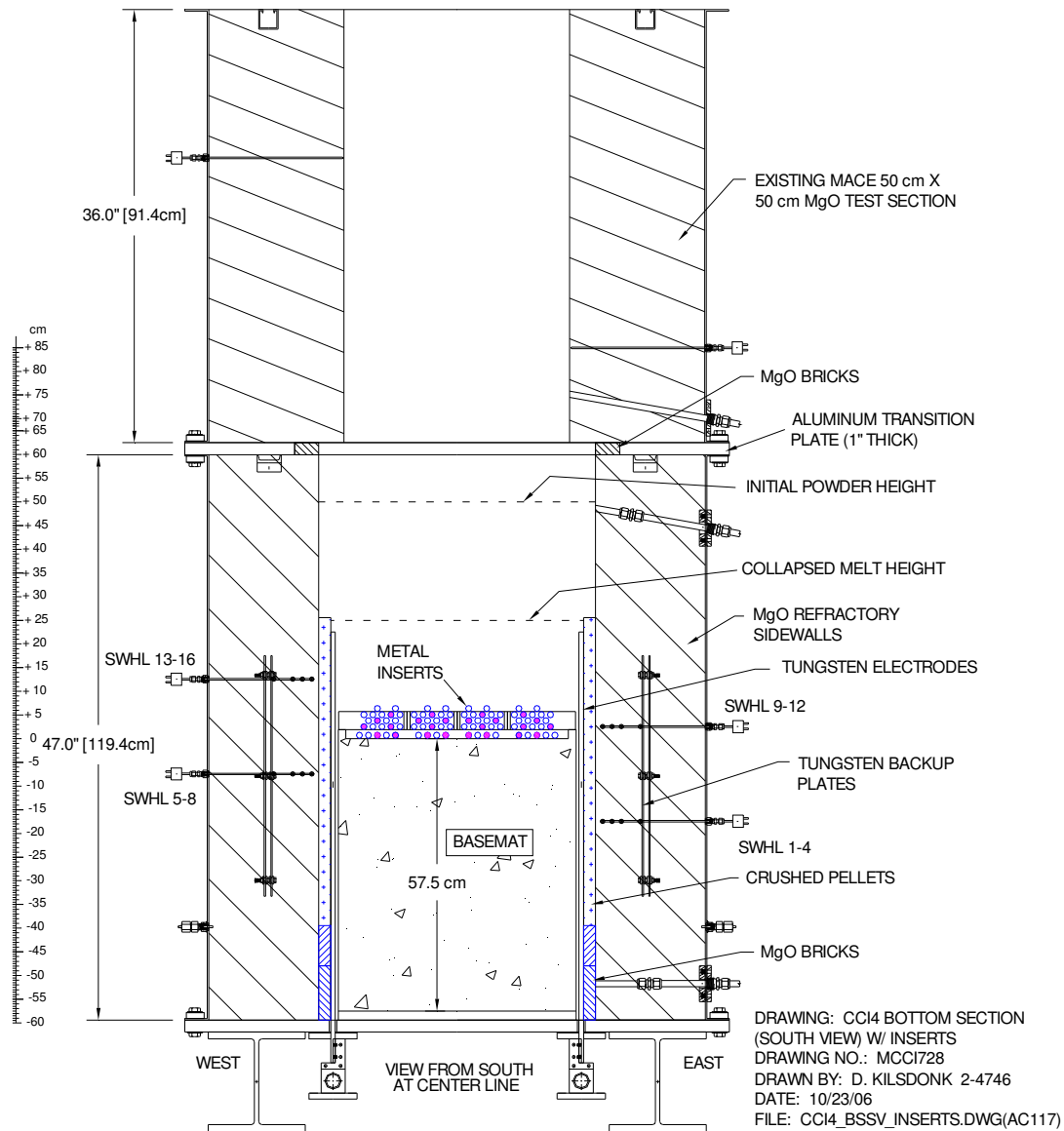


**Figure 2-3. Side View of Lower Test Section Showing Inert MgO Sidewall Sections.**

the balance of the existing test section components with an aluminum transition plate. The lower section was fabricated with vertical, flanged casting seams between the MgO and concrete so that the lower sidewalls could be disassembled to reveal the solidified corium following the test. The MgO sections were reusable, while the concrete sidewall remnants were retained as part of the test records. A layer of crushed UO<sub>2</sub> pellets was used to protect the interior surface of the MgO sidewalls against thermo-chemical attack by the corium. Tungsten plates were embedded in the sidewalls to stop erosion in case the UO<sub>2</sub> protective layer failed. Multi-junction Type C thermocouple assemblies were cast within the sidewalls so that the time-dependent heat loss from the melt could be calculated from the local temperature gradient and the thermal conductivity of the MgO.

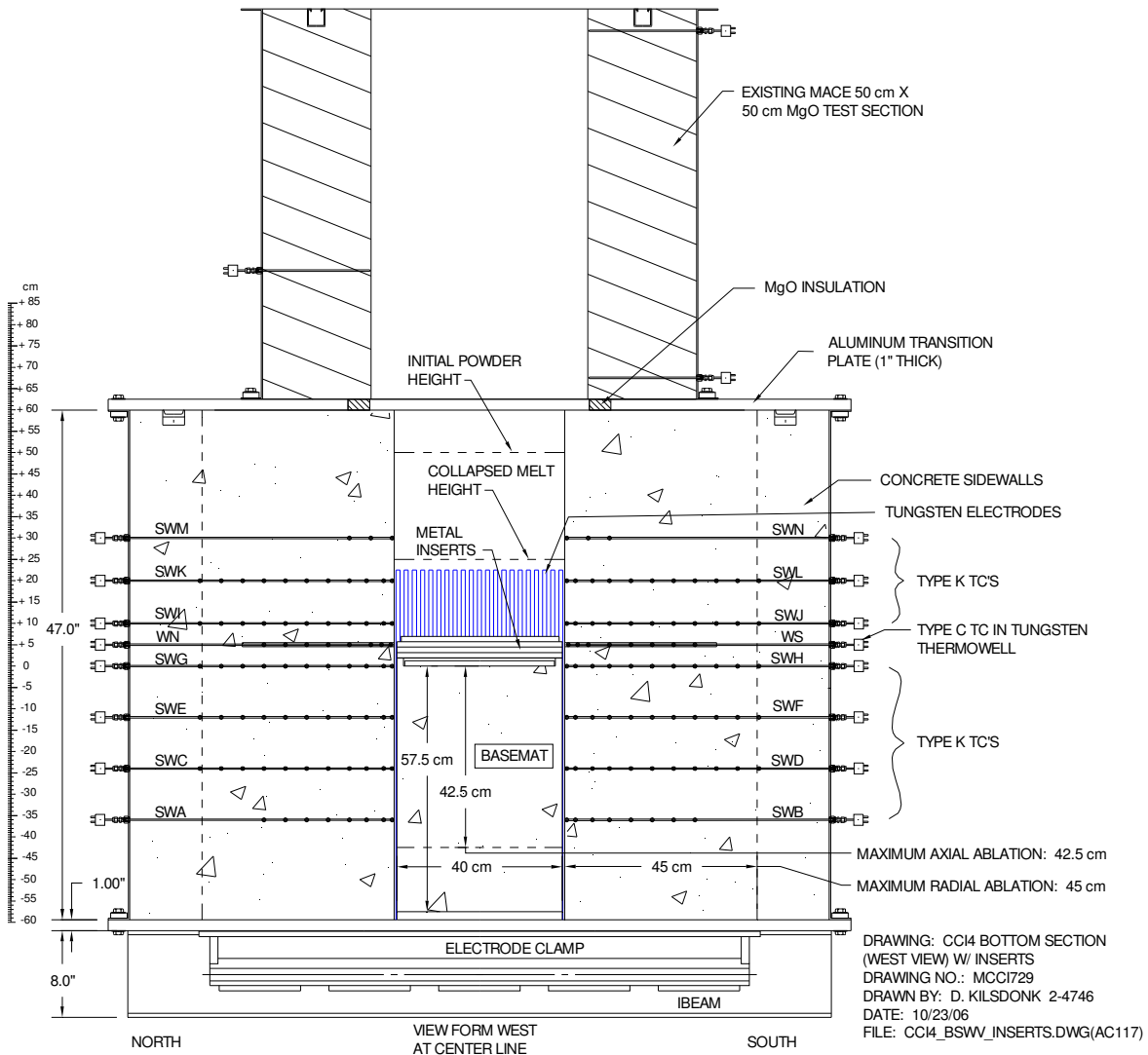


**Figure 2-4. Side View of Lower Test Section Showing Concrete Sidewall Sections.**

The melt was produced through an exothermic chemical reaction yielding the target mass over a timescale of ~ 30 seconds. After the chemical reaction, DEH simulating decay heat was applied through two banks of tungsten electrodes. As shown in Figures 2-2 and 2-3, the electrodes lined the interior surfaces of the two opposing MgO sidewalls. The electrodes were 9.5 cm in diameter and aligned in a row with a pitch of 1.9 cm. They were attached by copper clamps and water-cooled buss bars to a 560 kW AC power supply. As shown in Figure 2-2, the electrodes spanned a total width of 120 cm on each sidewall of the lower section. At the start of the experiment, the electrical current was drawn through the center, 40 cm-wide section of electrodes that were in direct contact with the melt. As the test progressed and the concrete sidewalls were eroded, additional electrodes were exposed to the corium. Current was drawn through these newly exposed heating elements, thereby maintaining a uniform internal heat pattern in the melt over the course of the experiment. With the overall electrode span of 120 cm, up to 40 cm of lateral sidewall ablation could be accommodated while ensuring that the entire melt cross-sectional area was in contact with the tungsten electrodes. However, melt that penetrated beyond this extra 40 cm would not be in direct contact with the electrodes.

Nonetheless, the results of previous tests [1] seem to indicate that melt mixing due to gas sparging from the concrete is sufficient to ensure that the heating input appears uniform. Thus, no significant distortion in the heating pattern was expected during this late stage of the test.

As shown in Figure 2-1, a large (15 cm diameter) gas line was used to vent the helium cover gas and the various gas species arising from the core-concrete interaction (i.e., CO, CO<sub>2</sub>, H<sub>2</sub>O, and H<sub>2</sub>) into two adjacent tanks that were partially filled with water. In the initial phase of the experiment when the cavity remained dry, the tanks served to cool the off-gases and filter aerosols generated from the core-concrete interaction. In the late phase after the cavity was flooded, the tanks served to condense the steam and, based on the measured condensation rate, provided data on the corium cooling rate. In either case, the helium cover gas and non-condensables (CO, CO<sub>2</sub>, and H<sub>2</sub>) passed through the tanks and were vented through an off gas system that included a demister, filters, and a gas flow meter. The gases eventually exhausted through the containment ventilation system and a series of high efficiency filters before finally being released from the building stack.

After a specified period of core-concrete interaction, the cavity was flooded using an instrumented water supply system. The water entered the test section through two weirs located in the opposing (non-electrode) sidewalls of the apparatus. The water supply system is shown in Figure 2-5. After a specified time with water present in the cavity, the crust formed at the melt-water interface was loaded with an insertable crust lance in an attempt to obtain data on the crust breach cooling mechanism. An illustration of the lance installed in the test section is shown in Figure 2-6. The lance was made from 2.54 cm diameter, 304 stainless steel rod with a pointed tip. The lance contained an electrical isolation hub so that there was no need to terminate power input to the melt during the crust loading procedure. As shown in Figure 2-6, the driving force for the lance was simply a 450 kg dead weight that was remotely lowered with the crane during the test.

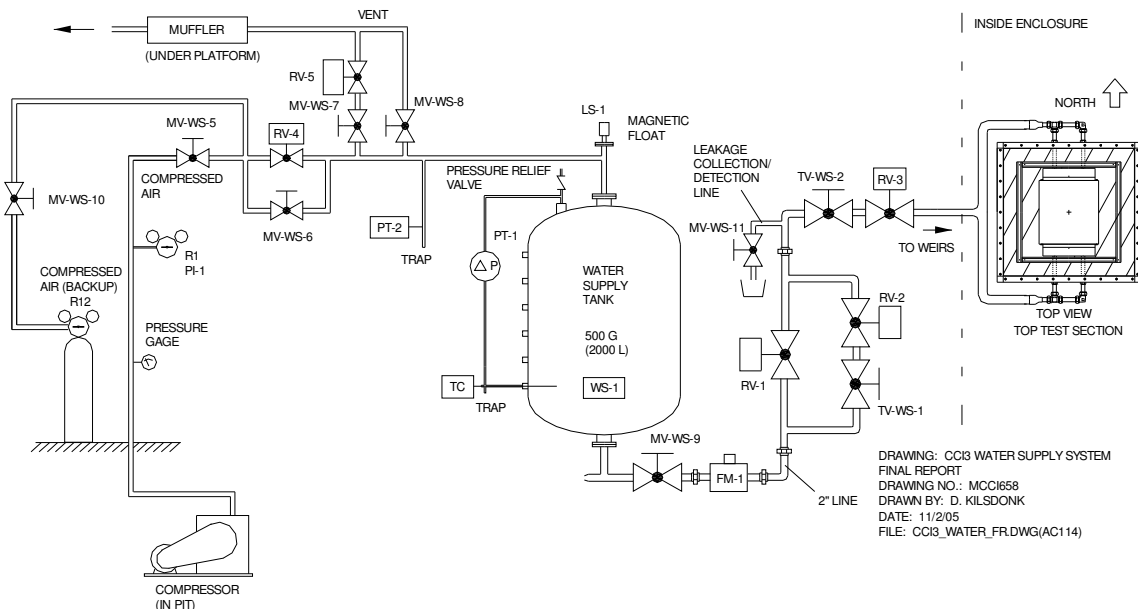


**Figure 2-5. Test Section Water Supply System.**

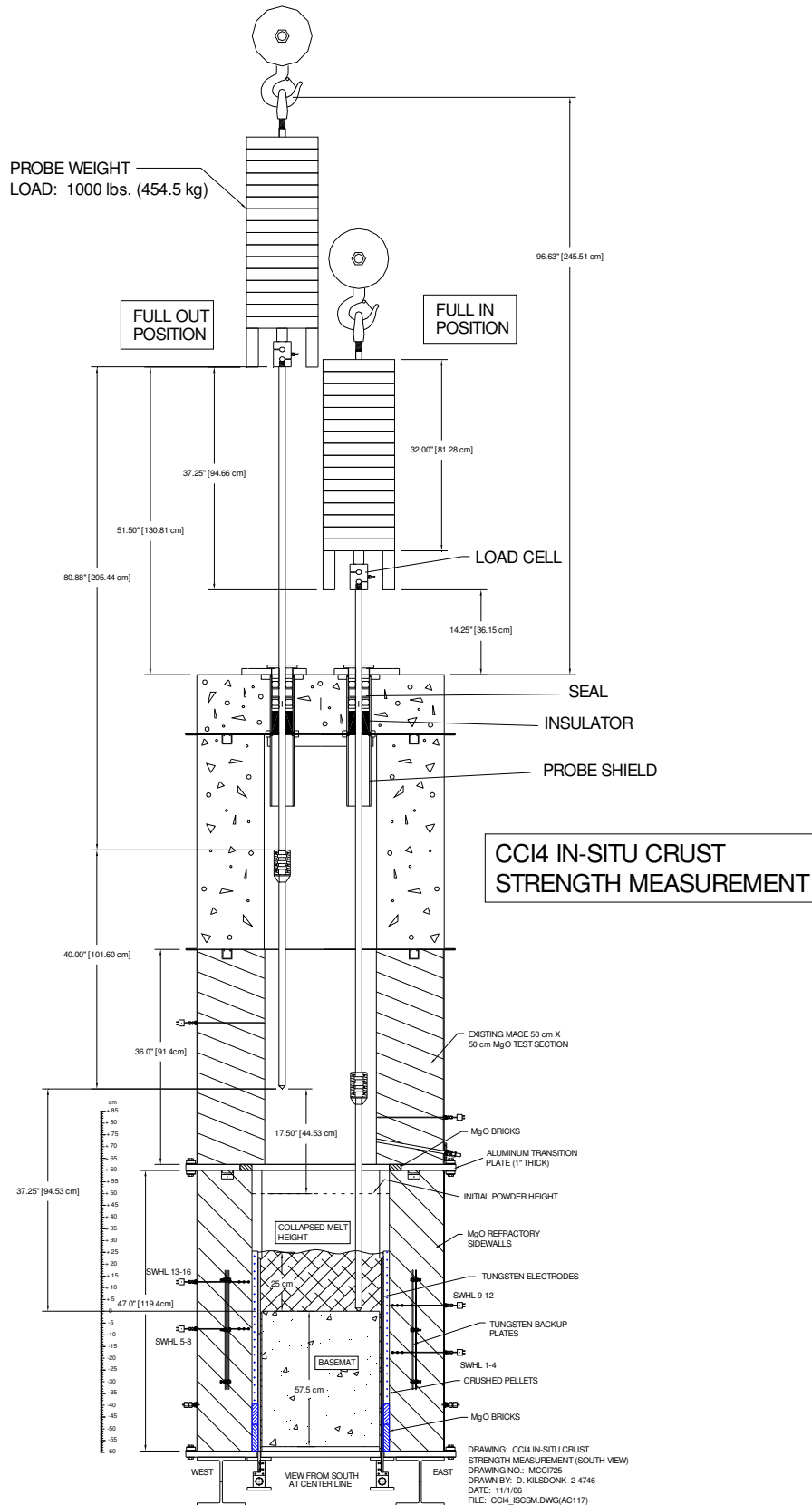
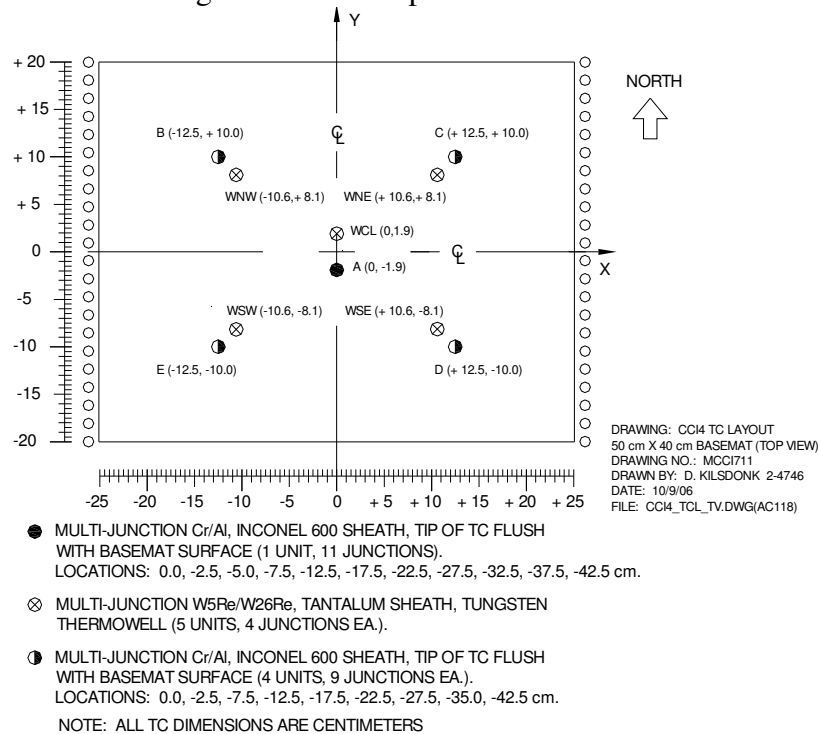


Figure 2-6. Illustration of CCI-4 Crust Lance Assembly Mounted in Test Section.

## 2.2 Instrumentation and Data Acquisition

The CCI facility was instrumented to monitor and guide experiment operation and to log data for evaluation of the lateral and axial erosion rates. Principal parameters that were monitored during the course of the test included the power supply voltage, current, and gross input power to the melt; melt temperature and temperatures within the concrete basemat and sidewalls; crust lance position and applied load; supply water flow rate; water volume and temperature within the test apparatus, and water volume and temperature within the quench system tanks. Other key data recorded by the DAS included temperatures within test section structural sidewalls, off gas temperature and flow rate, and pressures at various locations within the system. A detailed list of all instruments that were used in the experiment is provided in Appendix A. The description below focuses on the key instruments that were used to track the progression of the ablation front and melt temperature during the experiment. Descriptions of other instruments that were used to monitor system conditions are provided elsewhere [1].

Plan and elevation views of the basemat thermocouple layout are provided in Figures 2-7 and 2-8, respectively, while the concrete sidewall instrumentation locations are shown in Figure 2-4. Both the basemat and sidewalls of the test section were instrumented with multi-junction Type K thermocouple assemblies to determine the 2-D ablation profile as a function of time. In addition, Type C thermocouple assemblies in tungsten thermowells protruded upwards from the basemat and laterally inwards from the concrete sidewalls in several locations. The purpose of these instruments was to provide data on the axial and lateral melt temperature distribution as a function of time. Note that the thermocouple junction locations were repositioned to provide melt temperature and ablation front location data over the increased range of lateral and axial concrete ablation that were designed into this experiment.



**Figure 2-7. Plan View of Basemat Instrumentation Layout (dimensions are in cm).**

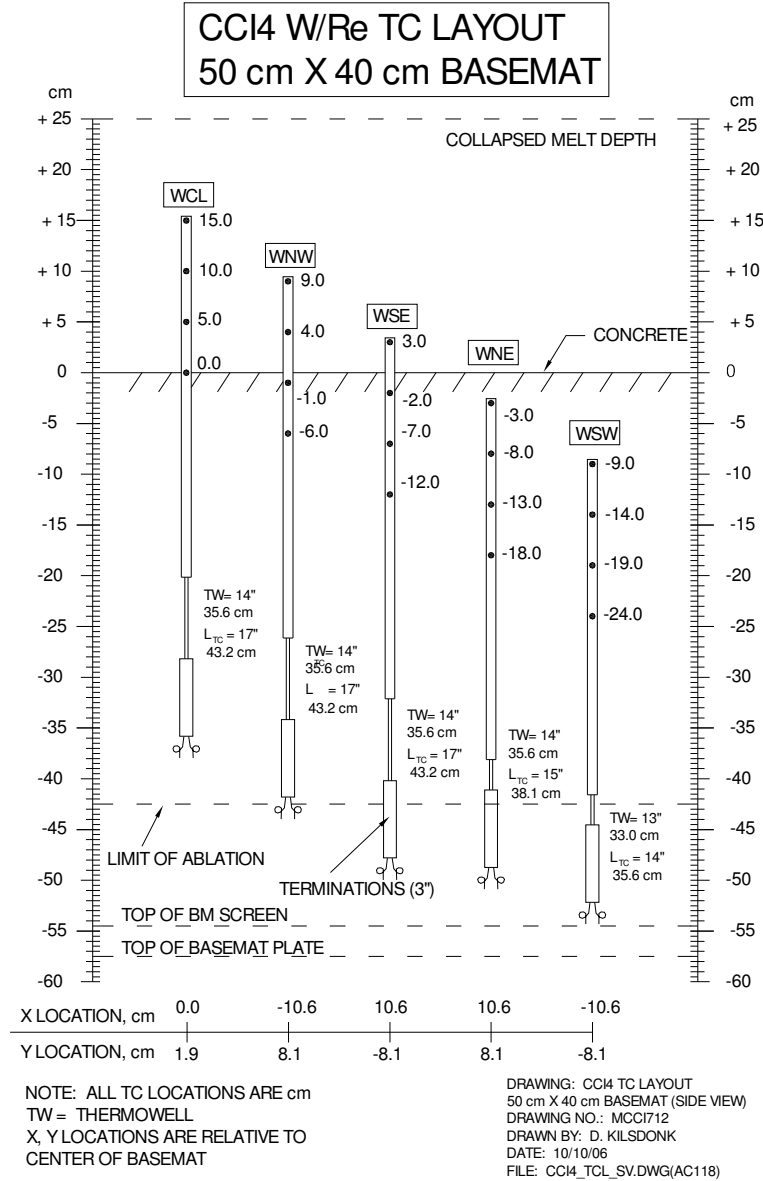


**Figure 2-8. Elevation View of Basemat Type C Thermocouple Locations.**

Other significant instrumentation included a stationary (lid mounted) video camera for observing physical characteristics of the core-concrete interaction.

All data acquisition and process control tasks were managed by a PC executing LabVIEW 6.i under Windows XP. Sensor output terminals were connected inside the test cell to model HP E1345A 16-channel multiplexers, which were integrated into a mainframe chassis in groups of eight. An illustration of the DAS setup is provided in Figure 2-9. The multiplexers directed signals to an HP E1326B 5 ½ digit multimeter incorporated into each chassis. Three independent 128 channel systems were used for a total capacity of 384 channels.

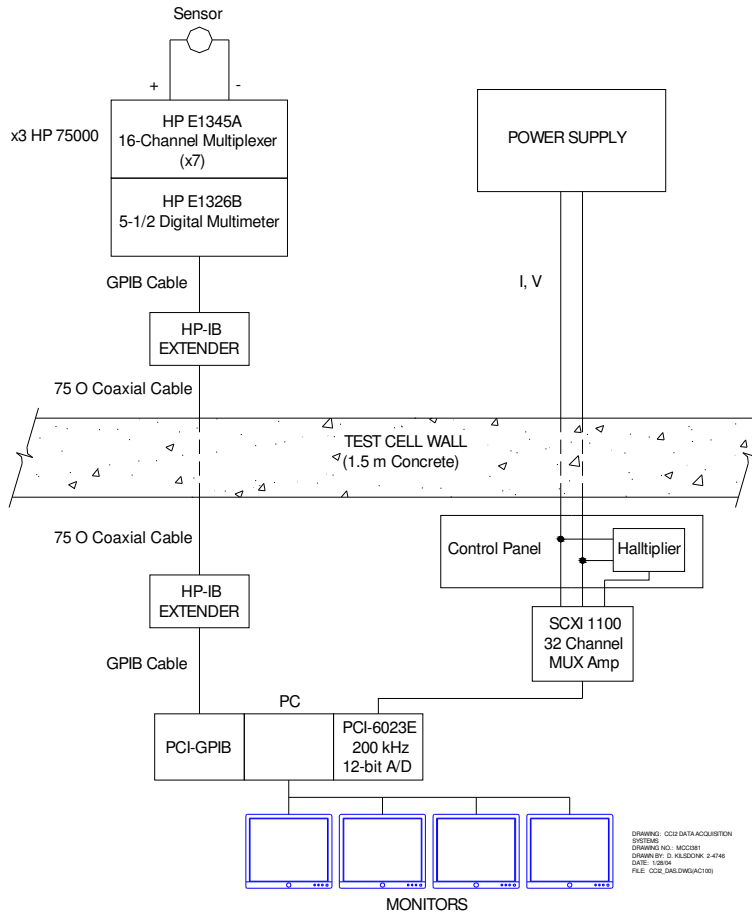


**Figure 2-9. CCI Data Acquisition and Control Systems.**

Signal noise was reduced by the digitizer through integration over a single power line cycle (16.7 ms). The digitized sensor readings were routed from the test cell to the PC in the control room via two HP-IB extenders. The extenders allowed the ASCII data from the HP to be sent through the cell wall over a BNC cable. The extender within the control room then communicated with a GPIB card within the PC. This configuration also permitted remote control of the multimeter through LabVIEW.

Integration of the signal over the period of a power line cycle limited the speed with which the multiplexer could scan the channel list. The minimum time for the digitizer to scan the channel list was  $\sim 1.7$  s (16.7 ms  $\cdot$  100 channels/chassis for this test). Though the three systems operated independently, implying the ability to update all 300 channels in roughly two seconds, the actual time required for the update was about 5.5 s.

### 2.3 Corium Composition and Concrete-Metal Inserts

As discussed earlier, one of the key objectives of this test was to increase the metal content of the melt to the highest practical level to more accurately mock up a prototypic BWR core melt at the time of vessel failure. The target value for the initial metal content was 15 wt %

[2]. The overall approach for satisfying this requirement was to place a metal-bearing concrete insert that overlaid the basemat for dissolution into the melt prior to onset of basemat ablation, thereby increasing the melt metal content to the target level. This technique was originally developed as part of the Advanced Containment Experiment Molten Core Concrete Interaction (ACE/MCCI) test series [3] that focused on quantifying fission product source term during core-concrete interaction. The metal content of the inserts, shown in cross-sectional view over the basemat in Figure 2-10, included Zr that represented unoxidized cladding plus iron that, when combined with the Cr metal reaction byproduct from the thermite reaction, produced a mixture that mocked up stainless steel from ablated vessel structures.

As part of this work, it was necessary to design and test a new thermite that, after complete oxidation of metallic cladding, yielded a melt composition with a fuel-to-cladding ratio of ~ 1 (molar basis) that is typical of many BWRs. Initially, a thermite was designed and tested that included both  $Fe_2O_3$  and  $CrO_3$  as oxidizers, so that a stainless steel-like metal byproduct was produced during the reaction that also added to the melt metal content. However, during mixing of the 1 kg sample for this test, the powders noticeably warmed, which is an indication of thermal instability. On this basis, a second thermite was designed and tested that only used  $CrO_3$  as the oxidizer, since this type of mixture is known to be thermally stable. With this approach, the Fe needed to obtain the stainless steel surrogate in the melt was placed in the inserts along with the Zr metal. Details regarding the thermite developmental tests are provided elsewhere. [4]

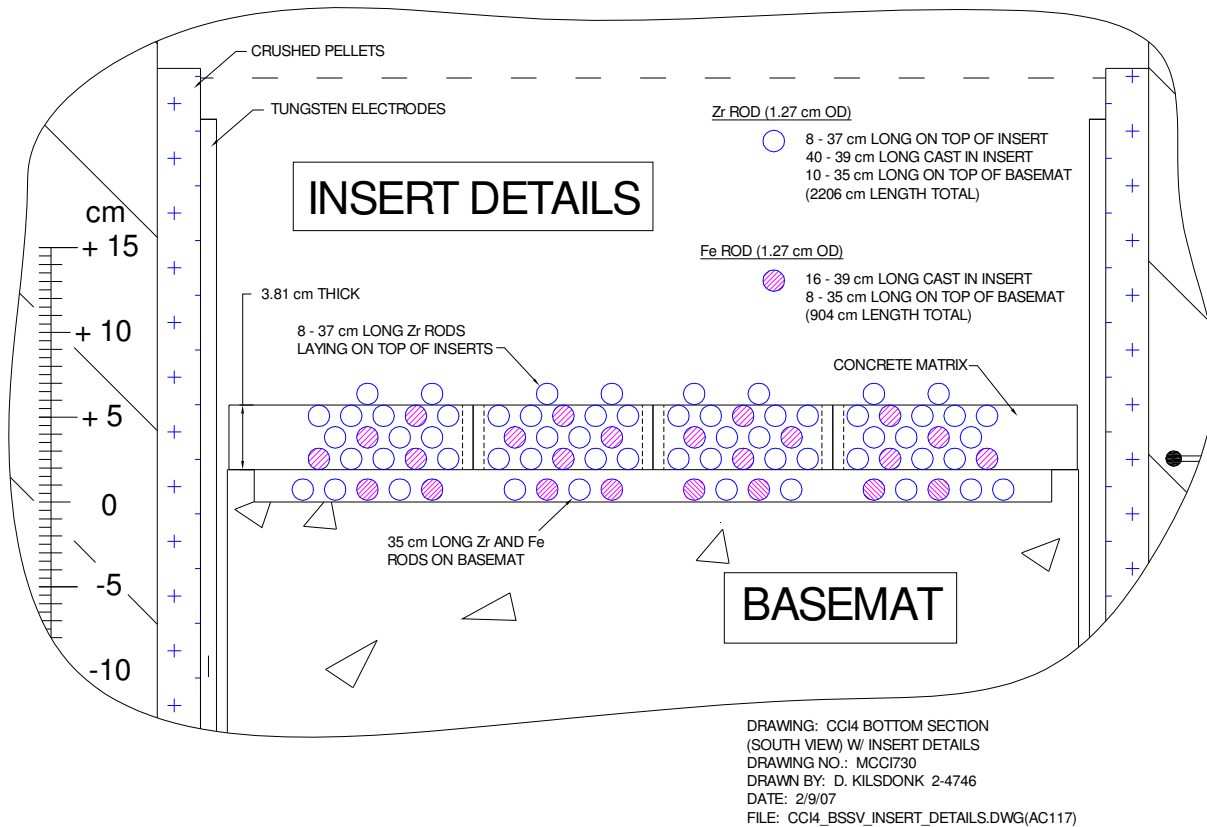
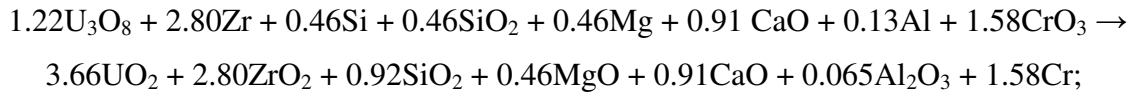


**Figure 2-10. Illustration of Concrete-Metal Inserts in Place over the Concrete Basemat.**

As shown in Table 1-1, the corium composition for CCI-4 was specified to be a 78 % oxidized BWR core melt containing 7.7 wt % stainless steel constituents and ~10.0 wt % limestone/common sand concrete. This was the best estimate melt composition after erosion of the concrete/metal inserts and at the start of basemat ablation, which defines time  $t = 0$  for the experiment (see Section 3). The composition estimate includes additional cladding (both Zr and  $ZrO_2$  from oxidation reactions that occurred during insert erosion), concrete slag, and steel constituents from the inserts. The thermite reaction that produced the initial melt composition over the inserts was of the form:



$$Q = -192.8 \text{ kJ/mole (1.64 MJ/kg);}$$

$$T_{\text{adiabatic}} = 2422 \text{ }^\circ\text{C}$$

$$T_{\text{actual}} \sim 2200 \text{ }^\circ\text{C}$$

The bulk composition of the melt produced from this reaction is summarized in Table 2-1, while the detailed pre- and post-reaction compositions are provided in Table 2-2. The reaction temperature of this thermite was measured as ~ 2200 °C during developmental tests [4].

**Table 2-1. Bulk Composition of CCI-4 Melt at Start of Interaction with Inserts.**

Constituent	Wt%
UO <sub>2</sub>	63.91
ZrO <sub>2</sub>	22.27
Calcined concrete <sup>a</sup>	8.51
Chromium metal	5.31
Total	100.00

<sup>a</sup>Calcined LCS concrete: 42.0/14.1/38.8/5.1 wt% SiO<sub>2</sub>/MgO/CaO/Al<sub>2</sub>O<sub>3</sub>

**Table 2-2. Detailed Pre- and Post-Reaction Thermite Compositions for CCI-4.**

Constituent	Reactant		Product	
	Wt %	Mass (kg)	Wt %	Mass (kg)
U <sub>3</sub> O <sub>8</sub>	66.44	176.07	-	-
UO <sub>2</sub>	-	-	63.91	169.36
Zr	16.48	43.67	-	-
ZrO <sub>2</sub>	-	-	22.27	59.02
Si	0.84	2.23	-	-
SiO <sub>2</sub>	1.79	4.74	3.58	9.48
Al	0.23	0.61	-	-
Al <sub>2</sub> O <sub>3</sub>	-	-	0.43	1.14
Mg	0.72	1.91	-	-
MgO	-	-	1.20	3.18
CaO	3.30	8.74	3.30	8.74
CrO <sub>3</sub>	10.20	27.03	-	-
Cr	-	-	5.31	14.08
Total	100.00	265.00	100.00	265.00

As noted earlier, the inserts contained all the Zr and Fe in the corium inventory. As shown in Figure 2-10, they were supported on a lip around the upper surface of the basemat. The composition of the inserts, which were 3.8 cm thick and weighed 36.58 kg, is shown in Table 2-3. The metals were in the form of 1.27 cm diameter rods that were cast into a concrete matrix. The rods ran parallel to the tungsten electrode banks so that an electrical shorting path between the electrode banks was not created. The Zr and Fe rods were intermixed to distribute the metals uniformly across the basemat.

The estimated bulk melt composition after erosion of the inserts and at the start of basemat ablation is shown in Table 2-4, while the detailed composition is provided in Table 2-5. These estimates include the expected oxidation of Zr with H<sub>2</sub>O and CO<sub>2</sub> gases that were liberated upon decomposition of the concrete in the inserts (concrete composition is provided in the next section). In particular, of the 17.88 kg of Zr rod, 4.06 kg was estimated to be oxidized to ZrO<sub>2</sub>, while the balance (13.82 kg) entered the melt in metallic form. As shown in Table 2-4, the corium metal content at the start of basemat ablation was 12.3 wt %, of which 4.6 wt% was unoxidized cladding, and 7.7 wt % was in the form of steel constituents. This metal content can be compared with the 15 wt % target level requested by the MB [2].

**Table 2-3. Composition of CCI-4 Concrete/Metal Inserts.**

Constituent	Wt%	Mass (kg)
Zr rod	48.88	17.88
Fe rod	24.52	8.97
Limestone/common sand concrete	26.60	9.73
Total	100.00	36.58

**Table 2-4. Bulk Melt Composition at Start of Basemat Ablation.**

Constituent	Wt%
UO <sub>2</sub>	56.52
ZrO <sub>2</sub>	21.53
Calcined concrete	9.65
Stainless steel components <sup>a</sup>	7.69
Unoxidized cladding	4.61
Total	100.00

<sup>a</sup>61.1/38.9 wt % Cr/Fe

**Table 2-5. Detailed Melt Composition at the Start of Basemat Ablation.**

Constituent	Wt %	Mass (kg)
UO <sub>2</sub>	56.52	169.36
ZrO <sub>2</sub>	21.53	64.51
SiO <sub>2</sub>	4.05	12.15
Al <sub>2</sub> O <sub>3</sub>	0.49	1.47
MgO	1.36	4.08
CaO	3.75	11.23
Zr	4.61	13.82
Cr	4.70	14.08
Fe	2.99	8.97
Total	100.00	299.67

## 2.4 Concrete Composition

As shown in Table 1-1, limestone/common sand concrete was specified for Test CCI-4. The estimated chemical composition for this concrete is provided in Table 2-6. This composition is based on analysis of a specimen taken from the CCI-2 concrete archive sample [1]. The actual composition of the concrete for Test CCI-4 will be determined through chemical analysis of a specimen that was collected during fabrication of the sidewall and basemat components.

**Table 2-6. Estimated Composition of CCI-4 Concrete (CCI-2 Basis [1]).**

Oxide	Wt%
Al <sub>2</sub> O <sub>3</sub>	2.49
CaO	25.88
Fe <sub>2</sub> O <sub>3</sub>	1.39
MgO	11.47
MnO	0.03
K <sub>2</sub> O	0.55
SiO <sub>2</sub>	21.61
Na <sub>2</sub> O	0.31
SrO	0.00
TiO <sub>2</sub>	0.135
SO <sub>3</sub>	0.505
CO <sub>2</sub>	29.71
H <sub>2</sub> O, Free	3.255
H <sub>2</sub> O, Bound	1.11
Total	98.47

## 3.0 TEST PROCEDURES

### 3.1 Pretest Operations

Assembly of the apparatus began by installing the tungsten electrodes (126 total; 63 per side) into machined copper electrode clamps. The electrode clamps were then attached to the bottom of the 2.54 cm thick aluminum support plate which served as the foundation for the entire apparatus. With the electrode clamps installed, the support plate was moved into position on the ZPR-9 reactor bed. The concrete basemat was then placed atop the support plate. The top surface of the basemat was insulated with a 3 mm thick layer of low density ZrO<sub>2</sub> felt. The basemat was then completely covered with a continuous sheet of 1.7 mil aluminized Saran film to prevent moisture contamination of the thermite powders from the basemat once the powders were loaded into the test section. The lower test section concrete and MgO sidewalls were then set in place. The concrete sidewalls were also covered with ZrO<sub>2</sub> felt and aluminized Saran before placement to prevent moisture contamination of the thermite from these components once the powders were loaded. The lower section flange bolts and clamping bars were then installed and torqued according to an approved procedure.

In parallel with test section assembly, the thermite powders were mixed in preparation for corium loading. As a precursor for initiating mixing, a gas sample test<sup>a</sup> was conducted to verify that the initial level of volatile impurities in a sample prepared from the CCI-4 thermite constituents was sufficiently low to preclude excessive gas release during the burn. The results of this test indicated moisture and nitrogen contents were within acceptable limits. On this basis, mixing was initiated.

Once the lower section was assembled, preparations for loading of the corium charge began. A single, large 1.7 mil aluminized Saran bag was preinstalled over the basemat. During loading, the 265 kg thermite charge was placed within this bag in order to reduce the amount of bagging material present in the thermite. As the powders were placed in the test section, the basemat melt temperature thermocouples were monitored to detect any localized heating in the corium powders. If heating was observed, the cell was to be evacuated immediately. As the thermite was placed, the gap between the tungsten electrodes and MgO sidewalls was filled with crushed UO<sub>2</sub> pellets. The crushed pellets served as a protective layer against excessive chemical/thermal attack by the corium during the test. Once loading was completed, two sparkler igniters were placed a few centimeters below the top of the powders near the center of the test section, and then the bag was folded and sealed.

Once loading was completed, a removable train containing a 1.0 kg bagged sample of thermite was installed over the powder bed; an illustration is provided in Figure 3-1. The sample train was removed weekly and the sample weighed to monitor the moisture pickup by the thermite during the period between loading and test initiation. Note from Figure 3-1 that the top portion of the train also contained a 4.5 kg canister of desiccant. The desiccant was provided to maintain the plenum gas as dry as possible during pretest operations. As an additional measure to prevent moisture accumulation in the powder bed, the lower test section was continuously purged with argon (2 slpm) from the time loading was completed until the test was initiated.

After installation of the sample train, the remainder of the test apparatus was assembled. This included installation of the transition plate, two upper sidewall sections, and finally the enclosure lid. Peripheral instrumentation was then installed on the lid and sidewalls of the test section. The main steamline run from the test section to the primary quench tank was completed, as well as the pressure relief line from the test section to the auxiliary tank. (The main steamline was closed off from the test section using an insertable blank-off plate throughout pretest operations to preclude moisture migration from the quench tank into the test section).

After assembly was completed, extensive system checkout procedures were performed to ensure that the facility was in proper working order. This included a proof test of the test section at 83 kPad, which is 20 % in excess of the pressure relief system activation pressure of 69 kPad. The pressurization gas for this test was argon. An insertable blind flange was installed upstream of the rupture disk in the pressure relief line to isolate this system. During the test, the apparatus

---

<sup>a</sup> The gas sample test procedure consists of igniting a representative sample of the thermite in a closed vessel. The amount of noncondensable gas produced is determined from the ideal gas law; the composition of the evolved gases is determined using gas mass spectroscopy.

was gradually pressurized to the proof pressure of 83 kPad. After a 1 minute hold at this pressure, the system was isolated to determine the leak rate. The leak rate of the CCI-4 test section was found to be 4.2 kPa/min (18 slpm) at a nominal pressure of 55 kPad, which was significantly below the acceptable leak rate of the fully assembled test section (i.e., < 2 % of the expected peak gas/vapor generation rate during the test).

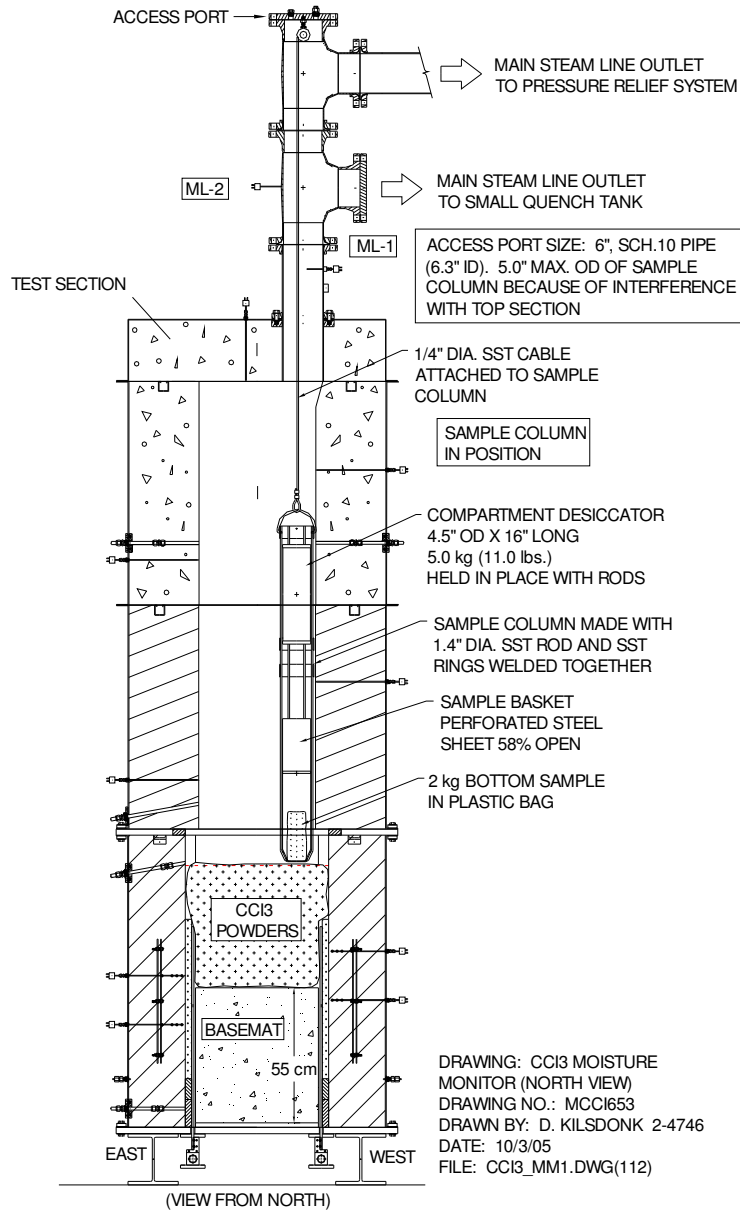


**Figure 3-1. Illustration of Thermite Sample Train Installed in Test Section.**

Pretest preparations for CCI-4 culminated with a final full system checkout that involved remotely running all equipment with the power supply in operation across a water cooled dummy load. Once the full system check was completed, final system preparations were carried out. These efforts included: (i) hookup of the power supply to the tungsten electrodes through water

cooled buss bars, (ii) installation of the final piping connection between the water supply tank and the test section, and (iii) removal of the sample train from within the test section. Following connection of the power supply to the electrode clamps, the key for the power supply lockout located in the cell, as well as the key for the interlock located on the control room console, were assigned to a custodian who kept the keys in their possession until the test was initiated. This step was taken to preclude inadvertent activation of the power supply.

Over the four week time interval spanning pretest operations, the moisture content of the removable sample of bagged thermite increased gradually from 0.18 wt % to 0.028 wt %. The final moisture content was within the maximum permissible level of 0.3 wt %. On this basis, final approval was granted to proceed with the execution of Test CCI-4.

### 3.2 Test Operations

The planned test operating procedure is described first, followed by a brief summary of the actual operating procedure.

As shown in Table 1-1, target power for the dry core-concrete interaction phase of the test was 95 kW.<sup>b</sup> After melt formation, the input power would be brought up to 95 kW and held there for the balance of dry cavity operations. The initial phase of the interaction would involve ablation of the concrete-metal inserts over the basemat, thereby incorporating the balance of the metals into the melt and producing the initial melt composition shown in Table 2-5. Onset of basemat ablation would define time  $t = 0$  for the experiment. After ablation began, the interaction would be permitted to proceed for 7.0 hours,<sup>c</sup> or until the ablation depth reached 40 cm laterally or 37.5 cm axially. After one of these criteria was met, the cavity would then be flooded. However, if a crust was present at the melt upper surface, the crust lance would be used to fail the crust prior to flooding so that the water would be able to contact the underlying melt. Following water addition, the power supply operation would be switched from constant power at 95 kW to a constant voltage operating mode. (With constant voltage, the input power density would remain relatively constant if a significant quench front developed). Thirty minutes after water addition, or after the debris cooling rate had been reduced to a relatively low level, the crust would be failed with the lance to obtain data on the transient crust breach cooling mechanism. After breach, power supply operations would continue for an additional 30 minutes, yielding a total operating period of 60 minutes with water present in the cavity, or until the ablation limit of 45 cm was reached laterally or 42.5 cm axially. At this point, the input power would be turned off and the test terminated.

CCI-4 was performed on 26 May 2007. On the evening prior to the experiment, the apparatus was inerted with a slow bleed of helium into the test section. On the day of the experiment, the apparatus was brought up to operating conditions, a final walk through

---

<sup>b</sup>The 95 kW power level for CCI-4 is scaled down from the 120 kW level used in Tests CCI-2 and CCI-3 [1] based on a surface area scaling that preserves the heat flux to the boundaries of the melt at the start of the interaction.

<sup>c</sup> The 7 hour limit on dry cavity ablation for CCI-4 is linearly scaled up from the 5.5 hour limit used in Tests CCI-2 and CCI-3 [1] based on the increase in maximum lateral erosion depth from 30 cm to 40 cm for CCI-4.

inspection was performed by operating personnel, the thermite igniter was hooked up, and finally the power supply was energized before the containment was evacuated and sealed. Data acquisition was initiated at 10:44 am. Coolant and cover gas flows were brought up to design conditions, and the cell ventilation system was closed and sealed per test procedures.

A brief event sequence for CCI-4 is provided in Table 3-1. In the discussion that follows, time  $t = 0$  corresponds to the onset of basemat ablation. The criteria used to define the onset of concrete ablation at a given location was that the local temperature reached the limestone/common sand concrete liquidus temperature of 1295 °C. [3]

**Table 3-1. CCI-4 Event Sequence (times relative to onset of ablation of the basemat).**

<b>Time (Minutes)</b>	<b>Event</b>
-48.6	DAS started.
-38.5	Power applied to thermite igniter wire.
-38.2	Thermite burn initiated; view of melt surface occluded by aerosol within 5 seconds.
-37.7	Thermite burn completed (burn time ~ 30 seconds); melt temperature ~2000 °C
-36.6	Target DEH input power of 95 kW reached.
-10.3	Temperatures in test section gas plenum increase sharply, and power supply operating parameters change (i.e., current decreases and voltage increases), indicating onset of insert ablation.
-6.54 to +4.41	Onset of basemat ablation detected at all five basemat locations; average time for all arrays is 0.0 minutes, which defines time $t = 0$ for the experiment.
23.1	DAQ communications failure halts data transmission between the PC and the analog to digital converters in the cell. Recovery efforts initiated.
41.0	Recovery operations completed and data acquisition restarted.
383.7	Sparks seen from beneath the test section bottom plate; DEH input power terminated.
384.9	Water addition to test section initiated.
458.3	Data acquisition terminated.

As shown in Table 3-1, data acquisition began at -48.6 minutes relative to initial melt contact with the basemat. As shown in Figure 3-2, power was applied to the nichrome wire/sparkler located at the top of the powder charge at -38.5 minutes. Based on video camera data from the test section and plenum gas temperature readings inside the test section, thermite ignition was announced and logged in the control room at -38.2 minutes. Based on readings from thermocouples located near the top of the concrete – metal inserts, the burn front reached the bottom of the powder bed in ~ 30 seconds (i.e., at -37.7 minutes), which was within the planning basis for the experiment. The readings from selected melt temperature thermocouples are shown in Figure 3-3 over the first few minutes of the interaction. As is evident from this

collection of data, peak melt temperatures near the center of the melt in the first 30 seconds of the interaction were in the range of 1910 to 2070 °C.

Following the thermite burn, there was a quiescent period during which concrete surfaces were protected by insulating crusts. However, at -10.3 minutes, plenum gas temperatures suddenly increased by several hundred degrees (Figure 3-4), and the power supply operating current dropped at constant power (Figure 3-5), indicating onset of concrete ablation within the test section.<sup>d</sup> The thermocouple data indicates that ablation of the concrete sidewalls was initiated at this time, as well as the concrete-metal inserts. Onset of basemat ablation was detected at the basemat centerline and in the four outer quadrants over the time interval from -6.54 to +4.41 minutes. The average time for all five arrays was 0.0 minutes, which defines time  $t = 0$  for the experiment.

At completion of the burn, a power supply current ramp up to the target power of 95 kW was initiated. This power level was reached at -36.6 minutes, where it was essentially maintained for the balance of the test involving dry cavity operations.

Near 23 minutes in the operating sequence, an unidentified DAQ communications failure halted transmission between the PC and the Hewlett Packard (HP) analog to digital converters in the cell. The cause is thought to be a transmission error between one of the HP units and one of the two repeaters between each HP and the PC. The error froze traffic along the General Purpose Interface Bus (GPIB) that linked all repeaters with the PC. Diagnostic and recovery operations were initiated, and communications were reestablished at 41 minutes, leaving a 16.9 minute gap in the recorded data. During this time, input power to the melt was maintained at 95 kW based on panel readouts in the control room that were independent of the data acquisition system.

After concrete ablation was initiated, input power was held constant at 95 kW, and concrete erosion continued. At 387.7 minutes, sparks were seen emanating from the bottom of the test section, indicating the development of a minor leak. At this time, power input to the melt was terminated. The cavity was flooded soon after (i.e., at 384.9 minutes) to obtain debris cooling data. The operators continued to log data until 458.3 minutes. At this point, the system was shutdown following the normal test termination procedures. The DAQ was restarted to record the long-term cool down data. The experiment was left unattended to cool down overnight.

---

<sup>d</sup> The decrease in current at constant power is due to the fact that the addition of concrete decomposition products to the melt causes the melt electrical resistance to increase.

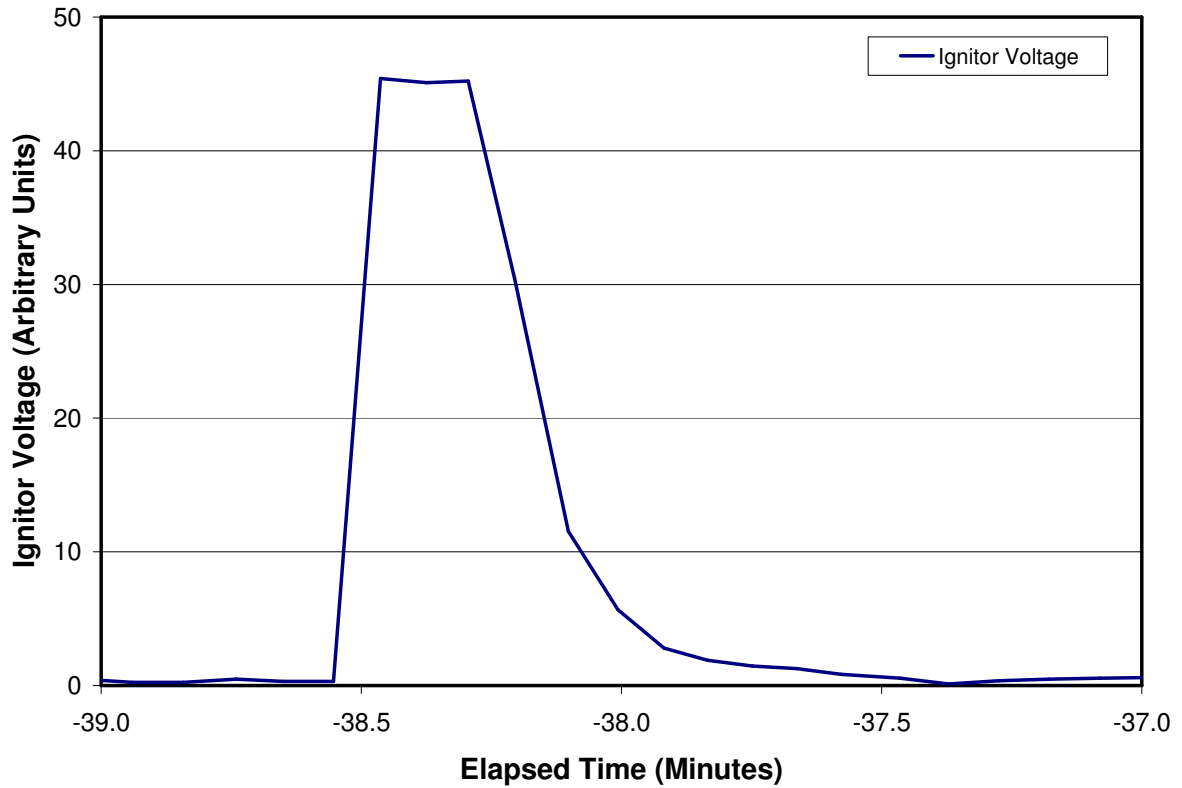


Figure 3-2. Voltage Reading Across Thermite Igniter Shunt.

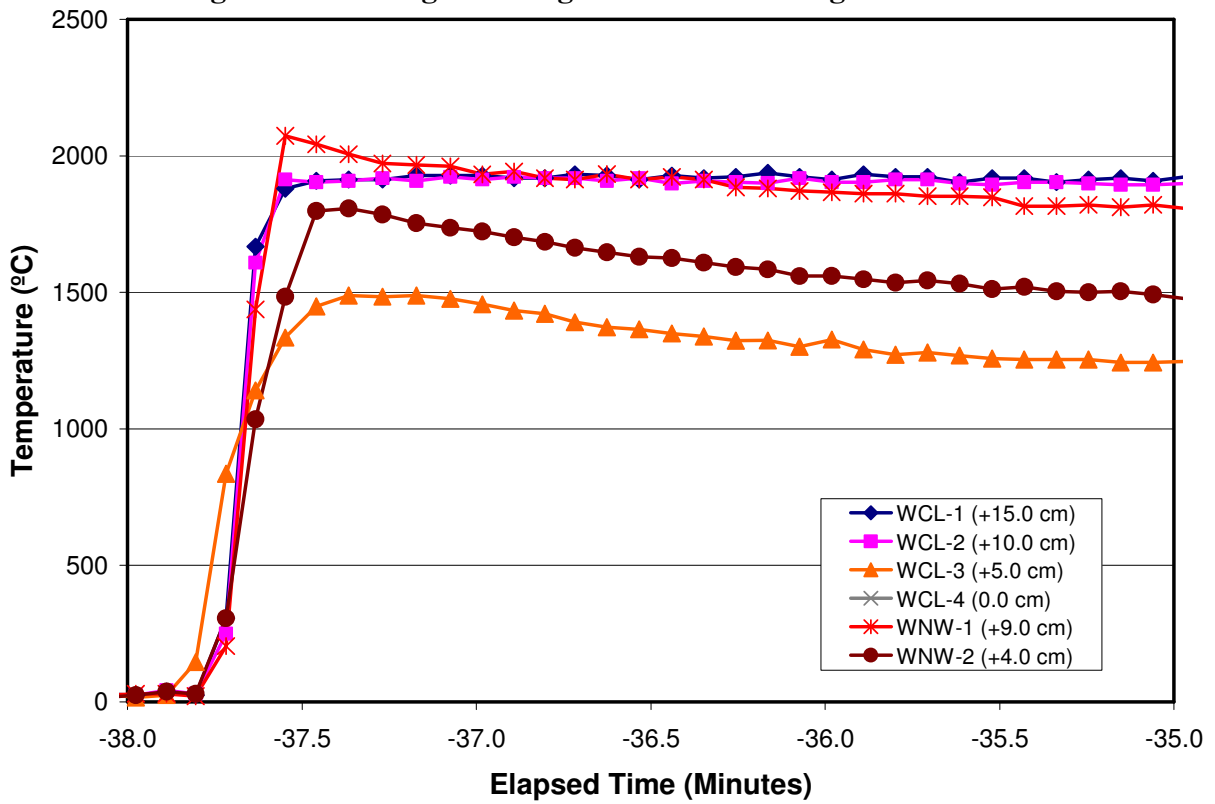
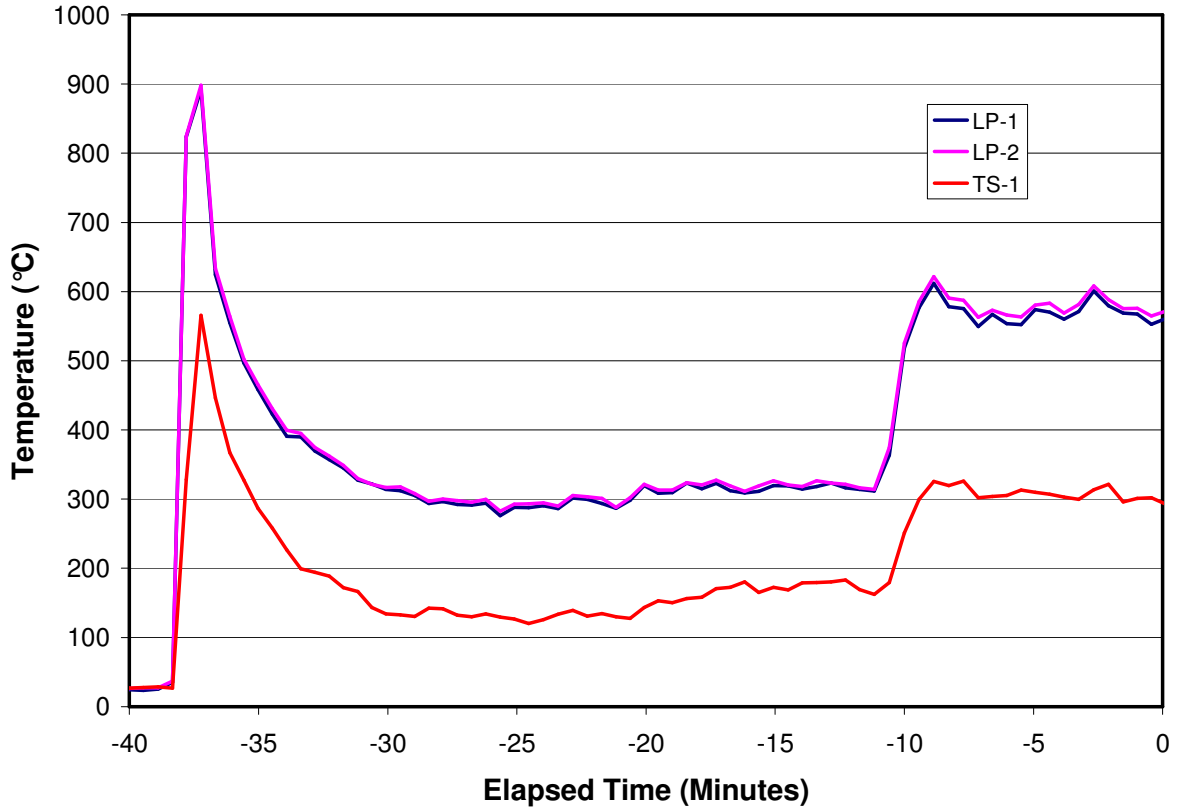
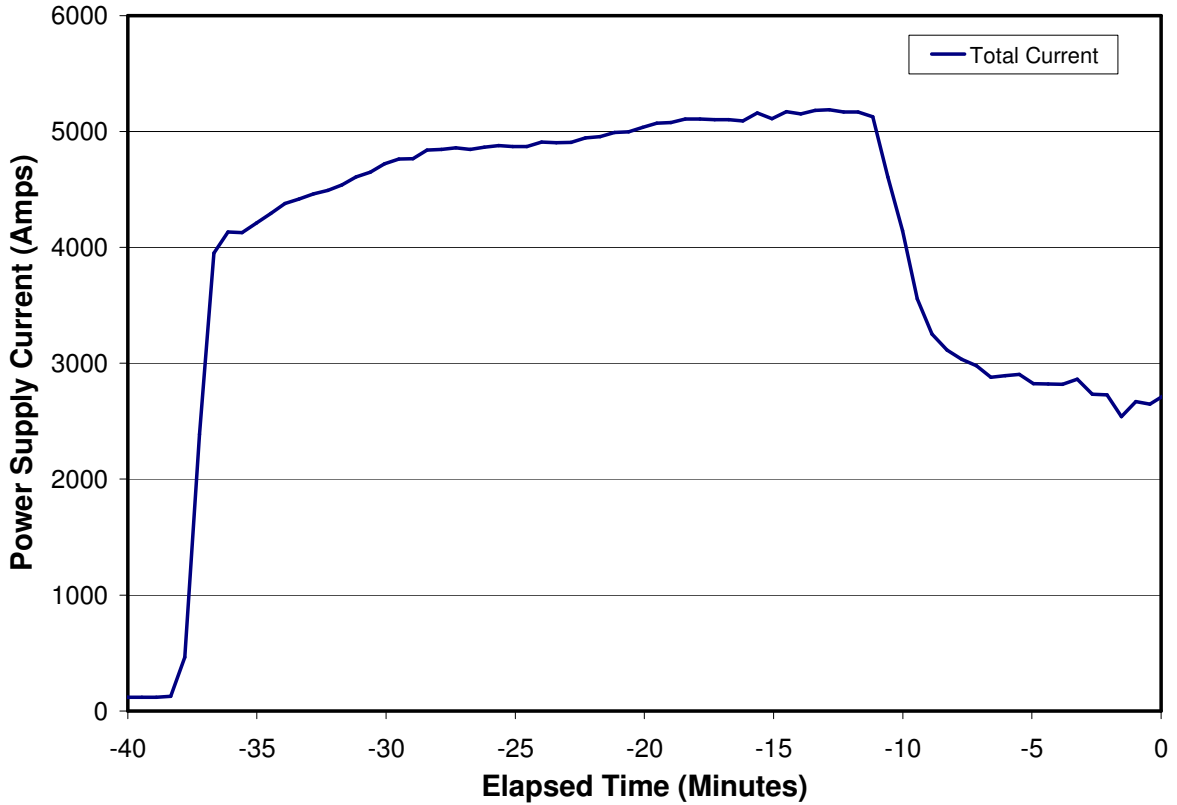


Figure 3-3. Bulk Melt Temperature Data Over the First 5 Minutes of the Interaction.



**Figure 3-4. Test Section Plenum Gas Temperatures During the Initial Interaction.**



**Figure 3-5. Power Supply Current During the Initial Interaction.**

## 4.0 RESULTS

A brief summary of the principal thermalhydraulic results from CCI-4 is provided in this section. A complete list of instruments used in the test is provided in Appendix A, while plots of all data logged from these instruments are provided in Appendix B.

### 4.1.1 Electric Power

The DEH power for CCI-4 is shown in Figure 4-1; the corresponding voltage and current traces are provided in Appendix B (see Figures B-45 and B-46, respectively). At completion of the thermite burn, the power supply voltage was steadily increased until the input power reached the target level of 95 kW at -36.6 minutes. Thereafter, input power was held constant in the range of  $95 \pm 5$  kW over the balance of dry cavity operations. Voltage tap changes were made at 20, 268, and 300 minutes in order to maintain constant power as the load resistance presented by the melt increased over the course of the test. Power input was terminated at 383.7 minutes when sparks were observed emanating from the bottom of the test section, indicating development of a minor leak.

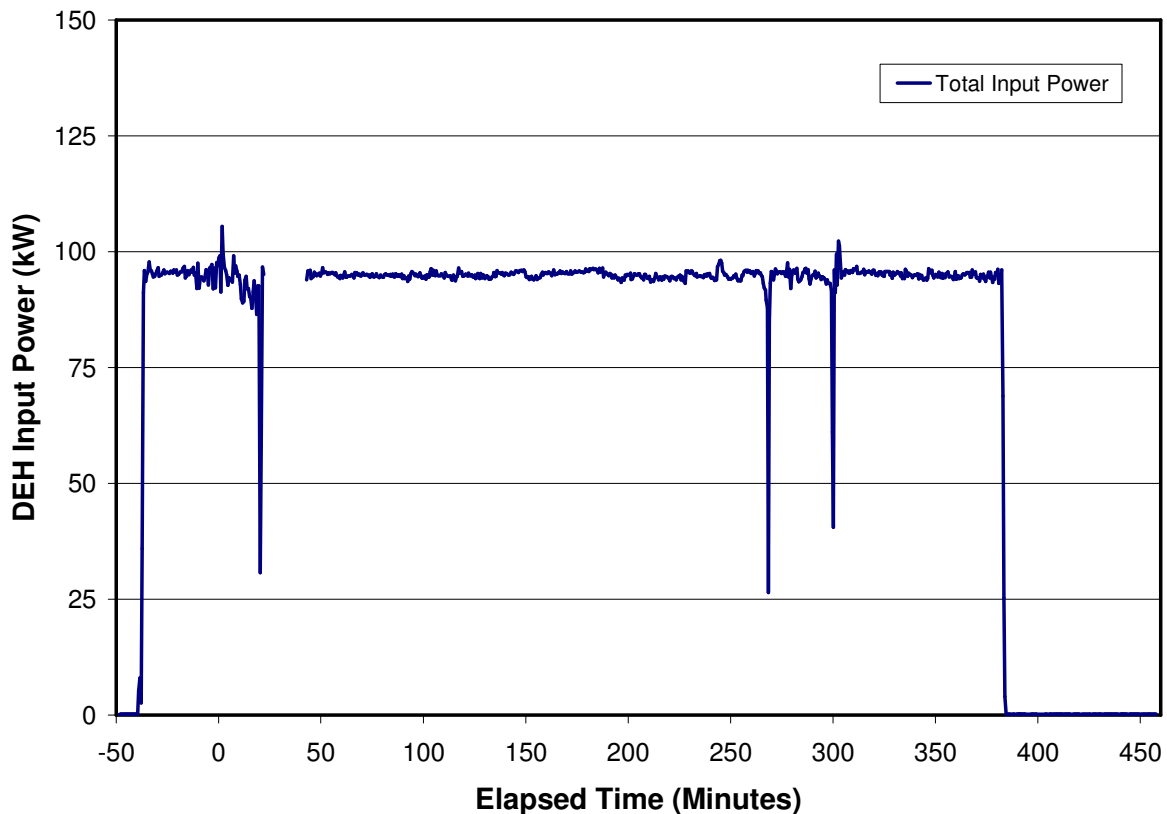


Figure 4-1. DEH Input Power.

## 4.2 Melt Temperatures

As described in Section 2.0, a total of thirty six W5%Re/W26%Re (Type C) thermocouple junctions were used to monitor melt temperatures at various axial and lateral

locations in CCI-4. The data from all of these thermocouples is shown collectively in Figure 4-2. To improve the readability of this data, two steps have been taken: i) the data have been averaged or 30 second time intervals, and ii) only data preceding the first off-scale reading by the thermocouples are shown. Data plots for each individual array are provided in Appendix B.

Examination of Figure 4-2 indicates that the average melt temperature declined from ~1900 °C during the first hour of the interaction, to ~ 1550 °C at the time input power was terminated and the cavity was flooded. The melt temperatures were fairly uniform across the extent of the interaction, generally clustering within a band of approximately  $\pm 50$  °C of the average at any given time. Several junctions showed an increase in melt temperature during insert ablation and the early stages of concrete ablation. This temperature escalation may be due to exothermic reaction between the metals (Zr, Cr, Fe) in the melt and sparging concrete decomposition gases (H<sub>2</sub>O, CO<sub>2</sub>).

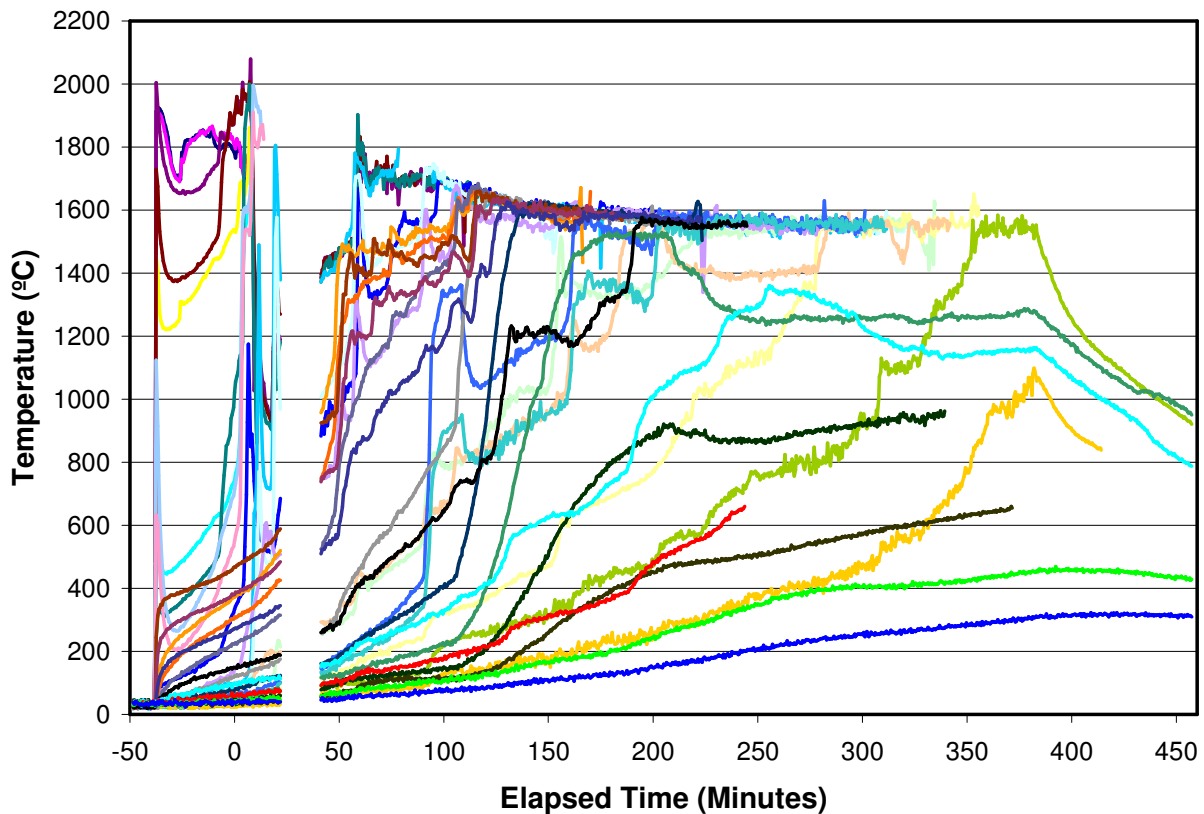


**Figure 4-2. Melt Temperatures Measured During CCI-4.**

### **4.3 Concrete Basemat and Sidewall Ablation Rates**

As described in Section 2.0, the basemat was instrumented with five multi-junction Type K thermocouple arrays to monitor the axial progression of the ablation front, while each concrete sidewall was instrumented with seven arrays to monitor the lateral ablation front progression at seven different elevations. When a thermocouple reached the LCS concrete liquidus temperature

of 1295 °C [3], the melt was considered to be in contact with the thermocouple at the junction location.

Figure 4-3 provides the axial ablation depth versus time based on the signal responses from the Type K basemat arrays, while Figures 4-4 and 4-5 provide the analogous plots of the lateral ablation depth in the North and South sidewalls, respectively. Examination of these figures indicates: i) no substantial differences between the lateral ablation rates on the North and South sidewalls, and ii) the lateral and axial ablation rates are similar. Additional information on the posttest cavity erosion profile is provided in Section 4.5.

#### 4.4 Corium Quench Rate

Another key test objective was to obtain data on the nature and extent of the corium quench process when flooding occurs late in the sequence. To first order, the quench rate can be estimated based on the steaming rate from the test section; i.e.

$$q'' = \frac{h_{lv} \cdot \dot{m}_s}{A}$$

where  $h_{lv}$  is the water latent heat of vaporization (2.256 MJ/kg),  $\dot{m}_s$  is the steam mass flow rate, and  $A$  is the surface area of the debris in contact with the coolant. The steam flow rate is calculated by first performing a 6-point (~30 second) running average on the cumulative water level data in the primary quench tank (see Figure B-52), and then calculating the derivative of the resultant dataset using a central differencing scheme. The corium cooling rate calculated using this approach is shown in Figure 4-6, assuming a test section cross-sectional area of 0.20 m<sup>2</sup>. The flux calculated based on this assumed area varied from 2.4 MW/m<sup>2</sup> immediately after flooding, down to ~ 200 kW/m<sup>2</sup> at the time the test was terminated. However, note that preliminary results of the posttest examinations indicated that a large mantle crust formed over the top of the debris, as occurred in Test CCI-2. [1] This crust completely occluded the test section, leaving a void beneath. Thus, the heat flux measured from the debris may have been limited by this mantle of material. Attempts to dislodge this material with the lance probe prior to cavity flooding were unsuccessful (see Figures B-42 and B-43).

#### 4.5 Posttest Cavity Erosion Profile

At the time this report was issued, the test section had been partially disassembled down to the lower section, and detailed measurements of the posttest debris cavity erosion profile had been initiated. A picture showing the debris after removal of the west MgO sidewall is provided in Figure 4-7. Also shown is the original cavity shape that has been superimposed as dark lines on the photograph to provide the reader with a sense of the change in cavity shape during the test. Consistent with the thermocouple measurements shown in Figures 4-3 through 4-5, the photograph indicates that the overall cavity erosion was fairly symmetrical in the lateral direction, and that the degree of axial ablation was comparable with the lateral ablation. More detailed characterization of the final cavity profile will be provided in the full data report for CCI-4.

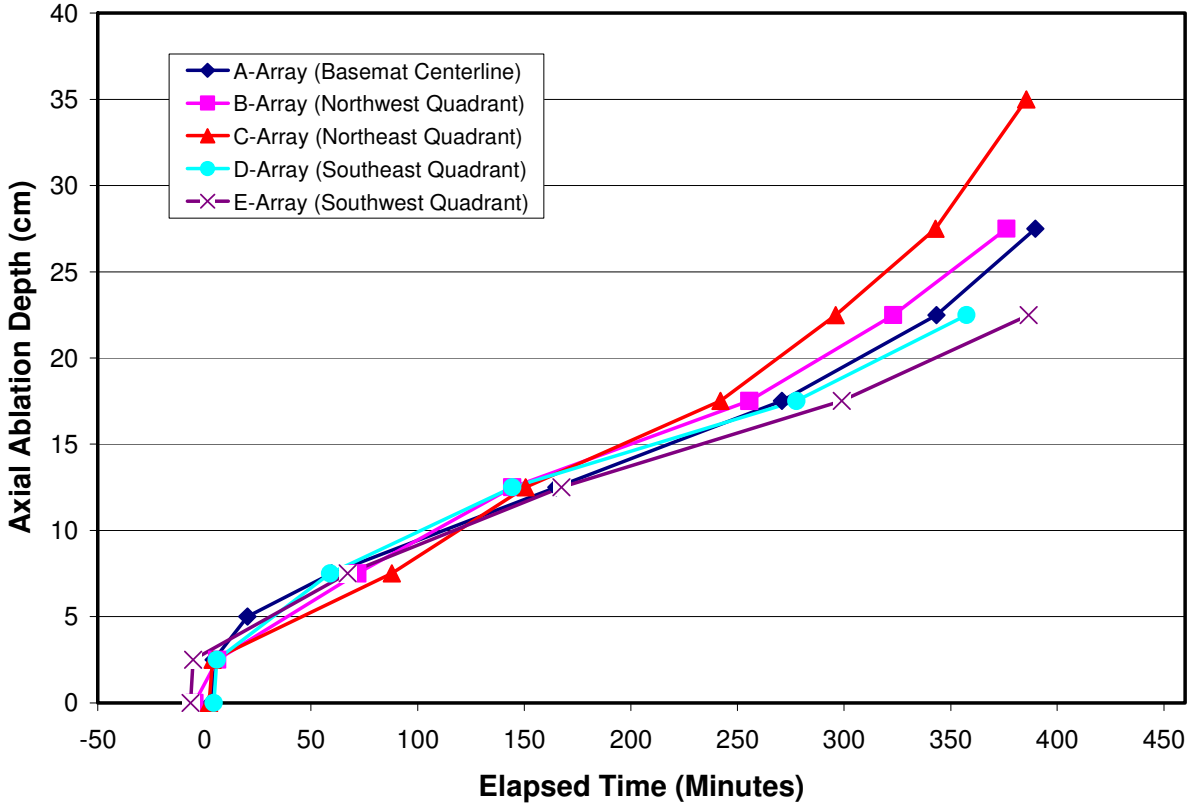


Figure 4-3. Basemat Axial Ablation Front Location.

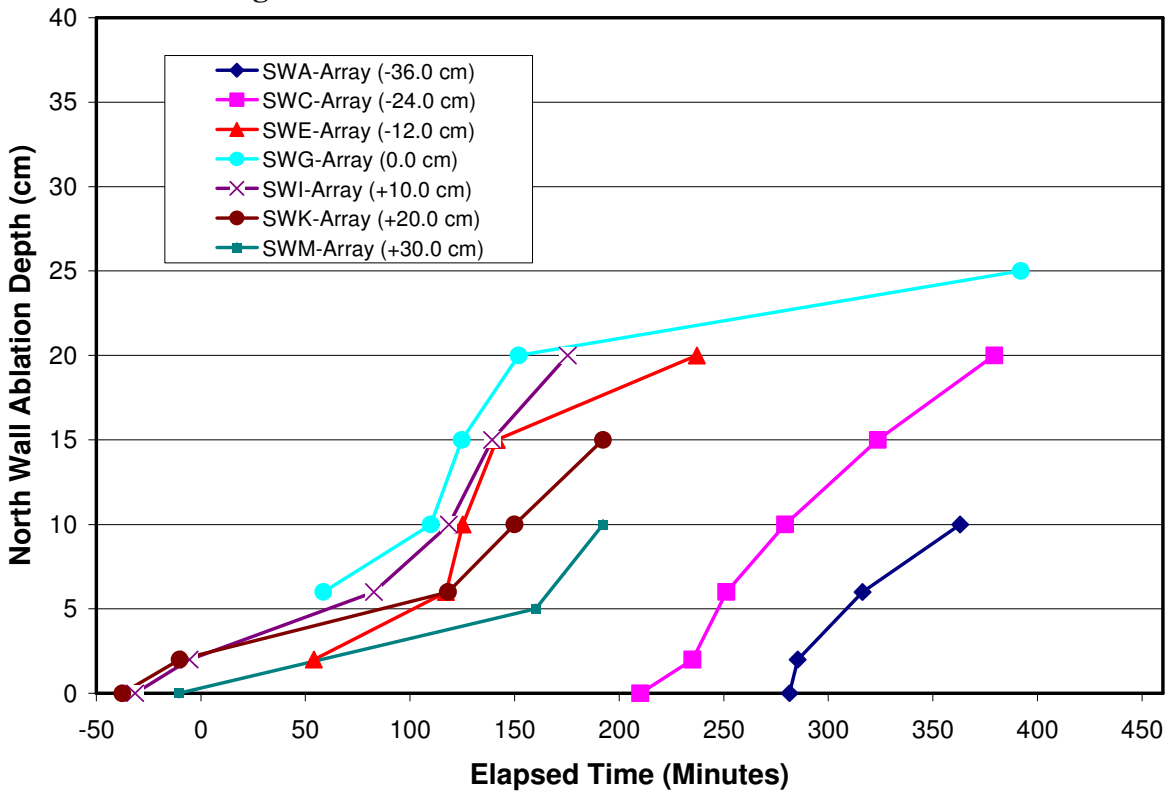


Figure 4-4. North Sidewall Lateral Ablation Front Location.

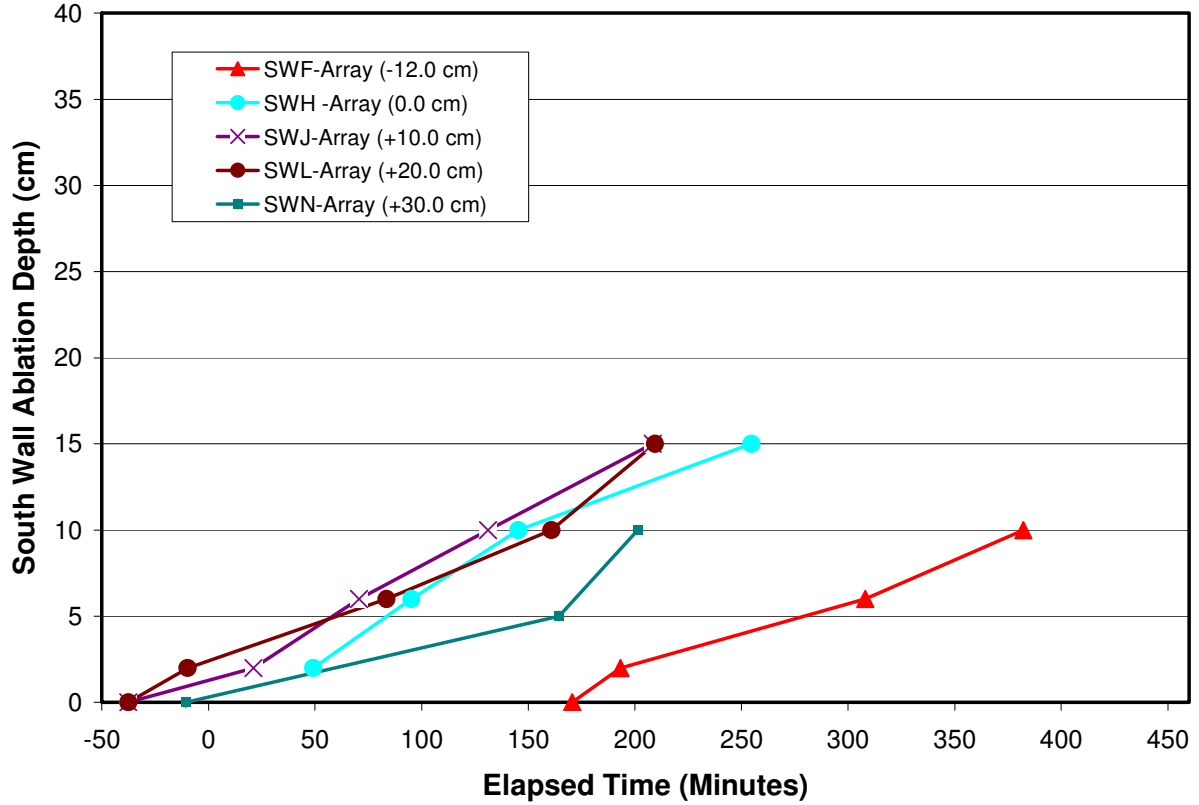


Figure 4-5. South Sidewall Lateral Ablation Front Location.

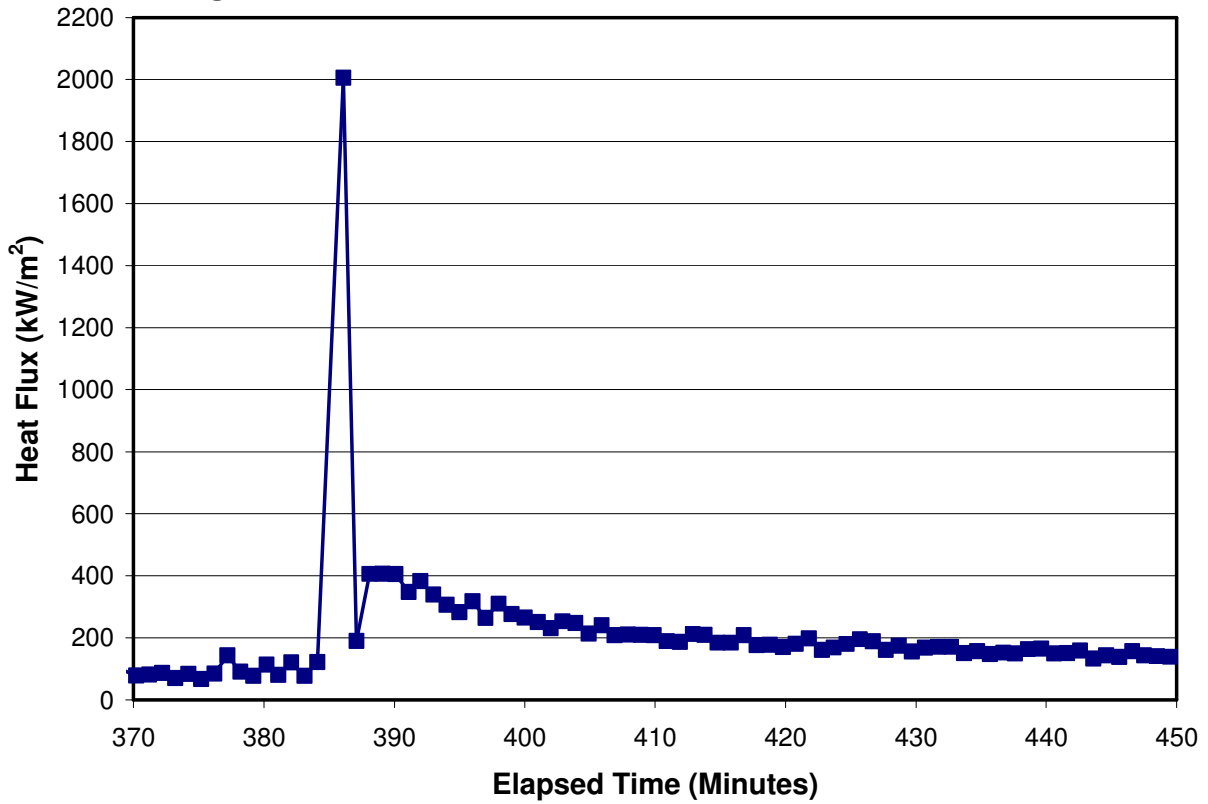
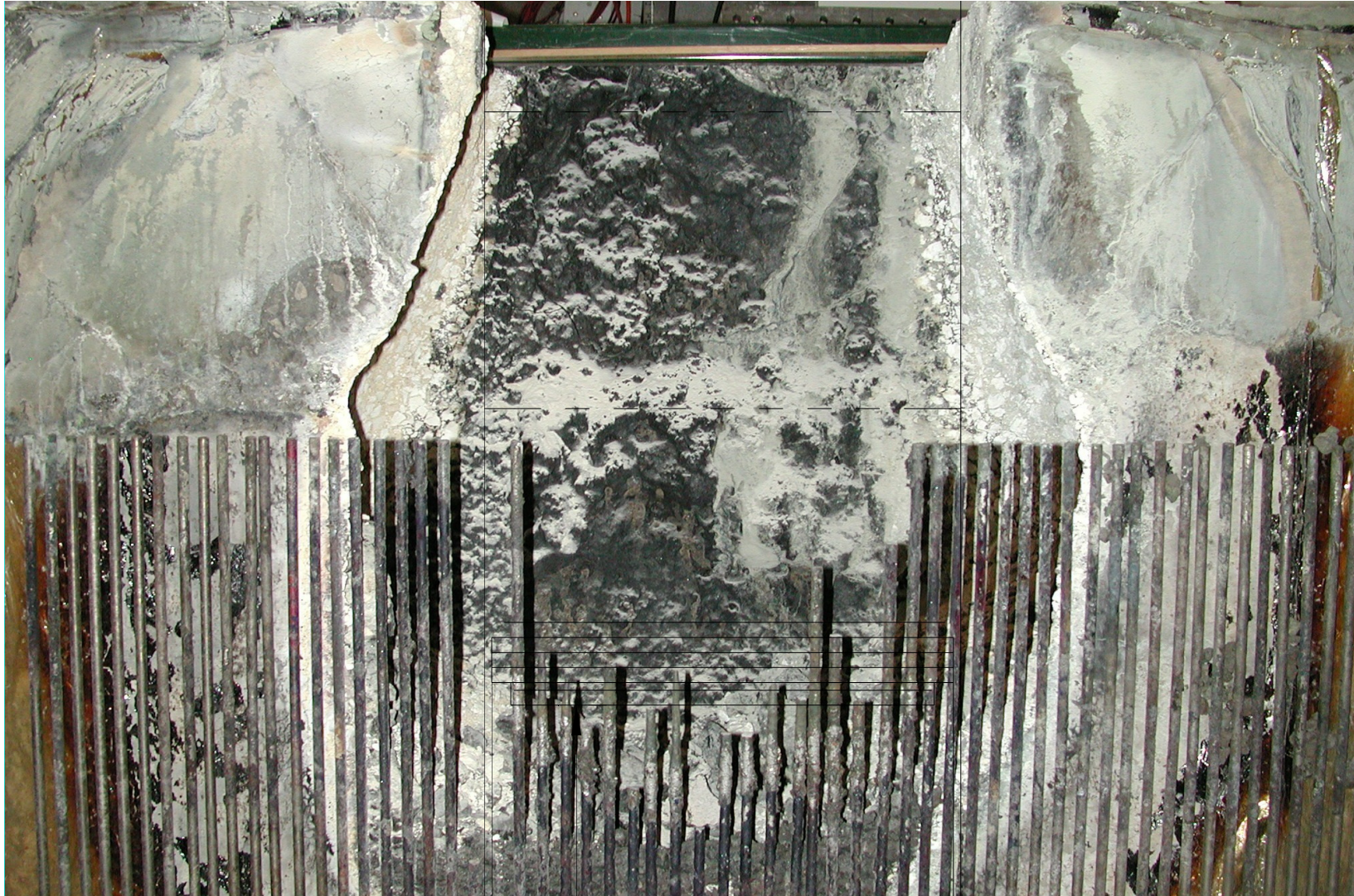


Figure 4-6. Melt-Water Heat Flux Based on Steam Formation Rate.



**Figure 4-7. Posttest Cavity Profile after Removal of West MgO Sidewall. (Original Cavity Profile Superimposed on Top of the Picture).**

## 5.0 REFERENCES

1. M. T. Farmer, S. Lomperski, D. J. Kilsdonk, and R. W. Aeschlimann, "OECD MCCI Project 2-D Core Concrete Interaction (CCI) Tests: Final Report," OECD/MCCI-2005-TR05, January 2, 2006.
2. Summary Record of the First Meeting of the Management Board of the OECD MCCI-2 Project, NEA Headquarters, Paris France 4-5 April 2006.
3. D. H. Thompson, M. T. Farmer, J. K. Fink, D. R. Armstrong, and B. W. Spencer, "ACE Phase C Final Report: Volume I-MCCI Thermalhydraulic Results," EPRI/ACE-TR-C42, September, 1997.
4. M. T. Farmer, D. J. Kilsdonk, S. Lomperski, and R. W. Aeschlimann, "2-D Core Concrete Interaction (CCI) Tests: CCI-4 Test Plan," OECD/MCCI-2007-TR03, Rev. 0, February, 2007.

**APPENDIX A**  
**Data Acquisition System Channel Assignments**

This Appendix provides the channel assignments for the three independent DAS systems that were used to record the data for CCI-4. For convenience, these three 128 channel systems were referred to the “Basemat”, “Power,” and “Quench” systems by operating personnel. The channel assignment lists for each of these three systems are provided in Tables A-1 through A-3. The data recorded on each of these channels is provided in Appendix B.

**Table A-1. "Basemat" DAS Channel Assignments for CCI-4.**

Channel	Variable	Sensor	Location	Level	Range/Limit	Accuracy	Notes
00	T	Diode Sensor	TC compensation Chs. B01-B49		130 C		
01	T	TC Type C	Basemat 0.0 cm, +1.9 cm WCL-1	+15.0 cm	2320 C	± 1%	
02	T	TC Type C	Basemat 0.0 cm, +1.9 cm WCL-2	+10.0 cm	2320 C	± 1%	
03	T	TC Type C	Basemat 0.0 cm, +1.9 cm WCL-3	+5.0 cm	2320 C	± 1%	
04	T	TC Type C	Basemat 0.0 cm, +1.9 cm WCL-4	0.0 cm	2320 C	± 1%	
05	T	TC Type C	Basemat -10.6 cm, +8.1 cm WNW-1	+9.0 cm	2320 C	± 1%	
06	T	TC Type C	Basemat -10.6 cm, +8.1 cm WNW-2	+4.0 cm	2320 C	± 1%	
07	T	TC Type C	Basemat -10.6 cm, +8.1 cm WNW-3	-1.0 cm	2320 C	± 1%	
08	T	TC Type C	Basemat -10.6 cm, +8.1 cm WNW-4	-6.0 cm	2320 C	± 1%	
09	T	TC Type C	Basemat +10.6 cm, +8.1 cm WNE-1	-3.0 cm	2320 C	± 1%	
10	T	TC Type C	Basemat +10.6 cm, +8.1 cm WNE-2	-8.0 cm	2320 C	± 1%	
11	T	TC Type C	Basemat +10.6 cm, +8.1 cm WNE-3	-13.0 cm	2320 C	± 1%	
12	T	TC Type C	Basemat +10.6 cm, +8.1 cm WNE-4	-18.0 cm	2320 C	± 1%	
13	T	TC Type C	Basemat +10.6 cm, -8.1 cm WSE-1	+3.0 cm	2320 C	± 1%	
14	T	TC Type C	Basemat +10.6 cm, -8.1 cm WSE-2	-2.0 cm	2320 C	± 1%	
15	T	TC Type C	Basemat +10.6 cm, -8.1 cm WSE-3	-7.0 cm	2320 C	± 1%	
16	T	TC Type C	Basemat +10.6 cm, -8.1 cm WSE-4	-12.0 cm	2320 C	± 1%	
17	T	TC Type C	Basemat -10.6 cm, -8.1 cm WSW-1	-9.0 cm	2320 C	± 1%	
18	T	TC Type C	Basemat -10.6 cm, -8.1 cm WSW-2	-14.0 cm	2320 C	± 1%	
19	T	TC Type C	Basemat -10.6 cm, -8.1 cm WSW-3	-19.0 cm	2320 C	± 1%	
20	T	TC Type C	Basemat -10.6 cm, -8.1 cm WSW-4	-24.0 cm	2320 C	± 1%	
21	T	TC Type C	N Sidewall, 0.0 cm deep, WN-1	+5.0 cm	2320 C	± 1%	
22	T	TC Type C	N Sidewall, 2.5 cm deep, WN-2	+5.0 cm	2320 C	± 1%	
23	T	TC Type C	N Sidewall, 5.0 cm deep, WN-3	+5.0 cm	2320 C	± 1%	
24	T	TC Type C	N Sidewall, 10.0 cm deep, WN-4	+5.0 cm	2320 C	± 1%	
25	T	TC Type C	S Sidewall, 0.0 cm deep, WS-1	+5.0 cm	2320 C	± 1%	

26	T	TC Type C	S Sidewall, 2.5 cm deep, WS-2	+5.0 cm	2320 C	± 1%	
27	T	TC Type C	S Sidewall, 5.0 cm deep, WS-3	+5.0 cm	2320 C	± 1%	
28	T	TC Type C	S Sidewall, 10.0 cm deep, WS-4	+5.0 cm	2320 C	± 1%	
29	T	TC Type K	Basemat 0.0 cm, -1.9 cm A-1	0.0 cm	1400 C	± 0.75%	
30	T	TC Type K	Basemat 0.0 cm, -1.9 cm A-2	-2.5 cm	1400 C	± 0.75%	
31	T	TC Type K	Basemat 0.0 cm, -1.9 cm A-3	-5.0 cm	1400 C	± 0.75%	
32	T	TC Type K	Basemat 0.0 cm, -1.9 cm A-4	-7.5 cm	1400 C	± 0.75%	
33	T	TC Type K	Basemat 0.0 cm, -1.9 cm A-5	-12.5 cm	1400 C	± 0.75%	
34	T	TC Type K	Basemat 0.0 cm, -1.9 cm A-6	-17.5 cm	1400 C	± 0.75%	
35	T	TC Type K	Basemat 0.0 cm, -1.9 cm A-7	-22.5 cm	1400 C	± 0.75%	
36	T	TC Type K	Basemat 0.0 cm, -1.9 cm A-8	-27.5 cm	1400 C	± 0.75%	
37	T	TC Type K	Basemat 0.0 cm, -1.9 cm A-9	-32.5 cm	1400 C	± 0.75%	
38	T	TC Type K	Basemat 0.0 cm, -1.9 cm A-10	-37.5 cm	1400 C	± 0.75%	
39	T	TC Type K	Basemat 0.0 cm, -1.9 cm A-11	-42.5 cm	1400 C	± 0.75%	
40	T	TC Type K	Basemat -12.5 cm, +10.0 cm B-1	0.0 cm	1400 C	± 0.75%	
41	T	TC Type K	Basemat -12.5 cm, +10.0 cm B-2	-2.5 cm	1400 C	± 0.75%	
42	T	TC Type K	Basemat -12.5 cm, +10.0 cm B-3	-7.5 cm	1400 C	± 0.75%	
43	T	TC Type K	Basemat -12.5 cm, +10.0 cm B-4	-12.5 cm	1400 C	± 0.75%	
44	T	TC Type K	Basemat -12.5 cm, +10.0 cm B-5	-17.5 cm	1400 C	± 0.75%	
45	T	TC Type K	Basemat -12.5 cm, +10.0 cm B-6	-22.5 cm	1400 C	± 0.75%	
46	T	TC Type K	Basemat -12.5 cm, +10.0 cm B-7	-27.5 cm	1400 C	± 0.75%	
47	T	TC Type K	Basemat -12.5 cm, +10.0 cm B-8	-35.0 cm	1400 C	± 0.75%	
48	T	TC Type K	Basemat -12.5 cm, +10.0 cm B-9	-42.5 cm	1400 C	± 0.75%	
49	T	TC Type K	N Sidewall 35.0 cm deep SWK-9	+20.0 cm	1400 C	± 0.75%	
50	T	Diode Sensor	TC compensation Chs. B51-B99		130 C		
51	T	TC Type K	Basemat +12.5 cm, +10.0 cm C-1	0.0 cm	1400 C	± 0.75%	
52	T	TC Type K	Basemat +12.5 cm, +10.0 cm C-2	-2.5 cm	1400 C	± 0.75%	
53	T	TC Type K	Basemat +12.5 cm, +10.0 cm C-3	-7.5 cm	1400 C	± 0.75%	

54	T	TC Type K	Basemat +12.5 cm, +10.0 cm C-4	-12.5 cm	1400 C	± 0.75%	
55	T	TC Type K	Basemat +12.5 cm, +10.0 cm C-5	-17.5 cm	1400 C	± 0.75%	
56	T	TC Type K	Basemat +12.5 cm, +10.0 cm C-6	-22.5 cm	1400 C	± 0.75%	
57	T	TC Type K	Basemat +12.5 cm, +10.0 cm C-7	-27.5 cm	1400 C	± 0.75%	
58	T	TC Type K	Basemat +12.5 cm, +10.0 cm C-8	-35.0 cm	1400 C	± 0.75%	
59	T	TC Type K	Basemat +12.5 cm, +10.0 cm C-9	-42.5 cm	1400 C	± 0.75%	
60	T	TC Type K	N Sidewall 40.0 cm deep SWK-10	+20.0 cm	1400 C	± 0.75%	
61	T	TC Type K	Basemat +12.5 cm, -10.0 cm D-1	0.0 cm	1400 C	± 0.75%	
62	T	TC Type K	Basemat +12.5 cm, -10.0 cm D-2	-2.5 cm	1400 C	± 0.75%	
63	T	TC Type K	Basemat +12.5 cm, -10.0 cm D-3	-7.5 cm	1400 C	± 0.75%	
64	T	TC Type K	Basemat +12.5 cm, -10.0 cm D-4	-12.5 cm	1400 C	± 0.75%	
65	T	TC Type K	Basemat +12.5 cm, -10.0 cm D-5	-17.5 cm	1400 C	± 0.75%	
66	T	TC Type K	Basemat +12.5 cm, -10.0 cm D-6	-22.5 cm	1400 C	± 0.75%	
67	T	TC Type K	Basemat +12.5 cm, -10.0 cm D-7	-27.5 cm	1400 C	± 0.75%	
68	T	TC Type K	Basemat +12.5 cm, -10.0 cm D-8	-35.0 cm	1400 C	± 0.75%	
69	T	TC Type K	Basemat +12.5 cm, -10.0 cm D-9	-42.5 cm	1400 C	± 0.75%	
70	T	TC Type K	N Sidewall 45.0 cm deep SWK-11	+20.0 cm	1400 C	± 0.75%	
71	T	TC Type K	Basemat -12.5 cm, -10.0 cm E-1	0.0 cm	1400 C	± 0.75%	
72	T	TC Type K	Basemat -12.5 cm, -10.0 cm E-2	-2.5 cm	1400 C	± 0.75%	
73	T	TC Type K	Basemat -12.5 cm, -10.0 cm E-3	-7.5 cm	1400 C	± 0.75%	
74	T	TC Type K	Basemat -12.5 cm, -10.0 cm E-4	-12.5 cm	1400 C	± 0.75%	
75	T	TC Type K	Basemat -12.5 cm, -10.0 cm E-5	-17.5 cm	1400 C	± 0.75%	
76	T	TC Type K	Basemat -12.5 cm, -10.0 cm E-6	-22.5 cm	1400 C	± 0.75%	
77	T	TC Type K	Basemat -12.5 cm, -10.0 cm E-7	-27.5 cm	1400 C	± 0.75%	
78	T	TC Type K	Basemat -12.5 cm, -10.0 cm E-8	-35.0 cm	1400 C	± 0.75%	
79	T	TC Type K	Basemat -12.5 cm, -10.0 cm E-9	-42.5 cm	1400 C	± 0.75%	
80	T	TC Type K	S Sidewall 35.0 cm deep SWL-9	+20.0 cm	1400 C	± 0.75%	
81	T	TC Type K	N Sidewall 0.0 cm deep SWA-1	-36.0 cm	1400 C	± 0.75%	

82	T	TC Type K	N Sidewall 2.0 cm deep SWA-2	-36.0 cm	1400 C	± 0.75%	
83	T	TC Type K	N Sidewall 6.0 cm deep SWA-3	-36.0 cm	1400 C	± 0.75%	
84	T	TC Type K	N Sidewall 10.0 cm deep SWA-4	-36.0 cm	1400 C	± 0.75%	
85	T	TC Type K	N Sidewall 15.0 cm deep SWA-5	-36.0 cm	1400 C	± 0.75%	
86	T	TC Type K	N Sidewall 20.0 cm deep SWA-6	-36.0 cm	1400 C	± 0.75%	
87	T	TC Type K	N Sidewall 25.0 cm deep SWA-7	-36.0 cm	1400 C	± 0.75%	
88	T	TC Type K	N Sidewall 30.0 cm deep SWA-8	-36.0 cm	1400 C	± 0.75%	
89	T	TC Type K	S Sidewall 0.0 cm deep SWB-1	-36.0 cm	1400 C	± 0.75%	
90	T	TC Type K	S Sidewall 2.0 cm deep SWB-2	-36.0 cm	1400 C	± 0.75%	
91	T	TC Type K	S Sidewall 6.0 cm deep SWB-3	-36.0 cm	1400 C	± 0.75%	
92	T	TC Type K	S Sidewall 10.0 cm deep SWB-4	-36.0 cm	1400 C	± 0.75%	
93	T	TC Type K	S Sidewall 15.0 cm deep SWB-5	-36.0 cm	1400 C	± 0.75%	
94	T	TC Type K	S Sidewall 20.0 cm deep SWB-6	-36.0 cm	1400 C	± 0.75%	
95	T	TC Type K	S Sidewall 25.0 cm deep SWB-7	-36.0 cm	1400 C	± 0.75%	
96	T	TC Type K	S Sidewall 30.0 cm deep SWB-8	-36.0 cm	1400 C	± 0.75%	
97	T	TC Type K	N Sidewall 0.0 cm deep SWC-1	-24.0 cm	1400 C	± 0.75%	
98	T	TC Type K	N Sidewall 2.0 cm deep SWC-2	-24.0 cm	1400 C	± 0.75%	
99	T	TC Type K	N Sidewall 6.0 cm deep SWC-3	-24.0 cm	1400 C	± 0.75%	

Explanation of Variable Notations

T = temperature

**Table A-2. "Power" DAS Channel Assignments for CCI-4.**

Channel	Variable	Sensor	Location	Level	Range/Limit	Accuracy	Notes
00	T	TC Type K	S Sidewall 40.0 cm deep SWL-10	+20.0 cm	1400 C	± 0.75%	
01	T	TC Type K	N Sidewall 10.0 cm deep SWC-4	-24.0 cm	1400 C	± 0.75%	
02	T	TC Type K	N Sidewall 15.0 cm deep SWC-5	-24.0 cm	1400 C	± 0.75%	
03	T	TC Type K	N Sidewall 20.0 cm deep SWC-6	-24.0 cm	1400 C	± 0.75%	
04	T	TC Type K	N Sidewall 25.0 cm deep SWC-7	-24.0 cm	1400 C	± 0.75%	
05	T	TC Type K	N Sidewall 30.0 cm deep SWC-8	-24.0 cm	1400 C	± 0.75%	
06	T	TC Type K	N Sidewall 35.0 cm deep SWC-9	-24.0 cm	1400 C	± 0.75%	
07	T	TC Type K	N Sidewall 40.0 cm deep SWC-10	-24.0 cm	1400 C	± 0.75%	
08	T	TC Type K	N Sidewall 45.0 cm deep SWC-11	-24.0 cm	1400 C	± 0.75%	
09	T	TC Type K	S Sidewall 0.0 cm deep SWD-1	-24.0 cm	1400 C	± 0.75%	
10	T	TC Type K	S Sidewall 2.0 cm deep SWD-2	-24.0 cm	1400 C	± 0.75%	
11	T	TC Type K	S Sidewall 6.0 cm deep SWD-3	-24.0 cm	1400 C	± 0.75%	
12	T	TC Type K	S Sidewall 10.0 cm deep SWD-4	-24.0 cm	1400 C	± 0.75%	
13	T	TC Type K	S Sidewall 15.0 cm deep SWD-5	-24.0 cm	1400 C	± 0.75%	
14	T	TC Type K	S Sidewall 20.0 cm deep SWD-6	-24.0 cm	1400 C	± 0.75%	
15	T	TC Type K	S Sidewall 25.0 cm deep SWD-7	-24.0 cm	1400 C	± 0.75%	
16	T	TC Type K	S Sidewall 30.0 cm deep SWD-8	-24.0 cm	1400 C	± 0.75%	
17	T	TC Type K	S Sidewall 35.0 cm deep SWD-9	-24.0 cm	1400 C	± 0.75%	
18	T	TC Type K	S Sidewall 40.0 cm deep SWD-10	-24.0 cm	1400 C	± 0.75%	
19	T	TC Type K	S Sidewall 45.0 cm deep SWD-11	-24.0 cm	1400 C	± 0.75%	
20	T	TC Type K	N Sidewall 0.0 cm deep SWE-1	-12.0 cm	1400 C	± 0.75%	
21	T	TC Type K	N Sidewall 2.0 cm deep SWE-2	-12.0 cm	1400 C	± 0.75%	
22	T	TC Type K	N Sidewall 6.0 cm deep SWE-3	-12.0 cm	1400 C	± 0.75%	
23	T	TC Type K	N Sidewall 10.0 cm deep SWE-4	-12.0 cm	1400 C	± 0.75%	
24	T	TC Type K	N Sidewall 15.0 cm deep SWE-5	-12.0 cm	1400 C	± 0.75%	
25	T	TC Type K	N Sidewall 20.0 cm deep SWE-6	-12.0 cm	1400 C	± 0.75%	

26	T	TC Type K	N Sidewall 25.0 cm deep SWE-7	-12.0 cm	1400 C	± 0.75%	
27	T	TC Type K	N Sidewall 30.0 cm deep SWE-8	-12.0 cm	1400 C	± 0.75%	
28	T	TC Type K	N Sidewall 35.0 cm deep SWE-9	-12.0 cm	1400 C	± 0.75%	
29	T	TC Type K	N Sidewall 40.0 cm deep SWE-10	-12.0 cm	1400 C	± 0.75%	
30	T	TC Type K	N Sidewall 45.0 cm deep SWE-11	-12.0 cm	1400 C	± 0.75%	
31	T	TC Type K	S Sidewall 0.0 cm deep SWF-1	-12.0 cm	1400 C	± 0.75%	
32	T	TC Type K	S Sidewall 2.0 cm deep SWF-2	-12.0 cm	1400 C	± 0.75%	
33	T	TC Type K	S Sidewall 6.0 cm deep SWF-3	-12.0 cm	1400 C	± 0.75%	
34	T	TC Type K	S Sidewall 10.0 cm deep SWF-4	-12.0 cm	1400 C	± 0.75%	
35	T	TC Type K	S Sidewall 15.0 cm deep SWF-5	-12.0 cm	1400 C	± 0.75%	
36	T	TC Type K	S Sidewall 20.0 cm deep SWF-6	-12.0 cm	1400 C	± 0.75%	
37	T	TC Type K	S Sidewall 25.0 cm deep SWF-7	-12.0 cm	1400 C	± 0.75%	
38	T	TC Type K	S Sidewall 30.0 cm deep SWF-8	-12.0 cm	1400 C	± 0.75%	
39	T	TC Type K	S Sidewall 35.0 cm deep SWF-9	-12.0 cm	1400 C	± 0.75%	
40	T	TC Type K	S Sidewall 40.0 cm deep SWF-10	-12.0 cm	1400 C	± 0.75%	
41	T	TC Type K	S Sidewall 45.0 cm deep SWF-11	-12.0 cm	1400 C	± 0.75%	
42	T	TC Type K	N Sidewall 0.0 cm deep SWG-1	0.0 cm	1400 C	± 0.75%	
43	T	TC Type K	N Sidewall 2.0 cm deep SWG-2	0.0 cm	1400 C	± 0.75%	
44	T	TC Type K	N Sidewall 6.0 cm deep SWG-3	0.0 cm	1400 C	± 0.75%	
45	T	TC Type K	N Sidewall 10.0 cm deep SWG-4	0.0 cm	1400 C	± 0.75%	
46	T	TC Type K	N Sidewall 15.0 cm deep SWG-5	0.0 cm	1400 C	± 0.75%	
47	T	TC Type K	N Sidewall 20.0 cm deep SWG-6	0.0 cm	1400 C	± 0.75%	
48	T	TC Type K	N Sidewall 25.0 cm deep SWG-7	0.0 cm	1400 C	± 0.75%	
49	T	TC Type K	N Sidewall 30.0 cm deep SWG-8	0.0 cm	1400 C	± 0.75%	
50	T	TC Type K	S Sidewall 45.0 cm deep SWL-11	+20.0 cm	1400 C	± 0.75%	
51	T	TC Type K	N Sidewall 35.0 cm deep SWG-9	0.0 cm	1400 C	± 0.75%	
52	T	TC Type K	N Sidewall 40.0 cm deep SWG-10	0.0 cm	1400 C	± 0.75%	
53	T	TC Type K	N Sidewall 45.0 cm deep SWG-11	0.0 cm	1400 C	± 0.75%	

54	T	TC Type K	S Sidewall 0.0 cm deep SWH-1	0.0 cm	1400 C	± 0.75%	
55	T	TC Type K	S Sidewall 2.0 cm deep SWH-2	0.0 cm	1400 C	± 0.75%	
56	T	TC Type K	S Sidewall 6.0 cm deep SWH-3	0.0 cm	1400 C	± 0.75%	
57	T	TC Type K	S Sidewall 10.0 cm deep SWH-4	0.0 cm	1400 C	± 0.75%	
58	T	TC Type K	S Sidewall 15.0 cm deep SWH-5	0.0 cm	1400 C	± 0.75%	
59	T	TC Type K	S Sidewall 20.0 cm deep SWH-6	0.0 cm	1400 C	± 0.75%	
60	T	TC Type K	S Sidewall 25.0 cm deep SWH-7	0.0 cm	1400 C	± 0.75%	
61	T	TC Type K	S Sidewall 30.0 cm deep SWH-8	0.0 cm	1400 C	± 0.75%	
62	T	TC Type K	S Sidewall 35.0 cm deep SWH-9	0.0 cm	1400 C	± 0.75%	
63	T	TC Type K	S Sidewall 40.0 cm deep SWH-10	0.0 cm	1400 C	± 0.75%	
64	T	TC Type K	S Sidewall 45.0 cm deep SWH-11	0.0 cm	1400 C	± 0.75%	
65	T	TC Type K	N Sidewall 0.0 cm deep SWI-1	+10.0 cm	1400 C	± 0.75%	
66	T	TC Type K	N Sidewall 2.0 cm deep SWI-2	+10.0 cm	1400 C	± 0.75%	
67	T	TC Type K	N Sidewall 6.0 cm deep SWI-3	+10.0 cm	1400 C	± 0.75%	
68	T	TC Type K	N Sidewall 10.0 cm deep SWI-4	+10.0 cm	1400 C	± 0.75%	
69	T	TC Type K	N Sidewall 15.0 cm deep SWI-5	+10.0 cm	1400 C	± 0.75%	
70	T	TC Type K	N Sidewall 20.0 cm deep SWI-6	+10.0 cm	1400 C	± 0.75%	
71	T	TC Type K	N Sidewall 25.0 cm deep SWI-7	+10.0 cm	1400 C	± 0.75%	
72	T	TC Type K	N Sidewall 30.0 cm deep SWI-8	+10.0 cm	1400 C	± 0.75%	
73	T	TC Type K	N Sidewall 35.0 cm deep SWI-9	+10.0 cm	1400 C	± 0.75%	
74	T	TC Type K	N Sidewall 40.0 cm deep SWI-10	+10.0 cm	1400 C	± 0.75%	
75	T	TC Type K	N Sidewall 45.0 cm deep SWI-11	+10.0 cm	1400 C	± 0.75%	
76	T	TC Type K	S Sidewall 0.0 cm deep SWJ-1	+10.0 cm	1400 C	± 0.75%	
77	T	TC Type K	S Sidewall 2.0 cm deep SWJ-2	+10.0 cm	1400 C	± 0.75%	
78	T	TC Type K	S Sidewall 6.0 cm deep SWJ-3	+10.0 cm	1400 C	± 0.75%	
79	T	TC Type K	S Sidewall 10.0 cm deep SWJ-4	+10.0 cm	1400 C	± 0.75%	
80	T	TC Type K	S Sidewall 15.0 cm deep SWJ-5	+10.0 cm	1400 C	± 0.75%	
81	T	TC Type K	S Sidewall 20.0 cm deep SWJ-6	+10.0 cm	1400 C	± 0.75%	

82	T	TC Type K	S Sidewall 25.0 cm deep SWJ-7	+10.0 cm	1400 C	± 0.75%	
83	T	TC Type K	S Sidewall 30.0 cm deep SWJ-8	+10.0 cm	1400 C	± 0.75%	
84	T	TC Type K	S Sidewall 35.0 cm deep SWJ-9	+10.0 cm	1400 C	± 0.75%	
85	T	TC Type K	S Sidewall 40.0 cm deep SWJ-10	+10.0 cm	1400 C	± 0.75%	
86	T	TC Type K	S Sidewall 45.0 cm deep SWJ-11	+10.0 cm	1400 C	± 0.75%	
87	T	TC Type K	N Sidewall 0.0 cm deep SWK-1	+20.0 cm	1400 C	± 0.75%	
88	T	TC Type K	N Sidewall 2.0 cm deep SWK-2	+20.0 cm	1400 C	± 0.75%	
89	T	TC Type K	N Sidewall 6.0 cm deep SWK-3	+20.0 cm	1400 C	± 0.75%	
90	T	TC Type K	N Sidewall 10.0 cm deep SWK-4	+20.0 cm	1400 C	± 0.75%	
91	T	TC Type K	N Sidewall 15.0 cm deep SWK-5	+20.0 cm	1400 C	± 0.75%	
92	T	TC Type K	N Sidewall 20.0 cm deep SWK-6	+20.0 cm	1400 C	± 0.75%	
93	T	TC Type K	N Sidewall 25.0 cm deep SWK-7	+20.0 cm	1400 C	± 0.75%	
94	T	TC Type K	N Sidewall 30.0 cm deep SWK-8	+20.0 cm	1400 C	± 0.75%	
95	T	TC Type K	S Sidewall 0.0 cm deep SWL-1	+20.0 cm	1400 C	± 0.75%	
96	T	TC Type K	S Sidewall 2.0 cm deep SWL-2	+20.0 cm	1400 C	± 0.75%	
97	T	TC Type K	S Sidewall 6.0 cm deep SWL-3	+20.0 cm	1400 C	± 0.75%	
98	T	TC Type K	S Sidewall 10.0 cm deep SWL-4	+20.0 cm	1400 C	± 0.75%	
99	T	TC Type K	S Sidewall 15.0 cm deep SWL-5	+20.0 cm	1400 C	± 0.75%	

Explanation of Variable Notations

T = temperature

**Table A-3. "Quench" DAS Channel Assignments for CCI-4.**

Channel	Variable	Sensor	Location	Level	Range/Limit	Accuracy	Notes
00	T	Diode Sensor	TC Compensation CH Q00-Q49		130 C		
01	T	TC Type K	S Sidewall 20.0 cm deep SWL-6	+20.0 cm	1400 C	± 0.75%	
02	T	TC Type K	S Sidewall 25.0 cm deep SWL-7	+20.0 cm	1400 C	± 0.75%	
03	T	TC Type K	S Sidewall 30.0 cm deep SWL-8	+20.0 cm	1400 C	± 0.75%	
04	T	TC Type C	E Sidewall 1.0 cm deep SWHL-1	-17.5 cm	2320 C	± 1.0%	
05	T	TC Type C	E Sidewall 2.0 cm deep SWHL-2	-17.5 cm	2320 C	± 1.0%	
06	T	TC Type C	E Sidewall 4.0 cm deep SWHL-3	-17.5 cm	2320 C	± 1.0%	
07	T	TC Type C	E Sidewall 8.0 cm deep SWHL-4	-17.5 cm	2320 C	± 1.0%	
08	T	TC Type C	W Sidewall 1.0 cm deep SWHL-5	-7.5 cm	2320 C	± 1.0%	
09	T	TC Type C	W Sidewall 2.0 cm deep SWHL-6	-7.5 cm	2320 C	± 1.0%	
10	T	TC Type C	W Sidewall 4.0 cm deep SWHL-7	-7.5 cm	2320 C	± 1.0%	
11	T	TC Type C	W Sidewall 8.0 cm deep SWHL-8	-7.5 cm	2320 C	± 1.0%	
12	T	TC Type C	E Sidewall 1.0 cm deep SWHL-9	+2.5 cm	2320 C	± 1.0%	
13	T	TC Type C	E Sidewall 2.0 cm deep SWHL-10	+2.5 cm	2320 C	± 1.0%	
14	T	TC Type C	E Sidewall 4.0 cm deep SWHL-11	+2.5 cm	2320 C	± 1.0%	
15	T	TC Type C	E Sidewall 8.0 cm deep SWHL-12	+2.5 cm	2320 C	± 1.0%	
16	T	TC Type C	W Sidewall 1.0 cm deep SWHL-13	+12.5 cm	2320 C	± 1.0%	
17	T	TC Type C	W Sidewall 2.0 cm deep SWHL-14	+12.5 cm	2320 C	± 1.0%	
18	T	TC Type C	W Sidewall 4.0 cm deep SWHL-15	+12.5 cm	2320 C	± 1.0%	
19	T	TC Type C	W Sidewall 8.0 cm deep SWHL-16	+12.5 cm	2320 C	± 1.0%	
20	L	Potentiometer	Lance Position Indicator		0-125 cm		
21	T	TC Type K	Steamline internal vertical run from vessel ML-1		1400 C	± 0.75%	
22	T	TC Type K	Steamline external vertical run from vessel ML-2		1400 C	± 0.75%	
23	T	TC Type K	Steamline external lateral run from vessel ML-3		1400 C	± 0.75%	
24	T	TC Type K	Steamline external vertical run to quench tank ML-4		1400 C	± 0.75%	
25	T	TC Type K	S Sidewall 0.0 cm deep SWHL-17	+67.5 cm	1400 C	± 0.75%	

26	T	TC Type K	S Sidewall 2.0 cm deep SWHL-18	+67.5 cm	1400 C	± 0.75%	
27	T	TC Type K	E Sidewall 0.0 cm deep SWHL -19	+81.6 cm	1400 C	± 0.75%	
28	FOR	Strain	Crust Force Load		0-44.6 kN		
29	T	TC Type K	Quench tank internal QT-1	21 cm	1400 C	± 0.75%	
30	T	TC Type K	Quench tank internal QT-2	55 cm	1400 C	± 0.75%	
31	T	TC Type C	N Sidewall, 15.0 cm deep, WN-5	+5.0 cm	2320 C	± 0.75%	
32	T	TC Type C	N Sidewall, 20.0 cm deep, WN-6	+5.0 cm	2320 C	± 0.75%	
33	T	TC Type K	N Sidewall 0.0 cm deep SWM-1	+30.0 cm	1400 C	± 0.75%	
34	T	TC Type K	N Sidewall 5.0 cm deep SWM-2	+30.0 cm	1400 C	± 0.75%	
35	T	TC Type K	Quench tank coil inlet QT-5		1400 C	± 0.75%	
36	T	TC Type K	Quench tank coil outlet QT-6		1400 C	± 0.75%	
37	T	TC Type K	Quench tank coil outlet QT-7		1400 C	± 0.75%	
38	T	TC Type K	Overflow tank internal OT-1	16 cm	1400 C	± 0.75%	
39	T	Voltage	Igniter Current		100 mV		
40	T	TC Type K	Spray tank internal ST-1	10 cm	1400 C	± 0.75%	
41	T	TC Type C	N Sidewall, 25.0 cm deep, WN-7	+5.0 cm	2320 C	± 1%	
42	T	TC Type K	E Sidewall 2.0 cm deep SWHL-20	+81.6 cm	1400 C	± 0.75%	
43	T	TC Type K	N Sidewall 0.0 cm deep SWHL-21	+92.2 cm	1400 C	± 0.75%	
44	T	TC Type K	N Sidewall 2.0 cm deep SWHL-22	+92.2 cm	1400 C	± 0.75%	
45	T	TC Type K	W Sidewall 0.0 cm deep SWHL-23	+122.4 cm	1400 C	± 0.75%	
46	T	TC Type K	W Sidewall 2.0 cm deep SWHL-24	+122.4 cm	1400 C	± 0.75%	
47	T	TC Type K	S Sidewall 0.0 cm deep SWHL-25	+148.8 cm	1400 C	± 0.75%	
48	T	TC Type K	S Sidewall 2.0 cm deep SWHL-26	+148.8 cm	1400 C	± 0.75%	
49	T	TC Type K	N Sidewall 10.0 cm deep SWM-3	+30.0 cm	1400 C	± 0.75%	
50	T	Diode Sensor	TC Compensation CH Q50-Q99		130 C		
51	T	TC Type K	S Sidewall 0.0 cm deep SWN-1	+30.0 cm	1400 C	± 0.75%	
52	T	TC Type K	S Sidewall 5.0 cm deep SWN-2	+30.0 cm	1400 C	± 0.75%	
53	T	TC Type C	N Sidewall, 30.0 cm deep, WN-8	+5.0 cm	2320 C	± 1%	

54	T	TC Type K	Internal, exhaust line OG-1		1400 C	± 0.75%	
55	T	TC Type K	Water supply tank internal WS-1	45 cm	1400 C	± 0.75%	
56	T	TC Type K	S Sidewall 10.0 cm deep SWN-3	+30.0 cm	1400 C	± 0.75%	
57	T	TC Type K	Water level probe LP-1	167/48 cm	1400 C	± 0.75%	
58	T	TC Type K	Water level probe LP-2	167/48 cm	1400 C	± 0.75%	
59	T	TC Type K	Test vessel plenum gas TS-1	223.0 cm	1400 C	± 0.75%	
60	L	Strain	Supply tank head PT-1		350-2000 l		D-6
61	P	Strain	Supply tank pressure PT-2		0-204 kPa		A-17
62	L	Strain	Test vessel head, insertion probe PT-3		63-150 l		D-3
63	L	Strain	Test vessel head, static probe PT-4		32-150 l		D-1
64	P	Strain	Test vessel plenum pressure PT-5		0-204 kPa		A-1
65	P	Strain	Basemat side pressure PT-6		0-204 kPa		A-3
66	Unused						
67	L	Strain	Quench tank head PT-8		80-590 l		D-9
68	P	Strain	Quench/overflow tank pressure PT-9		0-35 kPad		D-2
69	L	Strain	Overflow tank head PT-10		200-900 l		D-8
70	L	Strain	Spray tank head PT-11		240-1290 l		D-5
71	P	Strain	Spray tank pressure PT-12		0-35 kPad		D-4
72	L	Magnetic Float	Supply tank volume LS-1		350-2000 l		
73	L	Magnetic Float	Quench tank volume LS-2		80-590 l		
74	L	Magnetic Float	Overflow tank volume LS-3		200-900 l		
75	L	Magnetic Float	Spray tank volume LS-4		240-1290 l		
76	F	Paddlewheel	Water supply flow rate FM-1		680 lpm		
77	F	Paddlewheel	Quench tank coil flow rate FM-2		190 lpm		
78	Unused						
79	T	TC Type C	S Sidewall, 15.0 cm deep, WS-5	+5.0 cm	2320 C	± 1%	
80	T	TC Type C	S Sidewall, 20.0 cm deep, WS-6	+5.0 cm	2320 C	± 1%	
81	FC	Flow controller	Final Off gas Flow rate FC1a		0-5,600 lpm		

82		-	Calculated Water Volume in Test Section		0-150 l		
83	FC	Flow controller	Lid lights & camera cover gas flow rate FC-2		0-200 lpm		
84	Unused						
85		-	Calculated Total Current (Q92+Q93)		0 -10,000 A		
86	Unused	-	Calculated Total Power (Q94+Q95)		0-500 kW		
87	FC	Flow controller	Test vessel cover gas flow rate FC-6		0-100 lpm		
88	FC	Flow controller	Lid camera cover gas flow rate FC-7		0-350 lpm		
89	V		Pressure transducer power supply #1 voltage		0-30 V		
90	V		Pressure transducer power supply #2 voltage		0-30 V		
91	V	Voltmeter	Power supply voltage		0-200 V		
92	A	Transformer	Power supply current #2		5000 A		
93	A	Transformer	Power supply current #1		5000 A		
94	W	Hall Meter	Power supply power #2		1100 kW		
95	W	Hall Meter	Power supply power #1		1100 kW		
96	L	Strain	Auxiliary Tank Head PT-13		366-4080		D-10
97	T	TC Type K	Auxiliary Tank Internal AT-1	43 cm	1400 C	± 0.75%	
98	T	TC Type C	S Sidewall, 25.0 cm deep, WS-7	+5.0 cm	2320 C	± 1%	
99	T	TC Type C	S Sidewall, 30.0 cm deep, WS-8	+5.0 cm	2320 C	± 1%	

Explanation of variable notations

T = temperature P = Pressure FOR=Force L = Level V = Voltage F = Flow rate A = Current W = Power FC = Flow Controller

## **APPENDIX B**

### **Test Data**

This Appendix provides plots of all data recorded during Test CCI-4. The complete channel assignment list is provided in Appendix A. Time  $t = 0$  in all plots is referenced to the time at which axial ablation of the concrete basemat was nominally initiated. This corresponds to 48.6 minutes after onset of data acquisition; see Table 3-1. All data was logged at  $\sim 5.5$  second time intervals during the test. Selected channels have been averaged over 30 second time intervals to improve readability.

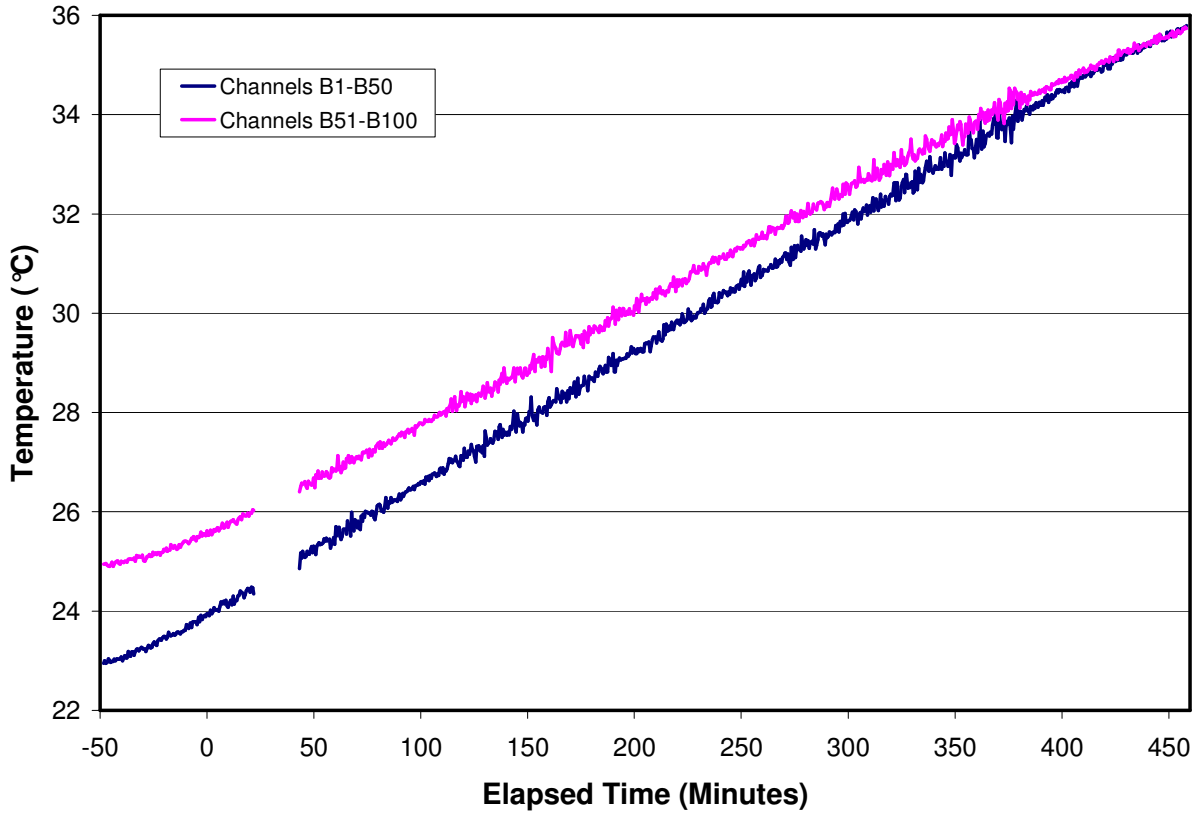


**Figure B-1. Compensator Temperature, Channels B1-B50 and B51-B100.**

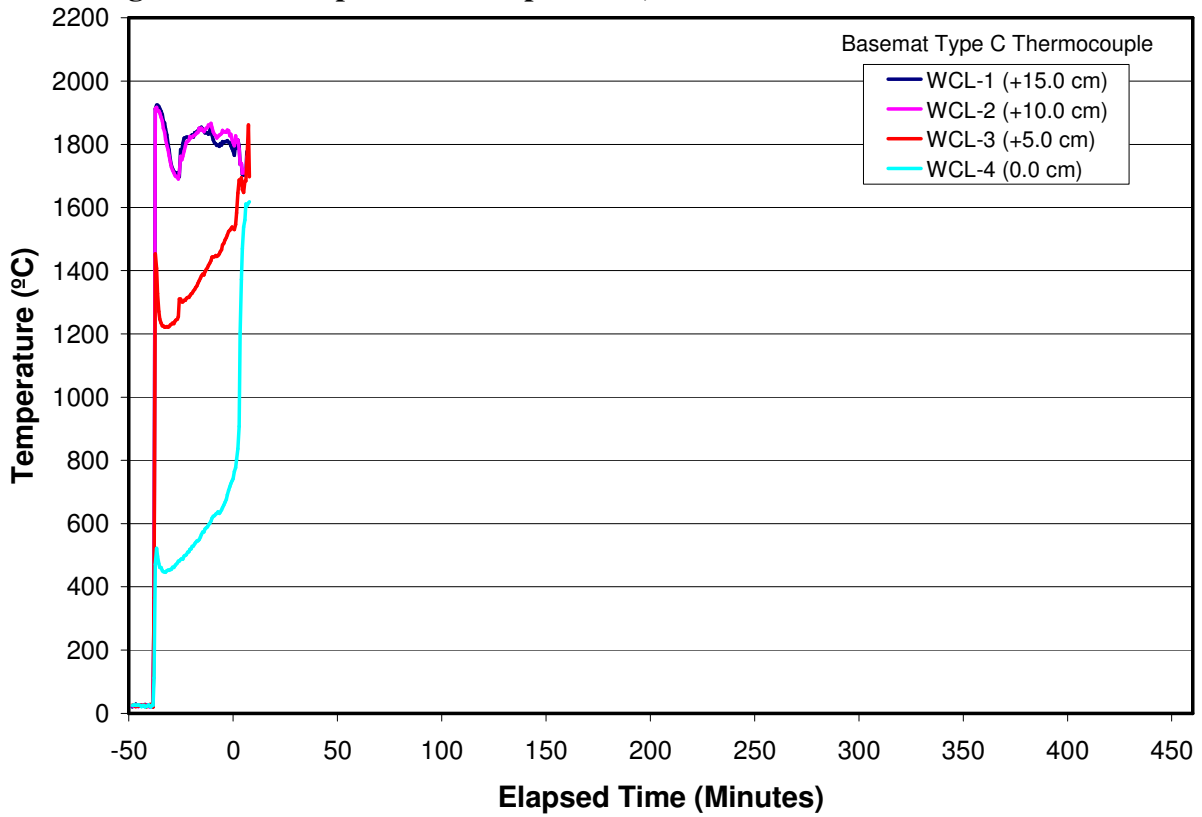


**Figure B-2. Basemat Type C “WCL” Array Data.**

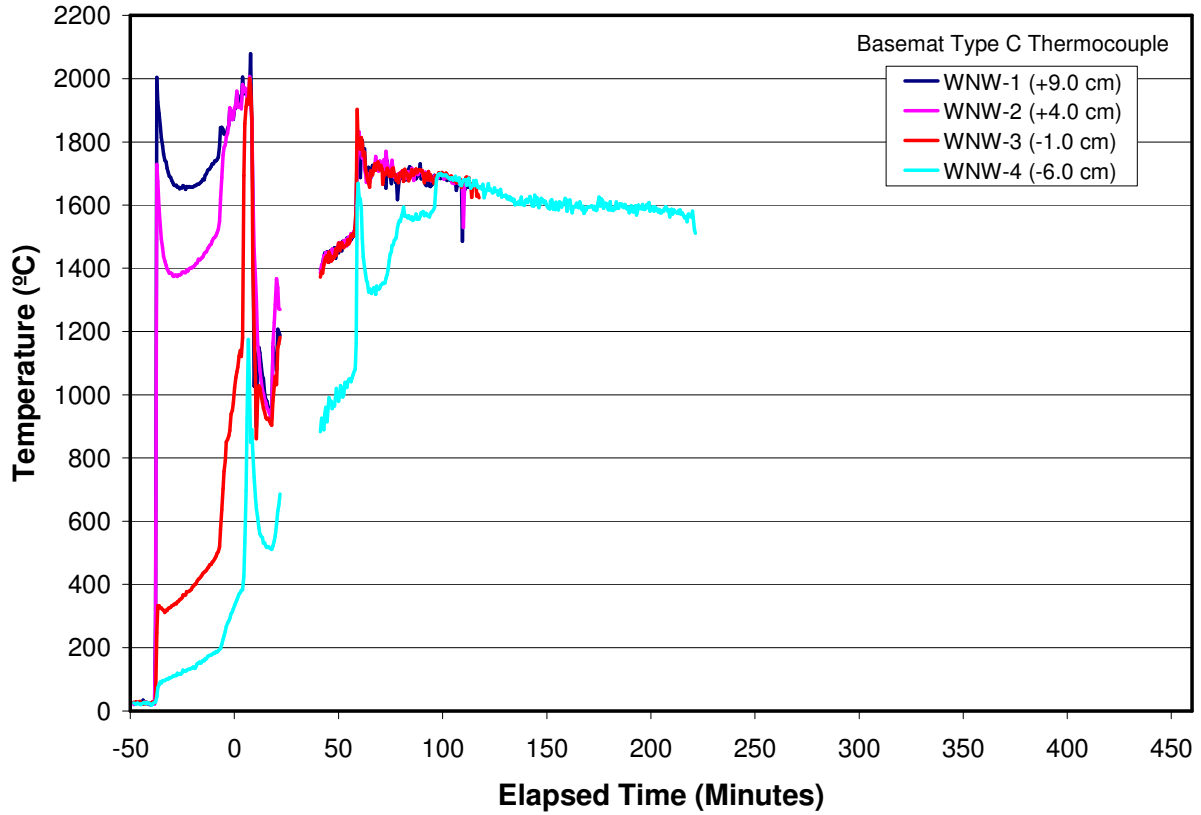


Figure B-3. Basemat Type C “WNW” Array Data.

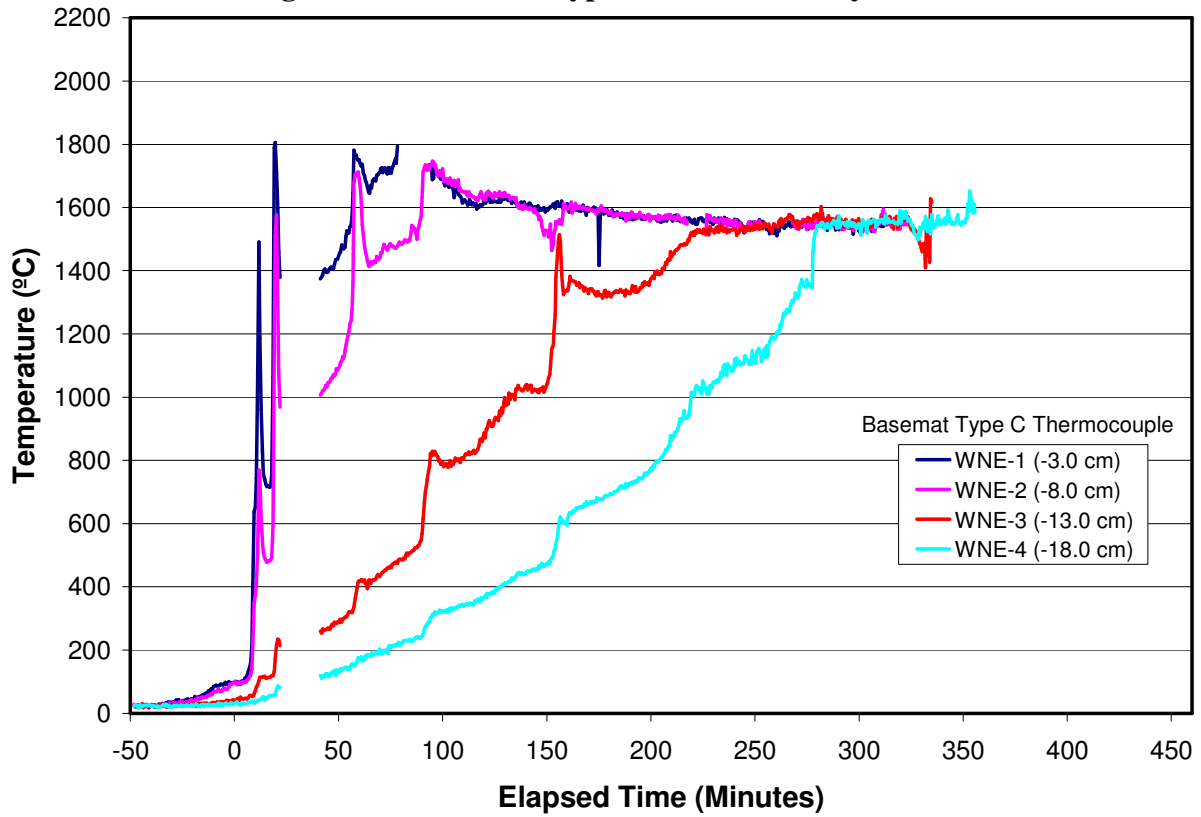


Figure B-4. Basemat Type C “WNE” Array Data.

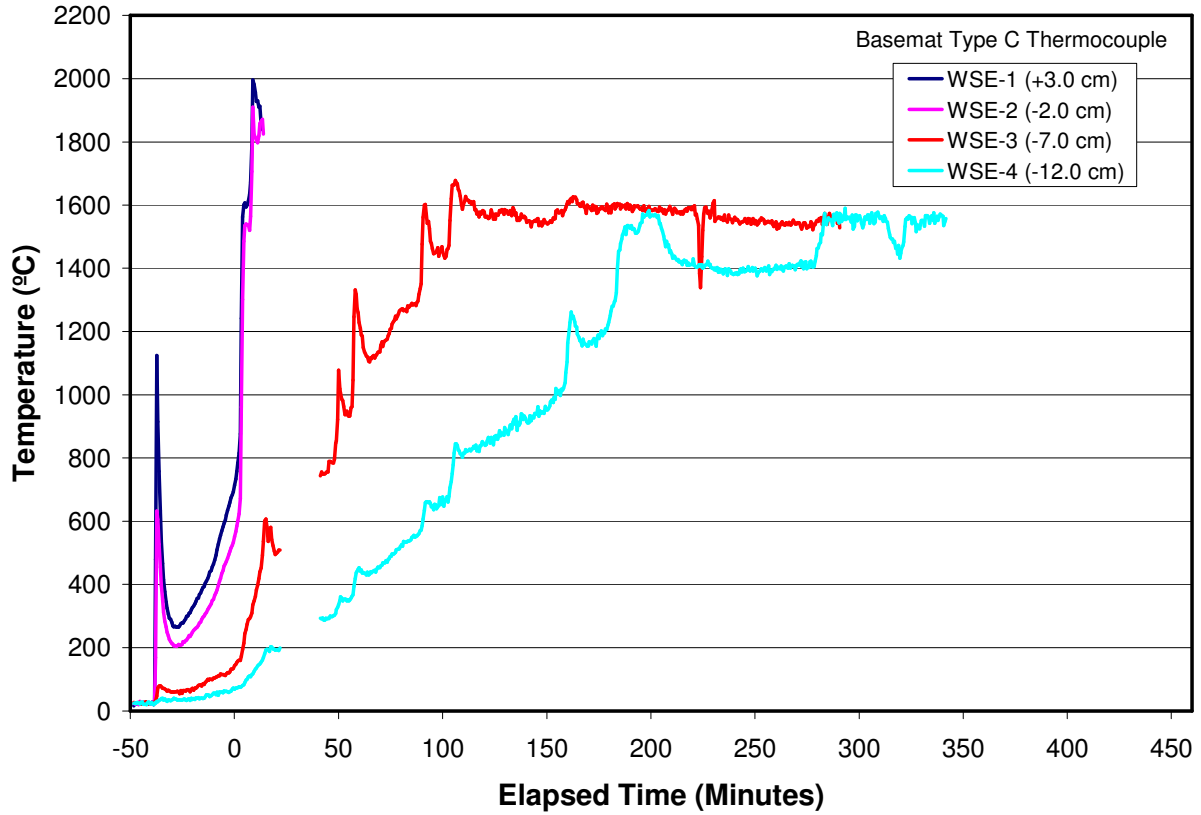


Figure B-5. Basemat Type C “WSE” Array Data.

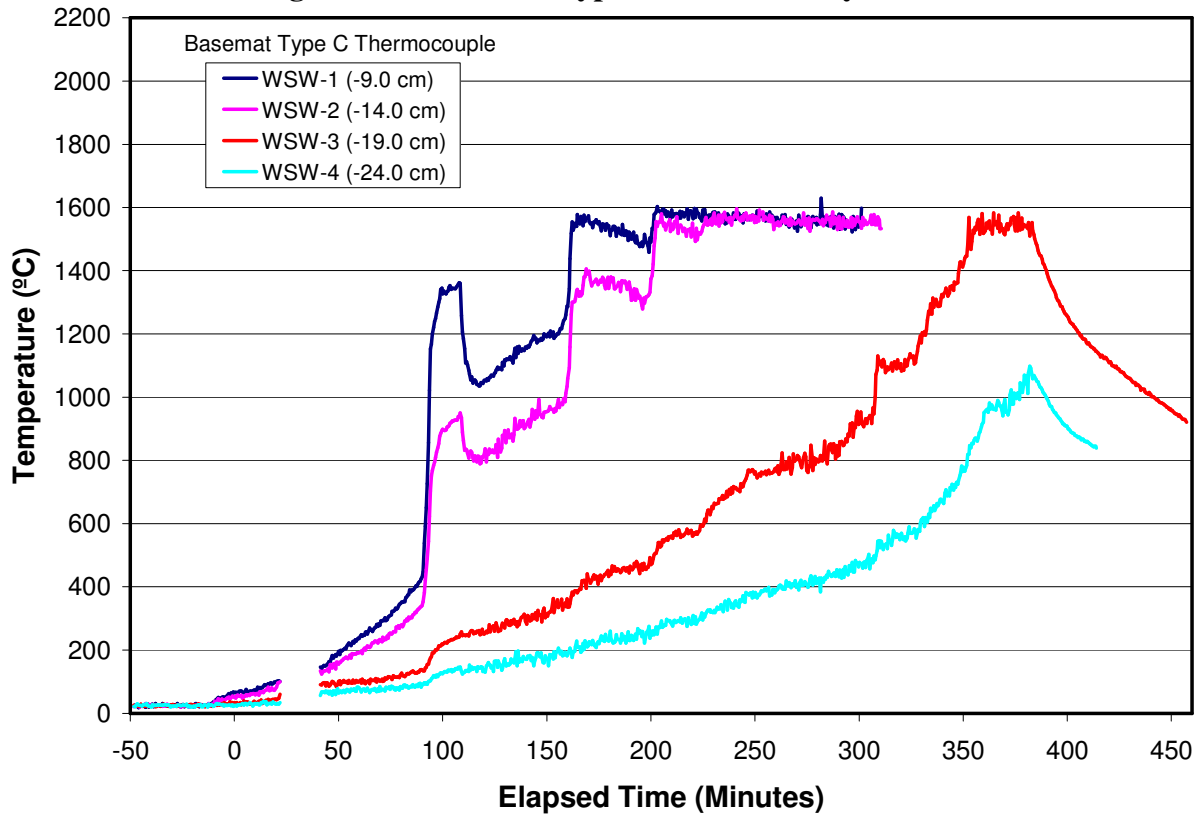


Figure B-6. Basemat Type C “WSW” Array Data.

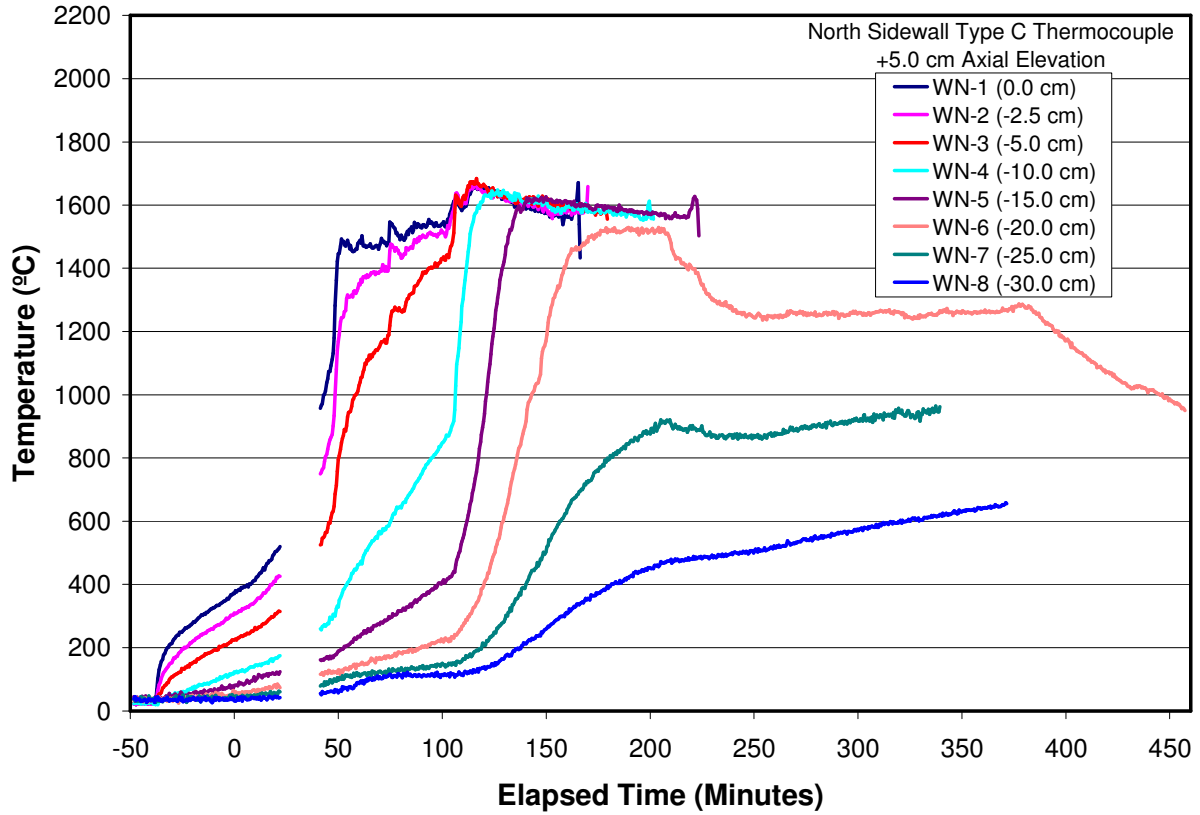


Figure B-7. North Sidewall Type C “WN” Array Data.

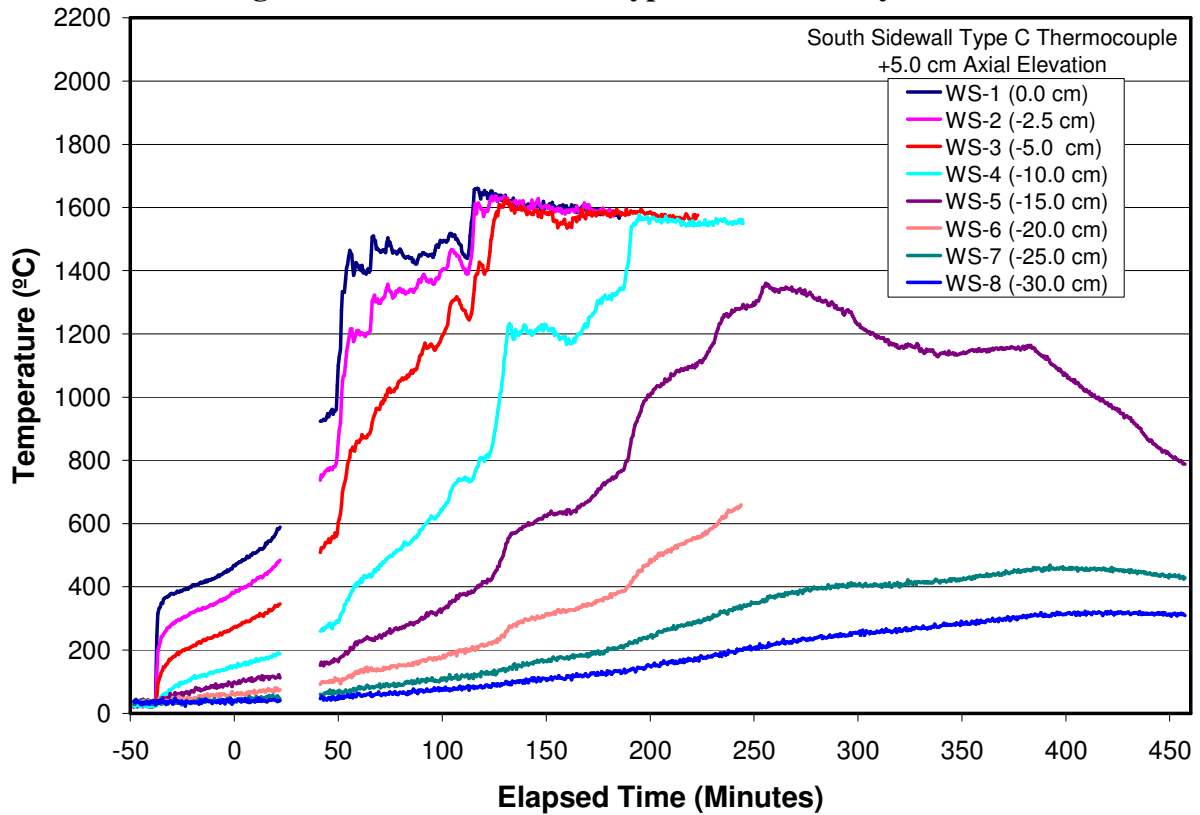


Figure B-8. South Sidewall Type C “WS” Array Data.

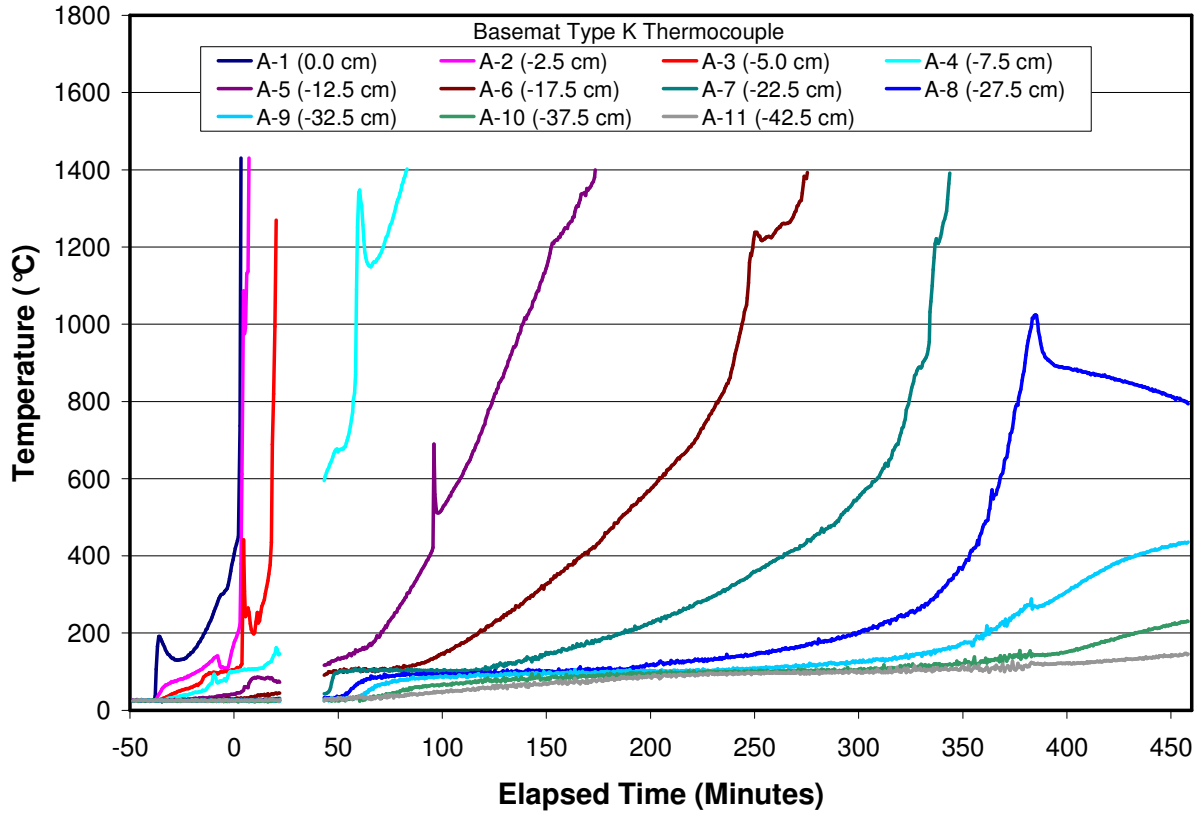


Figure B-9. Basemat Type K "A" Array Data.

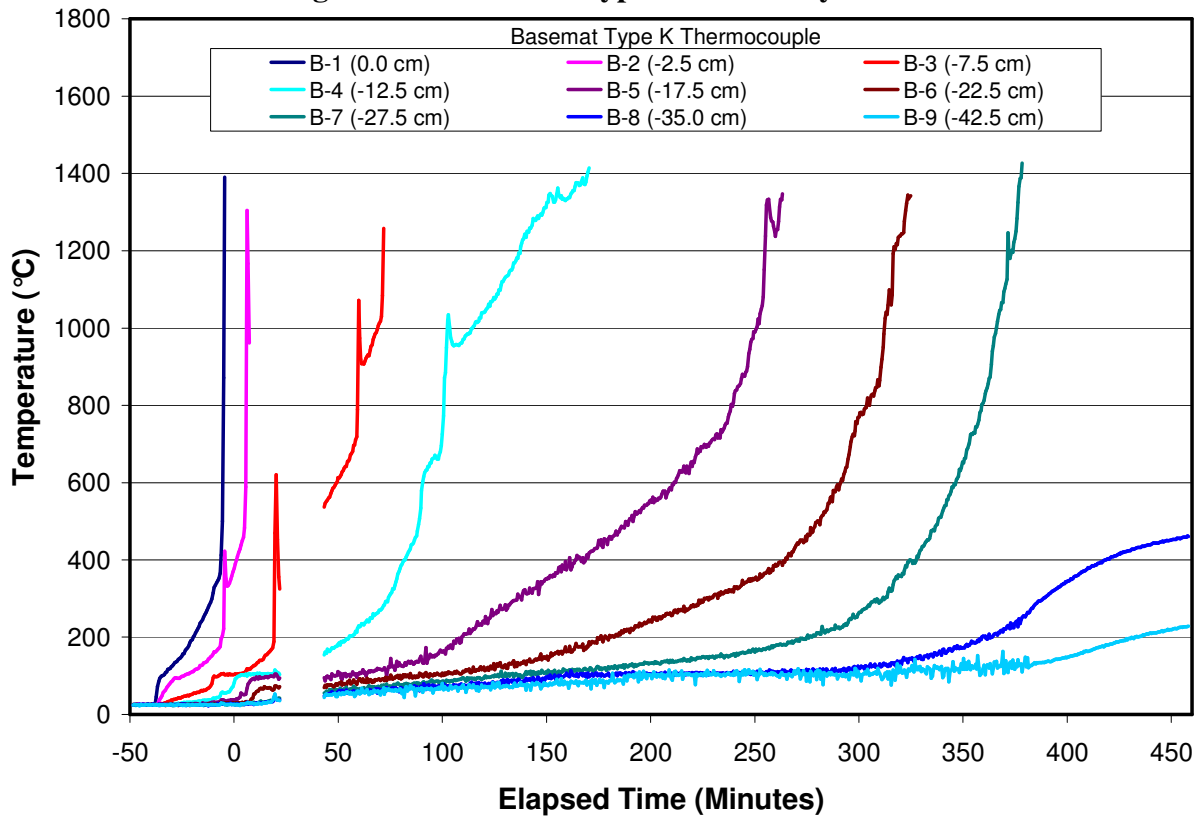


Figure B-10. Basemat Type K "B" Array Data.

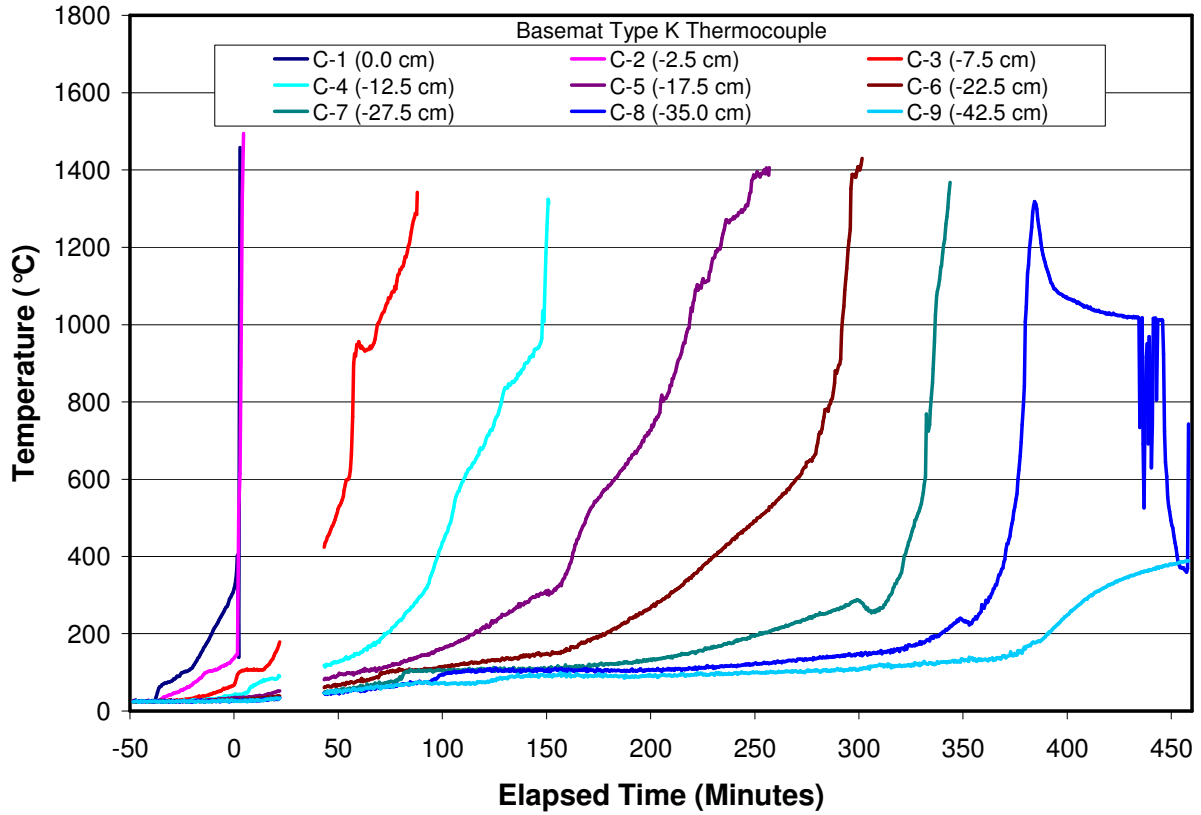


Figure B-11. Basemat Type K “C” Array Data.

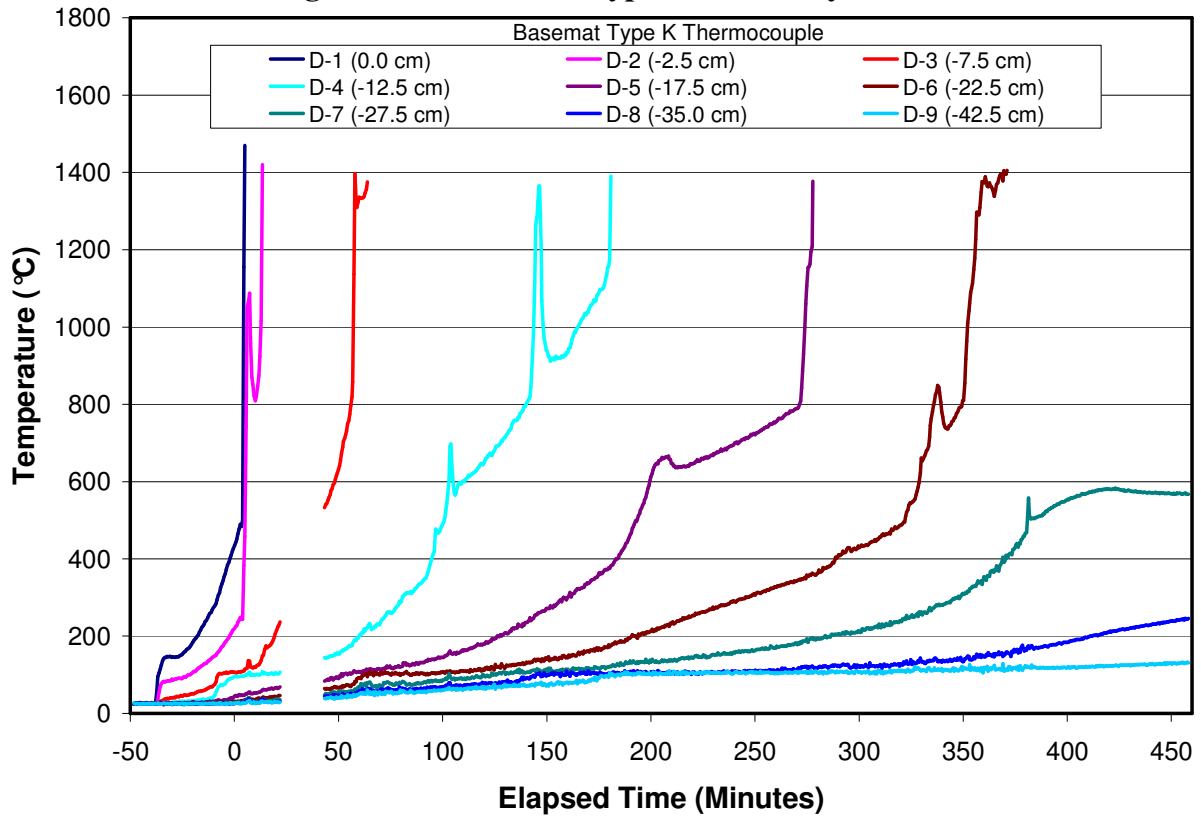


Figure B-12. Basemat Type K “D” Array Data.

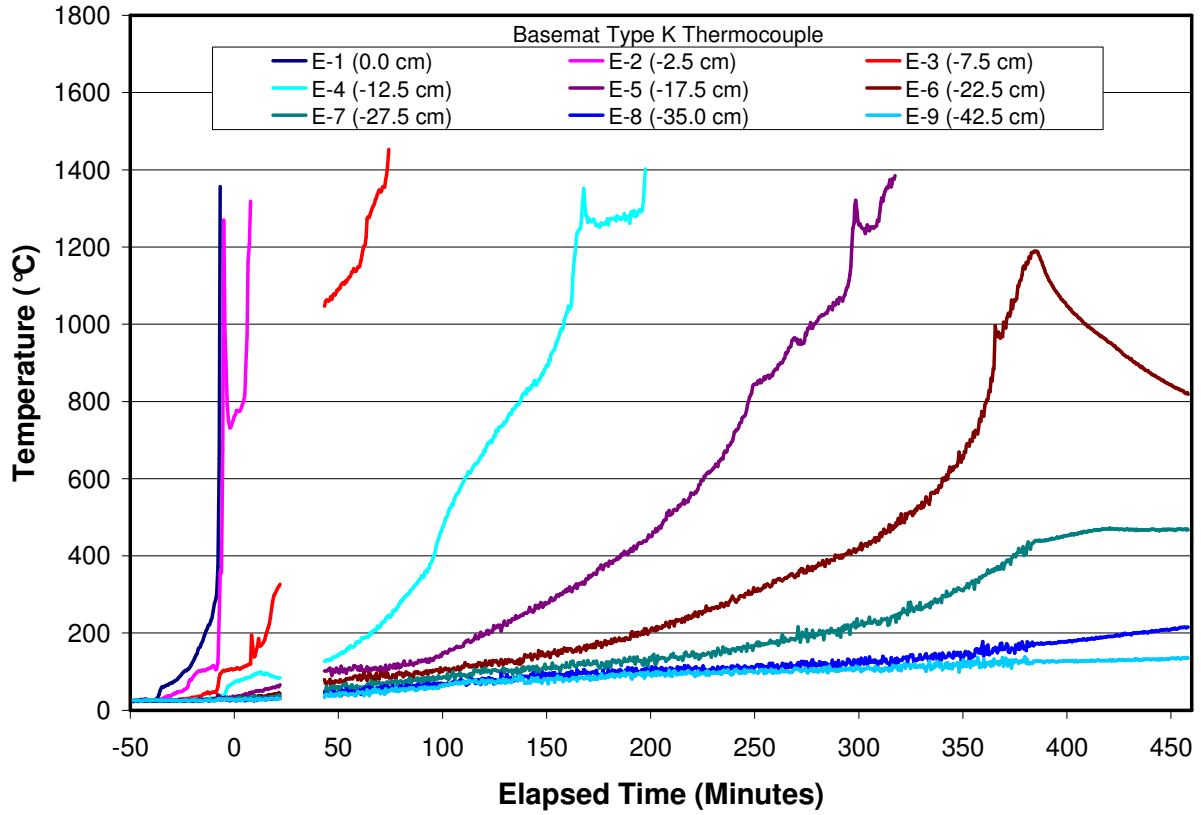


Figure B-13. Basemat Type K “E” Array Data.

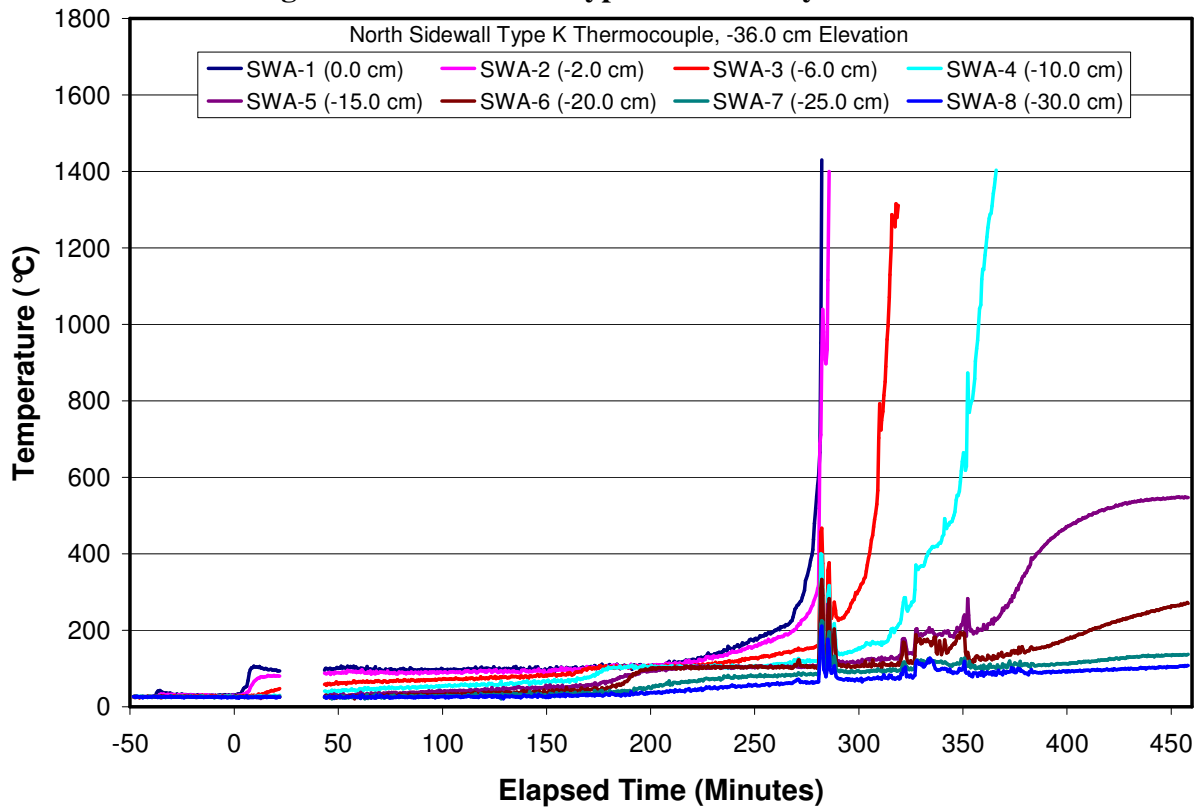


Figure B-14. North Sidewall Type K “SWA” Array Data.

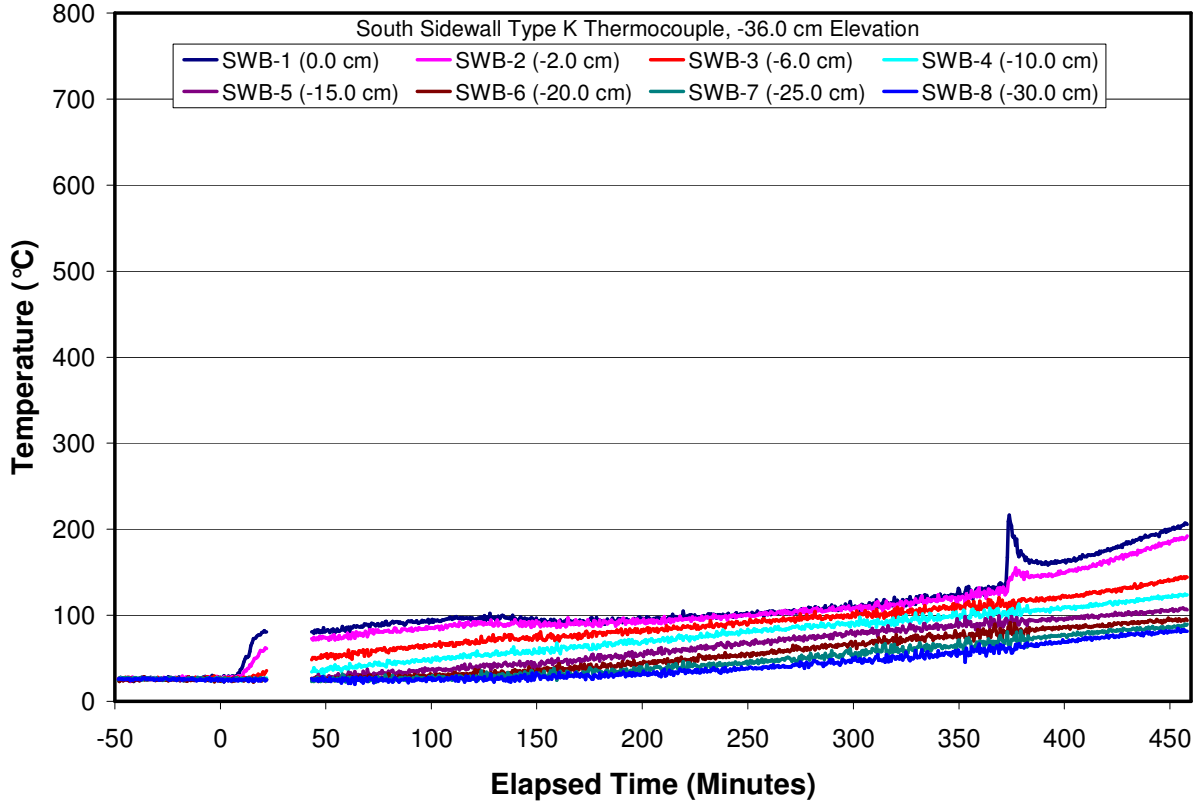


Figure B-15. South Sidewall Type K “SWB” Array Data.

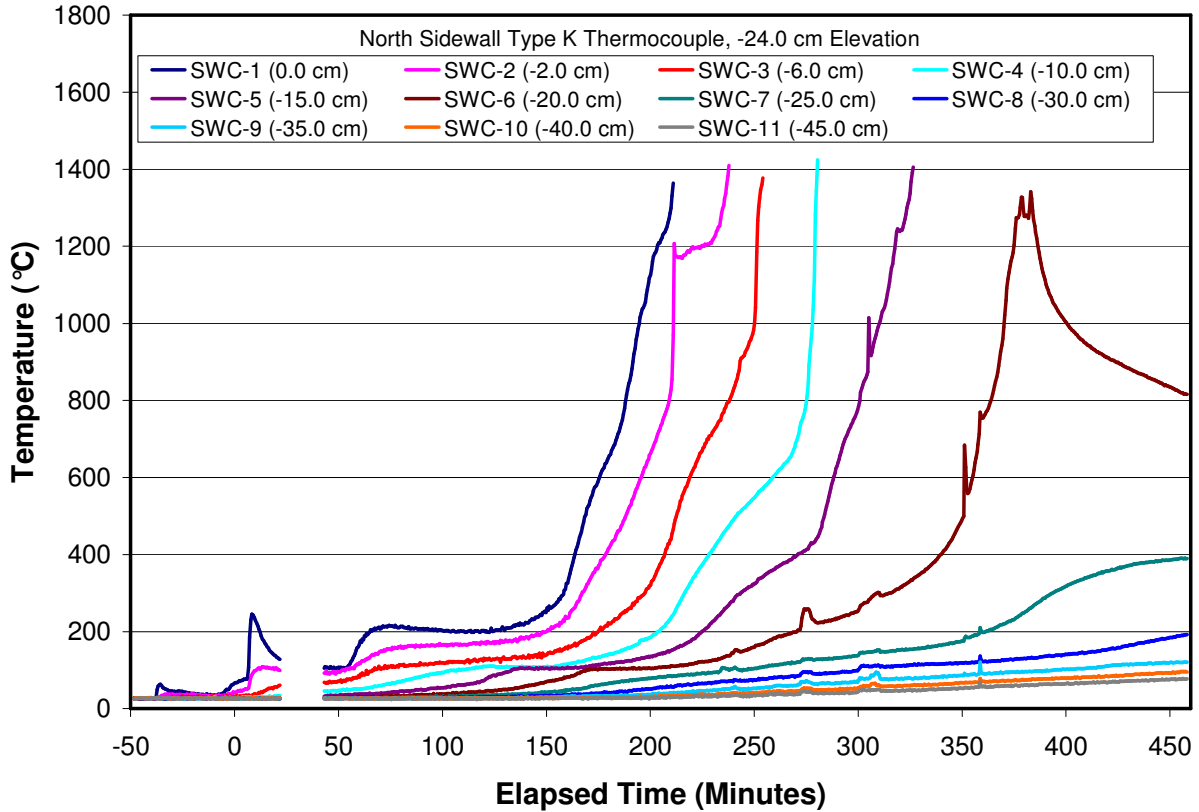


Figure B-16. North Sidewall Type K “SWC” Array Data.

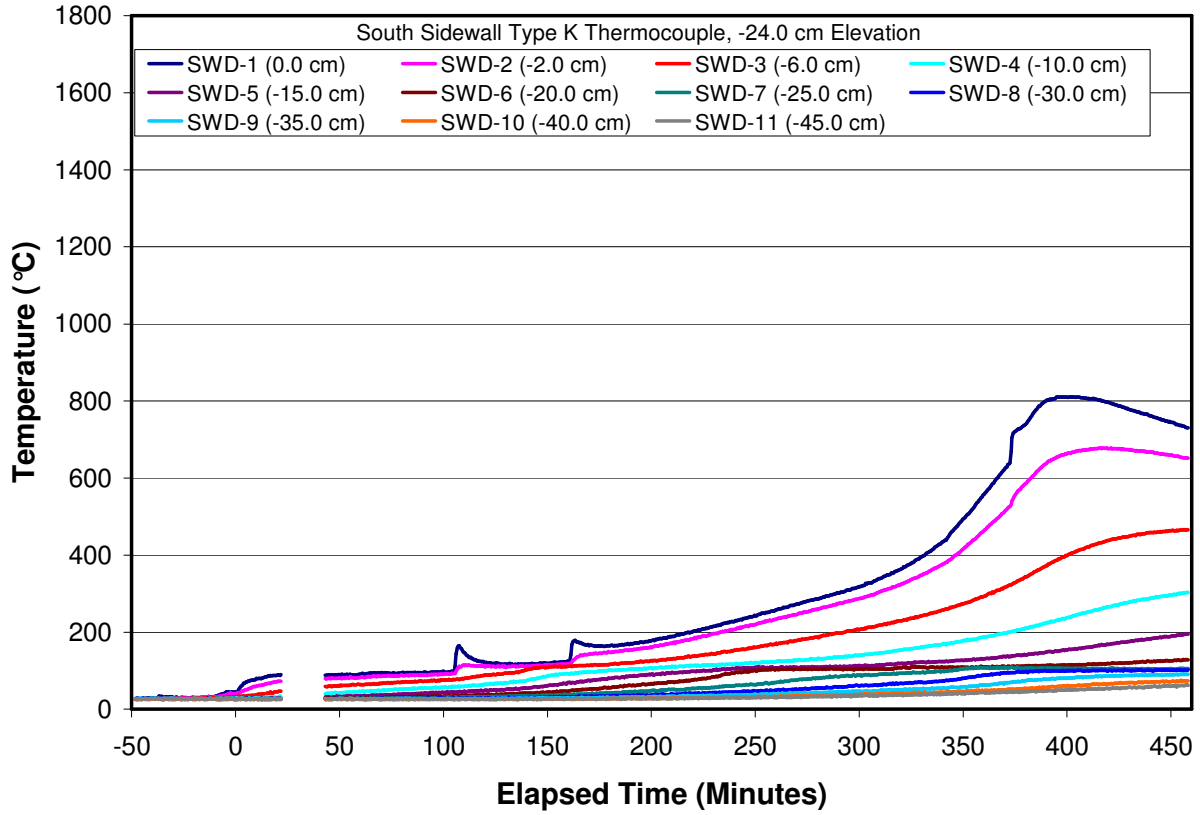


Figure B-17. South Sidewall Type K “SWD” Array Data.

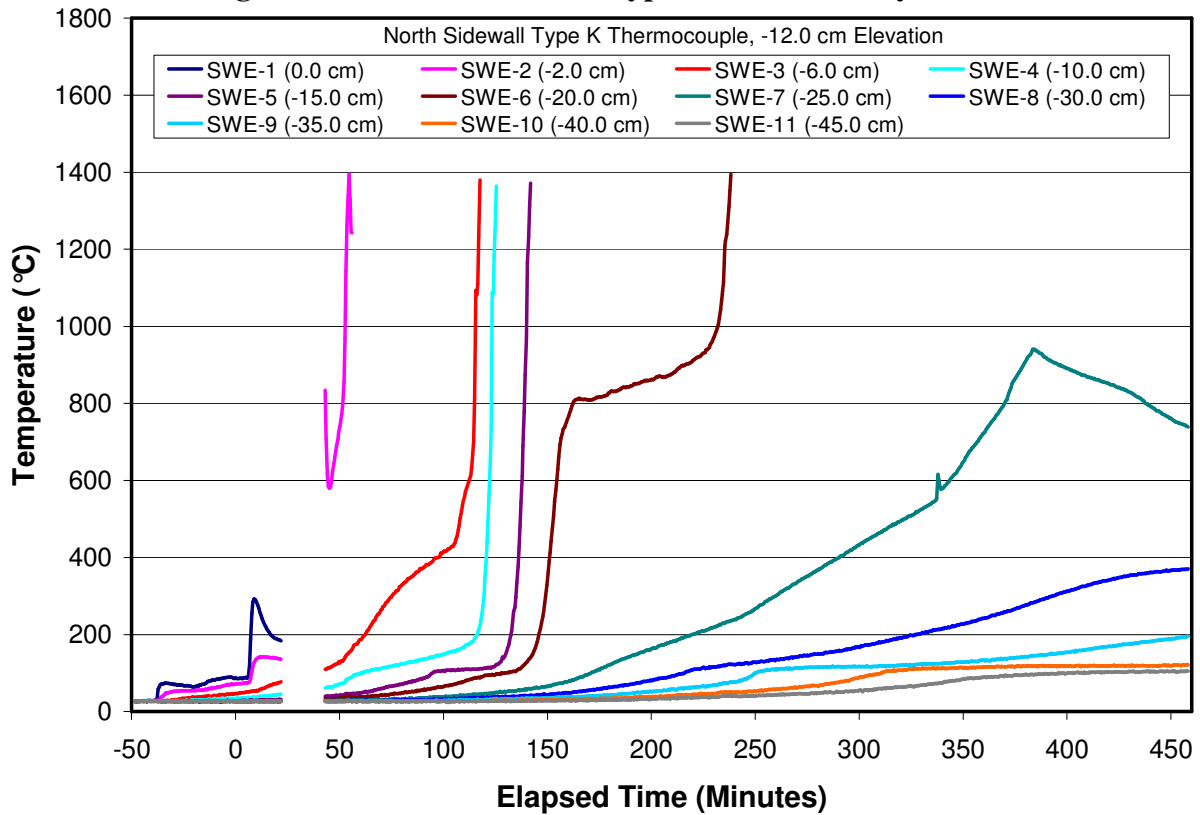
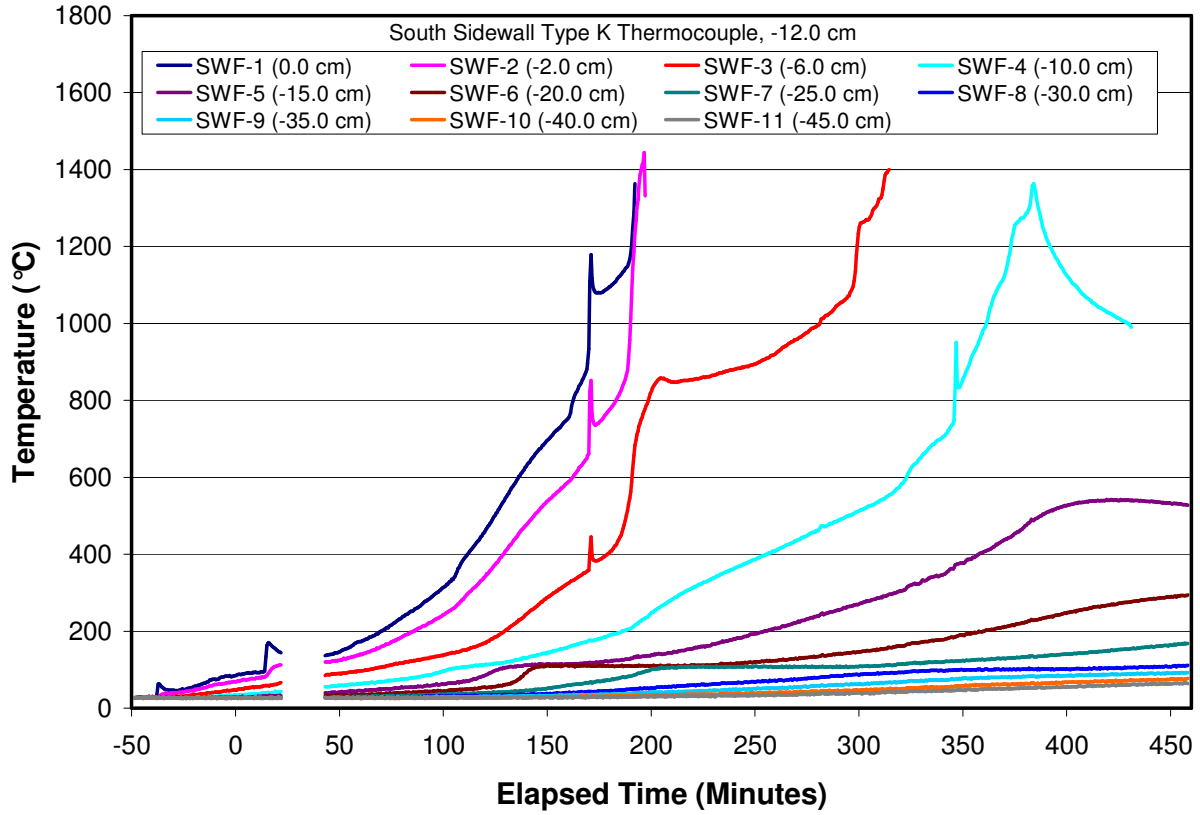
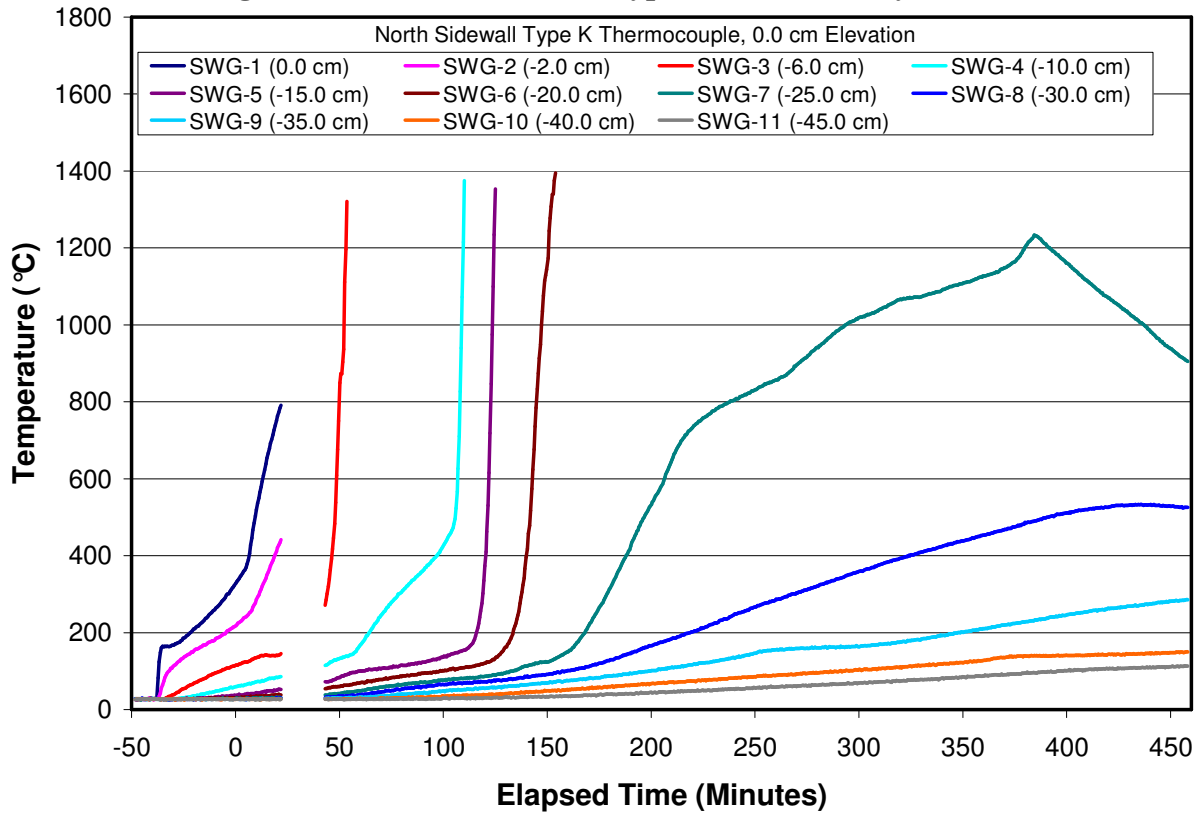


Figure B-18. North Sidewall Type K “SWE” Array Data.



**Figure B-19. South Sidewall Type K “SWF” Array Data.**



**Figure B-20. North Sidewall Type K “SWG” Array Data.**

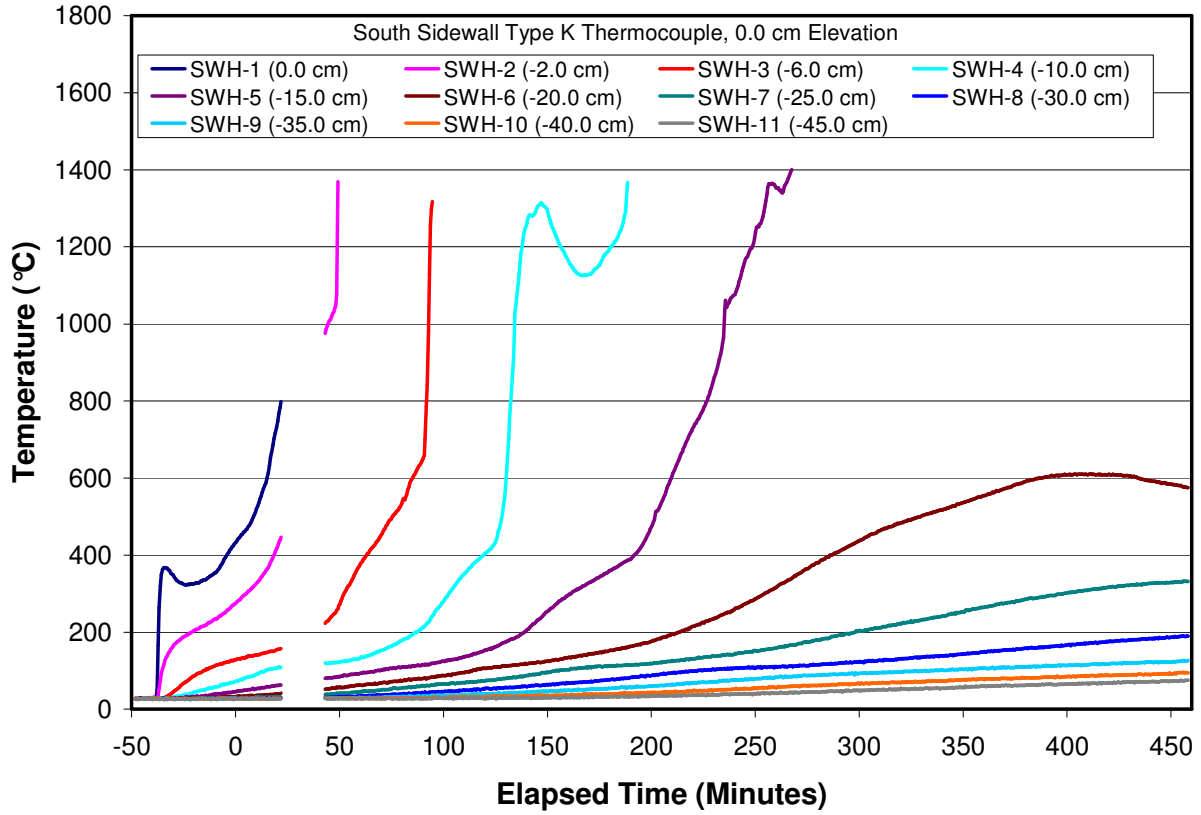


Figure B-21. South Sidewall Type K “SWH” Array Data.

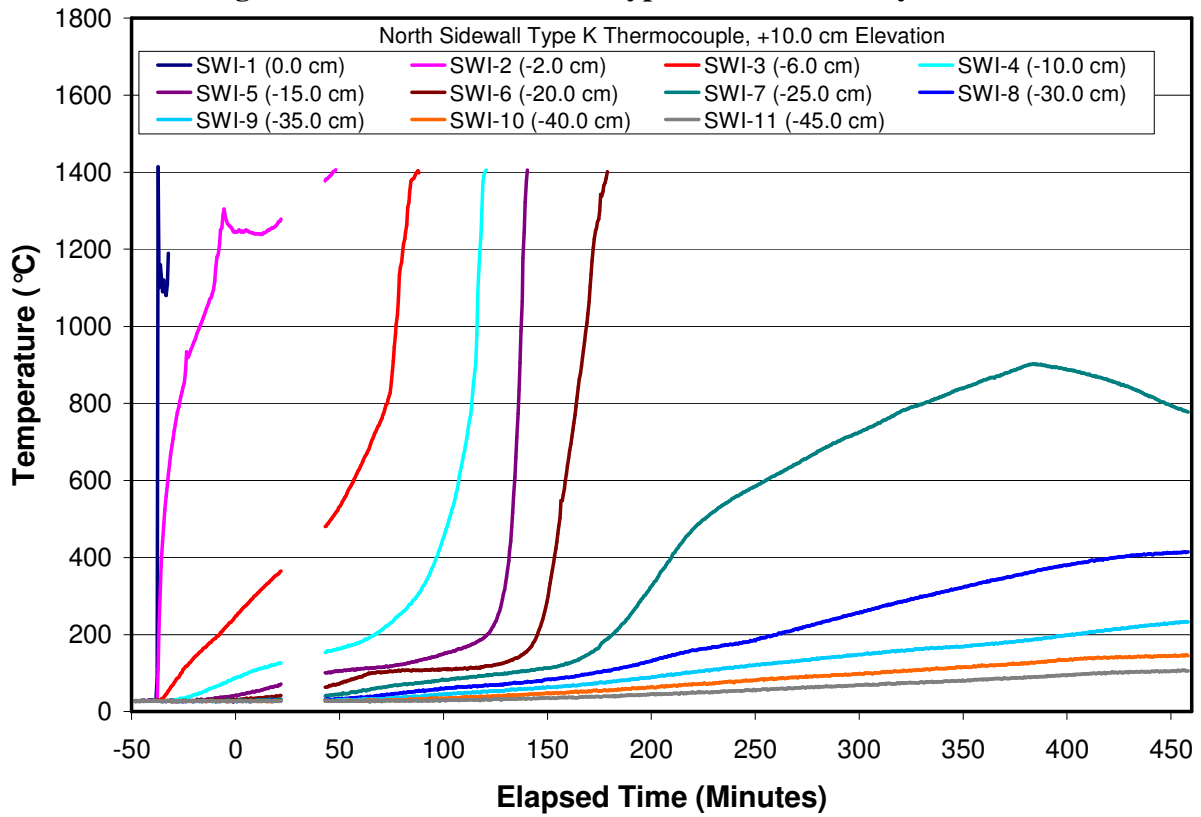
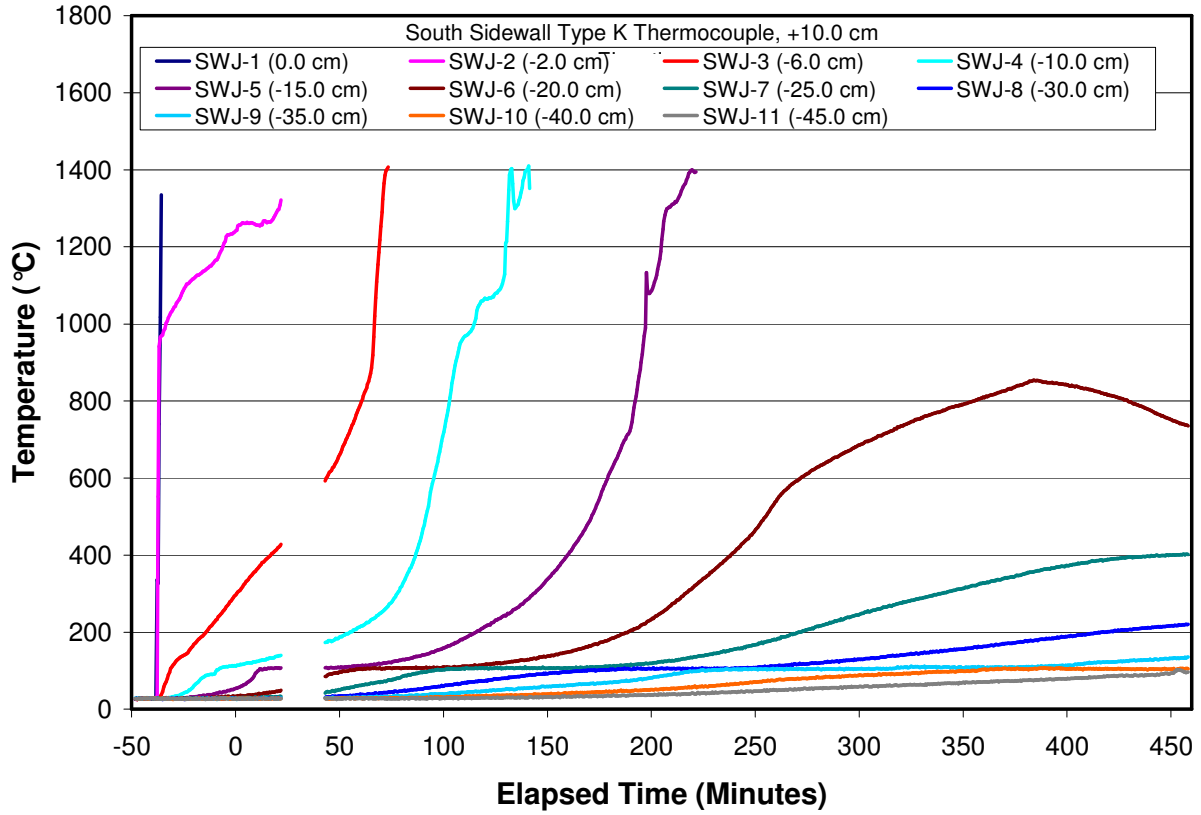
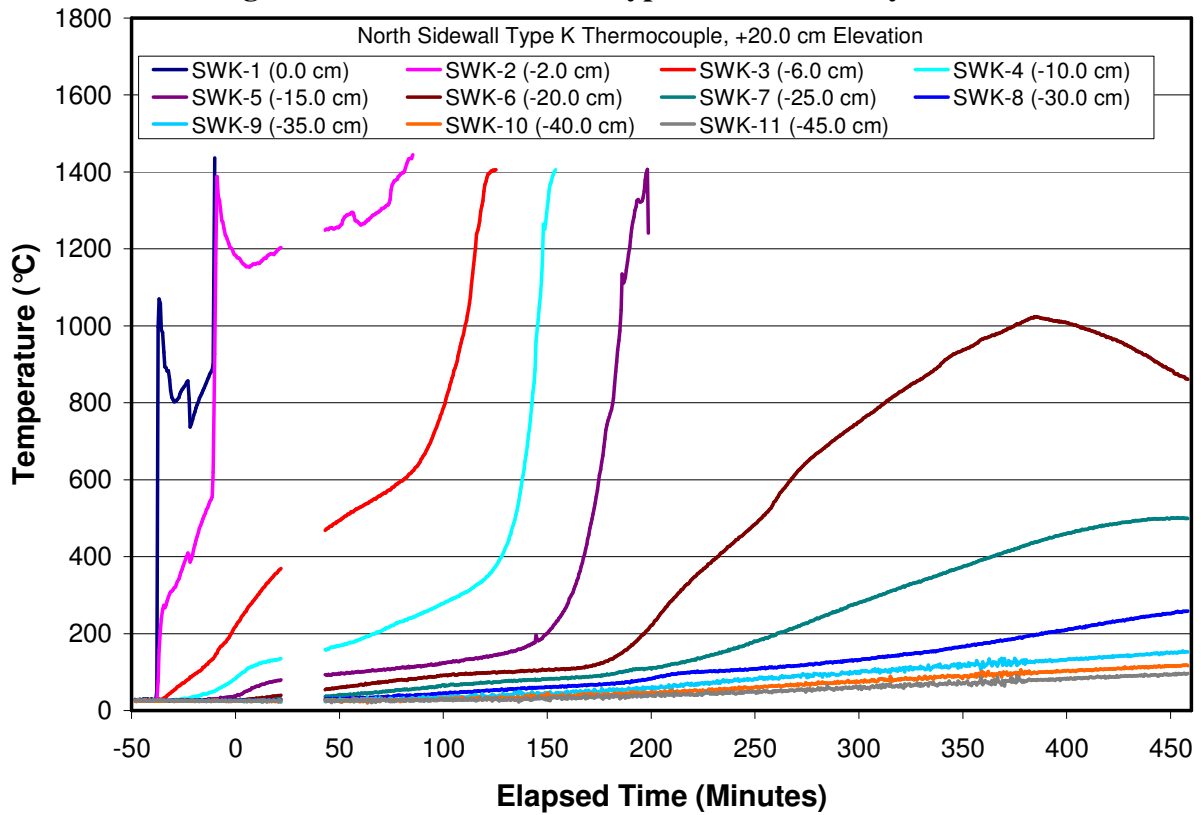


Figure B-22. North Sidewall Type K “SWI” Array Data.



**Figure B-23. South Sidewall Type K “SWJ” Array Data.**



**Figure B-24. North Sidewall Type K “SWK” Array Data.**

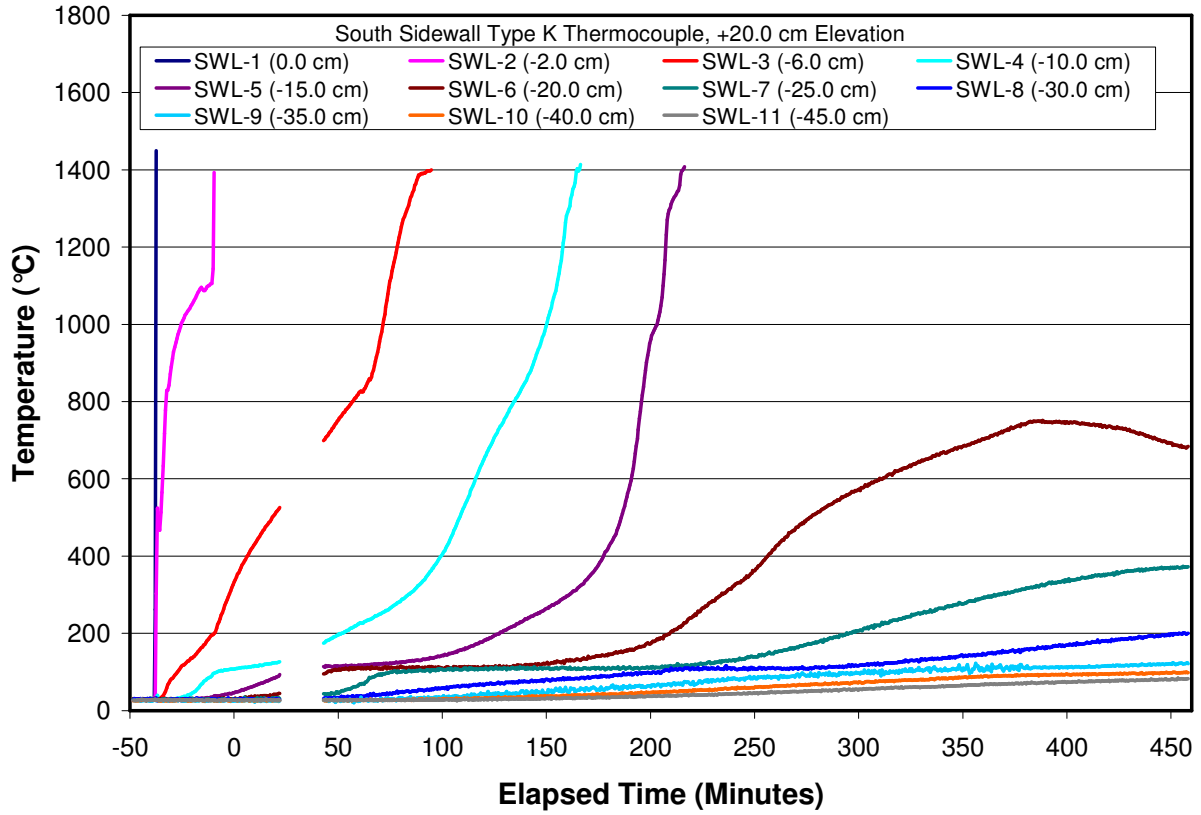


Figure B-25. South Sidewall Type K “SWL” Array Data.

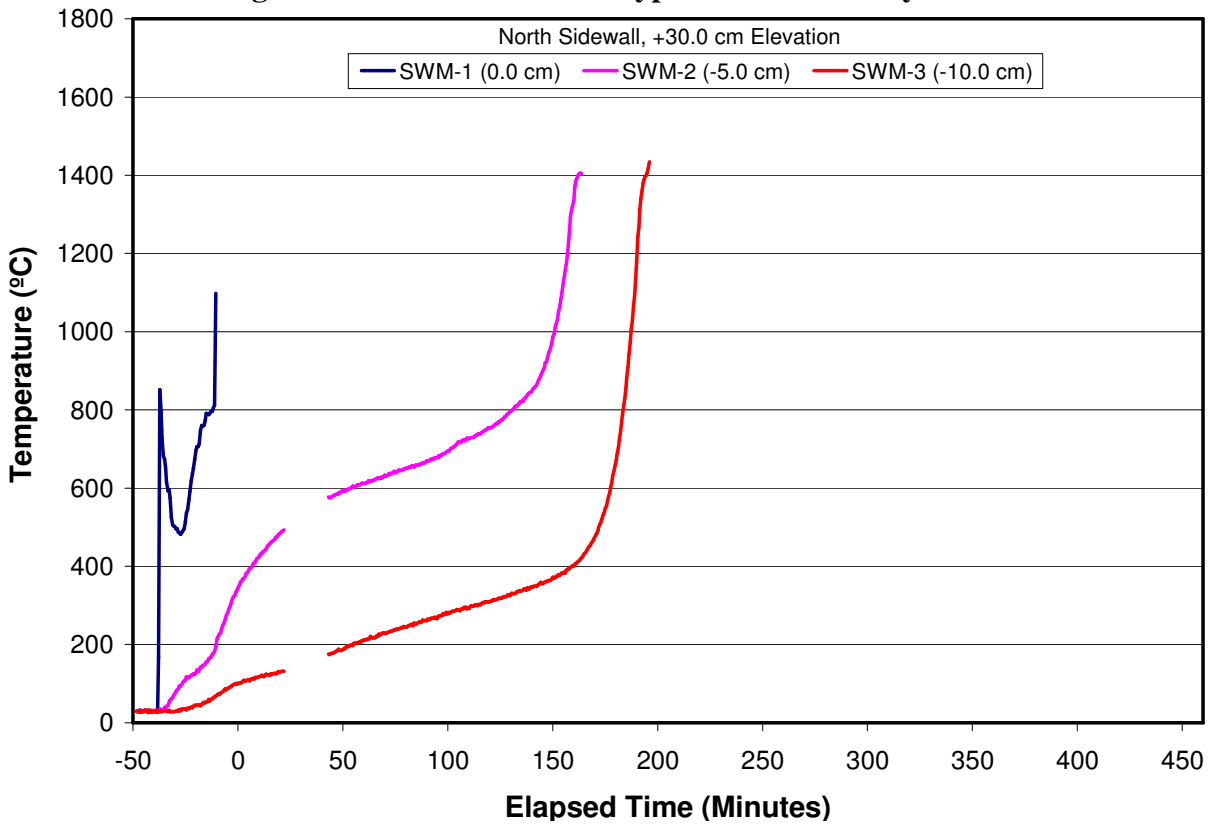


Figure B-26. North Sidewall Type K “SWM” Array Data.

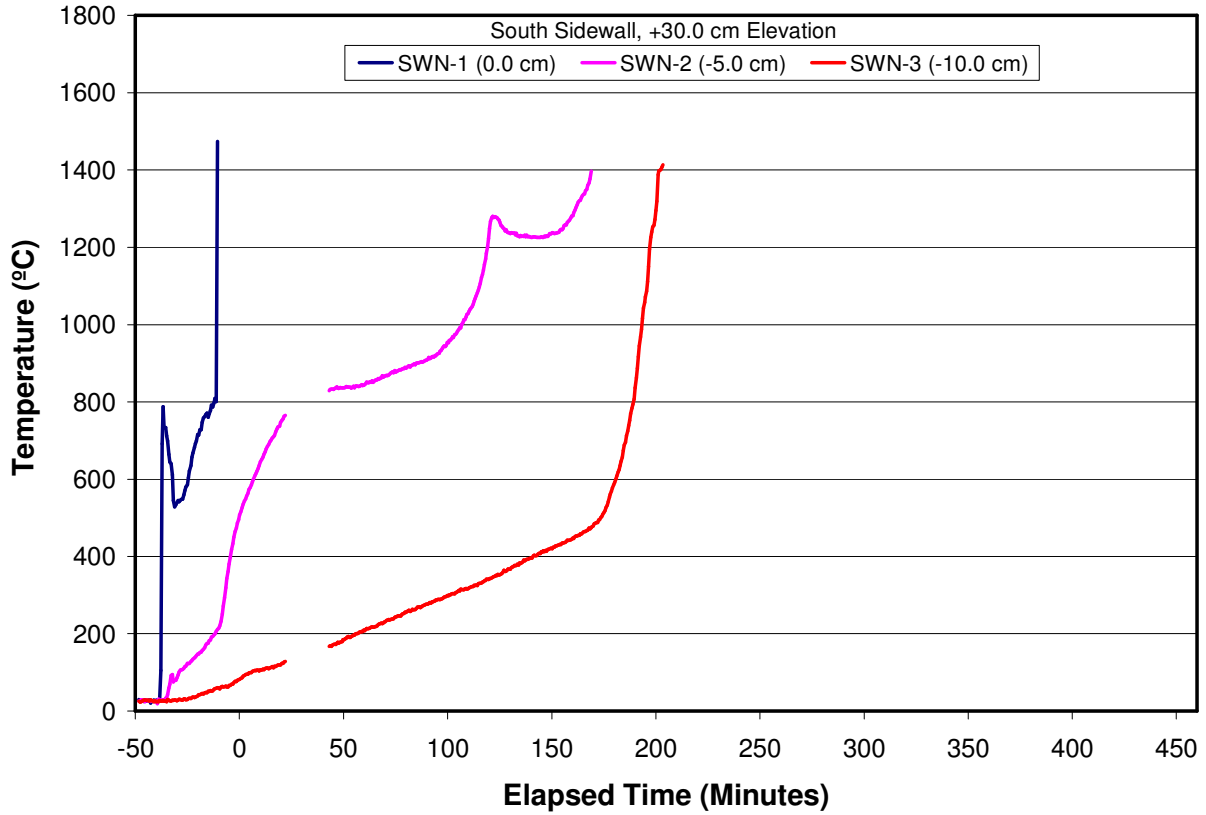


Figure B-27. South Sidewall Type K “SWN” Array Data.

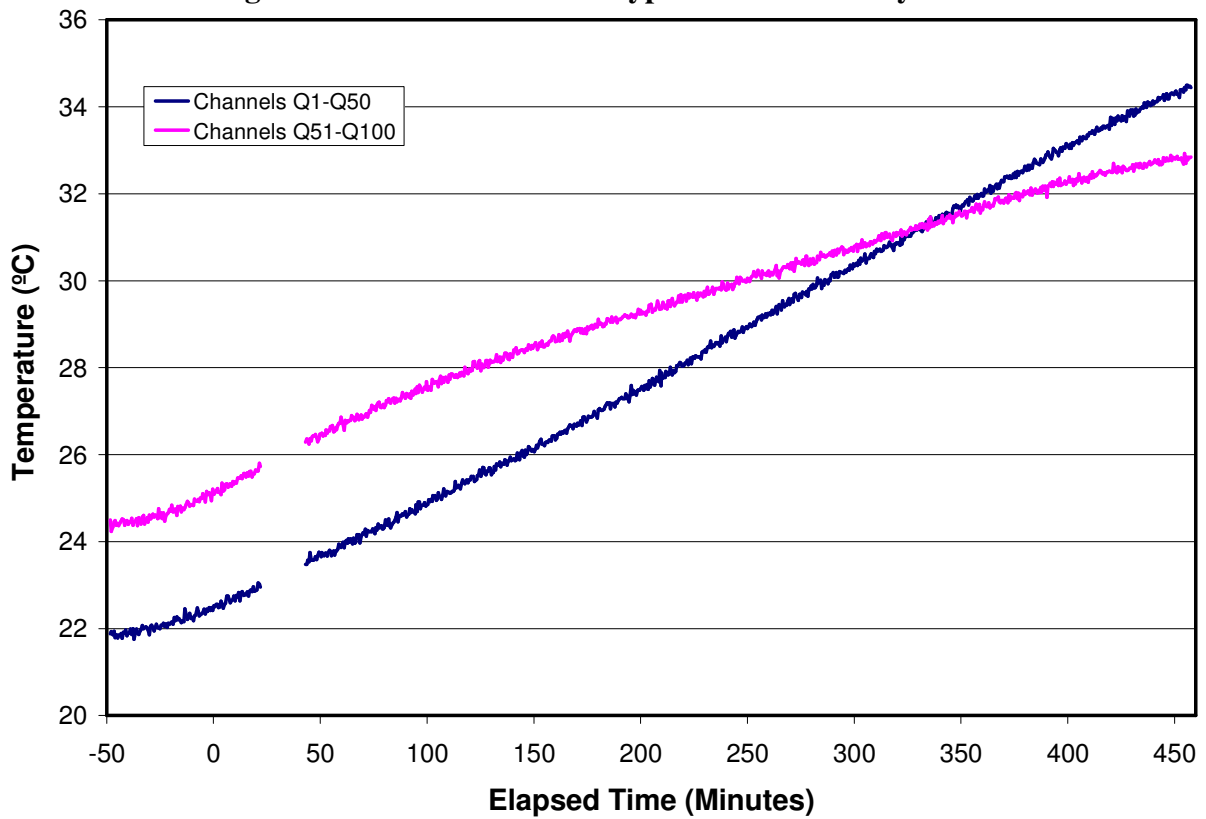


Figure B-28. Thermocouple Compensator Data for Channels Q1-Q50 and Q51-Q100.

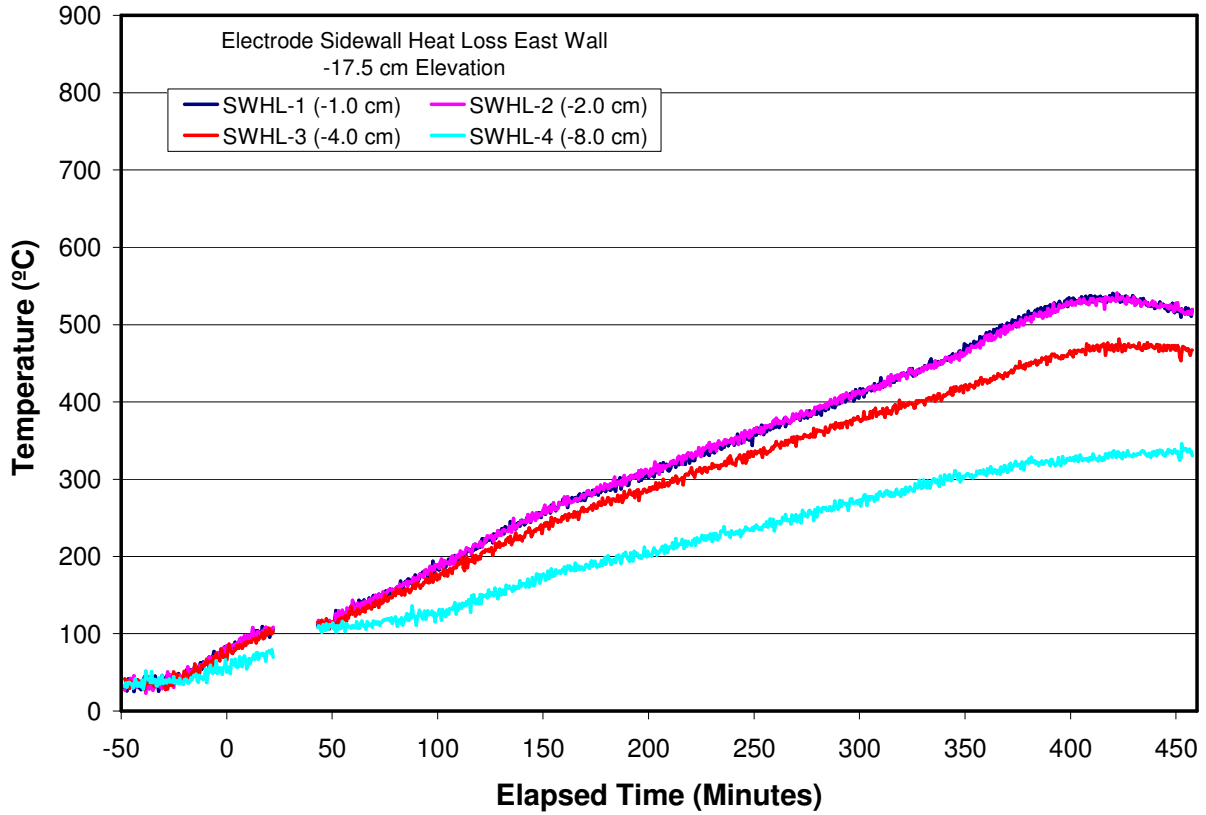


Figure B-29. Test Section Sidewall Heat Loss Data at -17.5 cm Elevation.

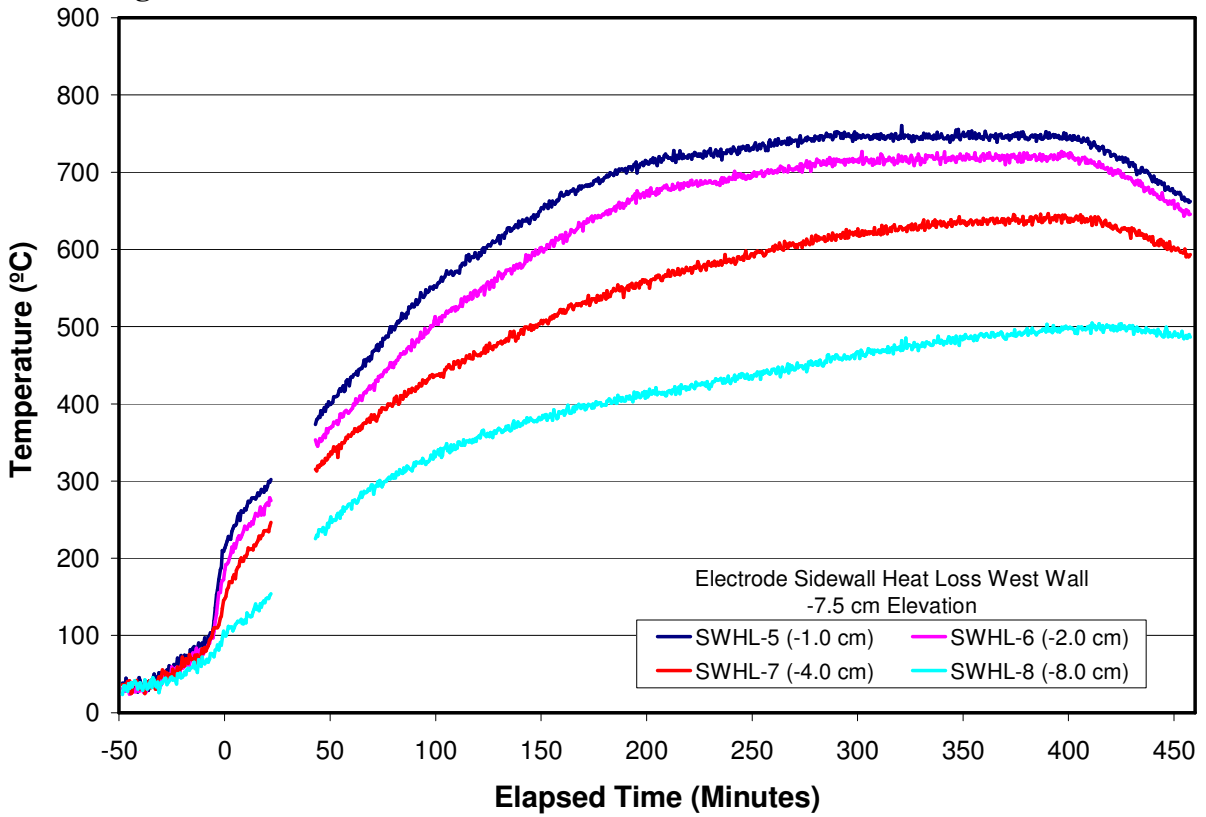
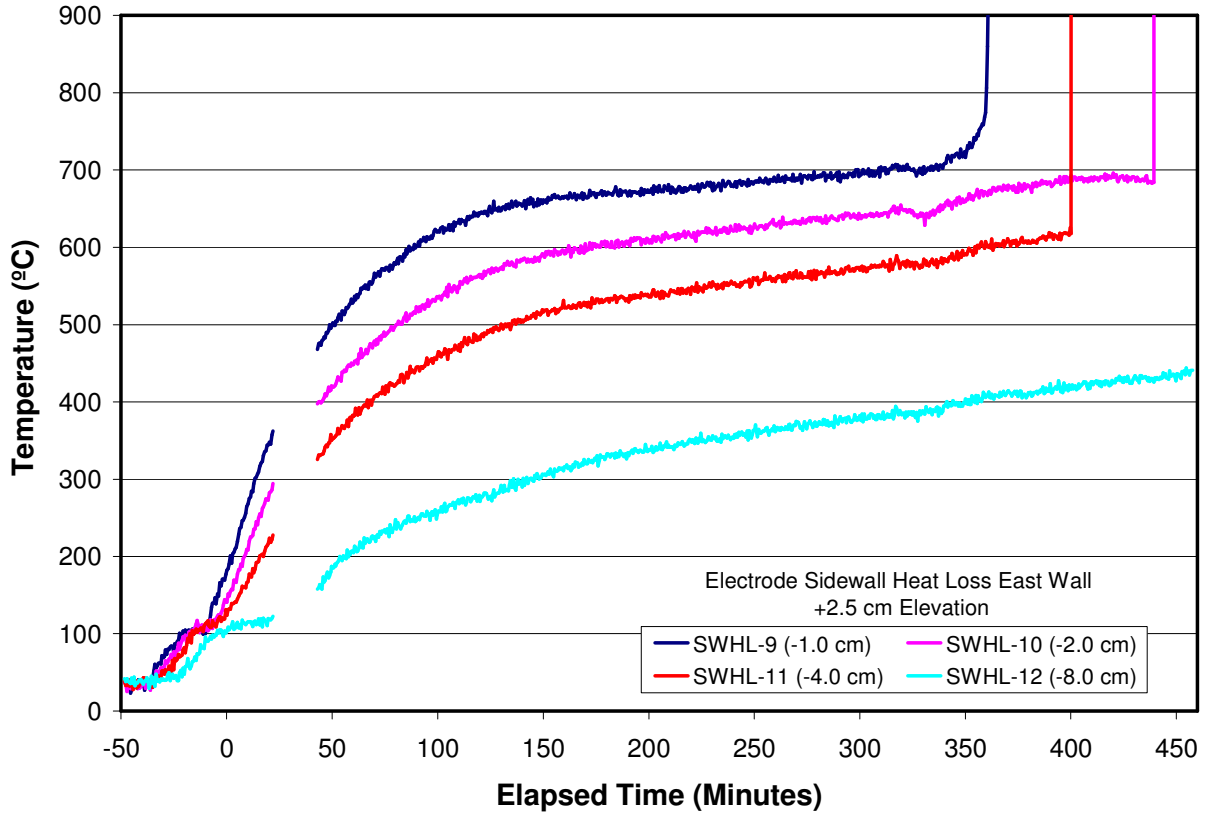
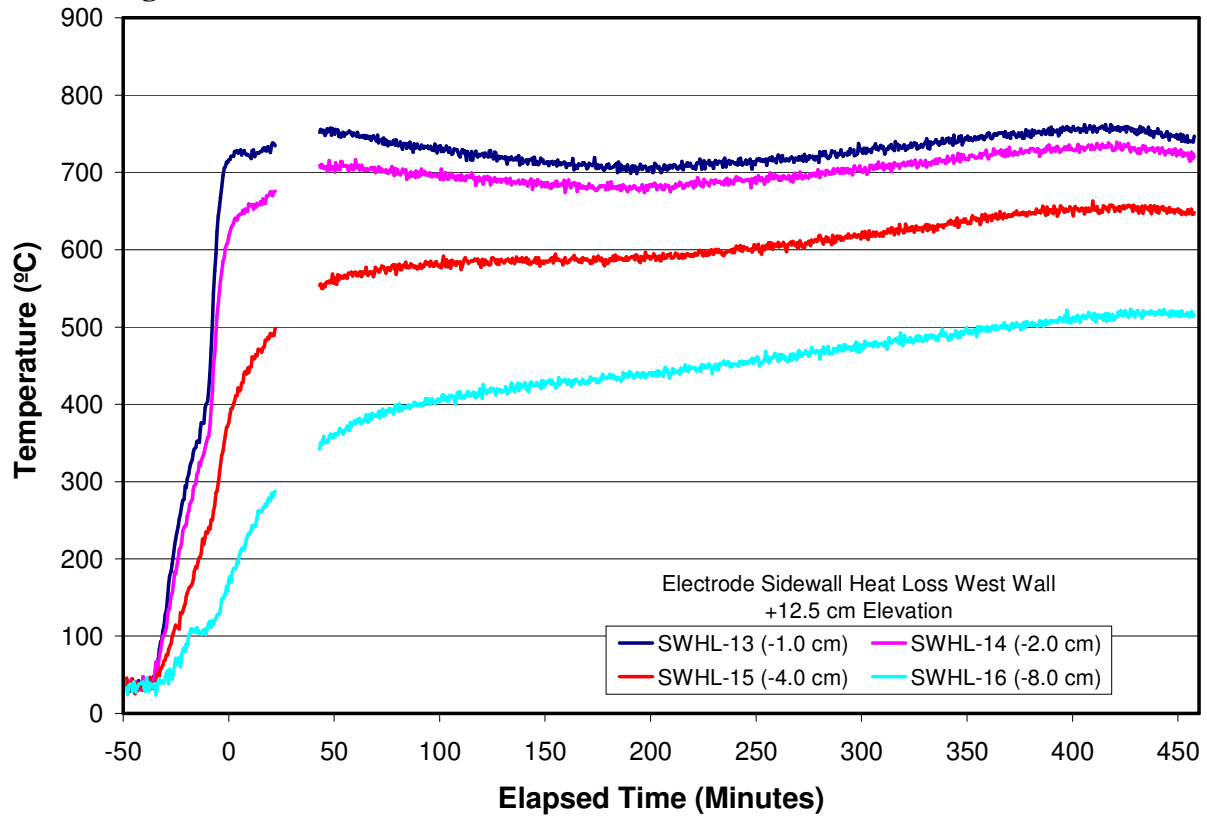


Figure B-30. Test Section Sidewall Heat Loss Data at -7.5 cm Elevation.



**Figure B-31. Test Section Sidewall Heat Loss Data at +2.5 cm Elevation.**



**Figure B-32. Test Section Sidewall Heat Loss Data at +12.5 cm Elevation.**

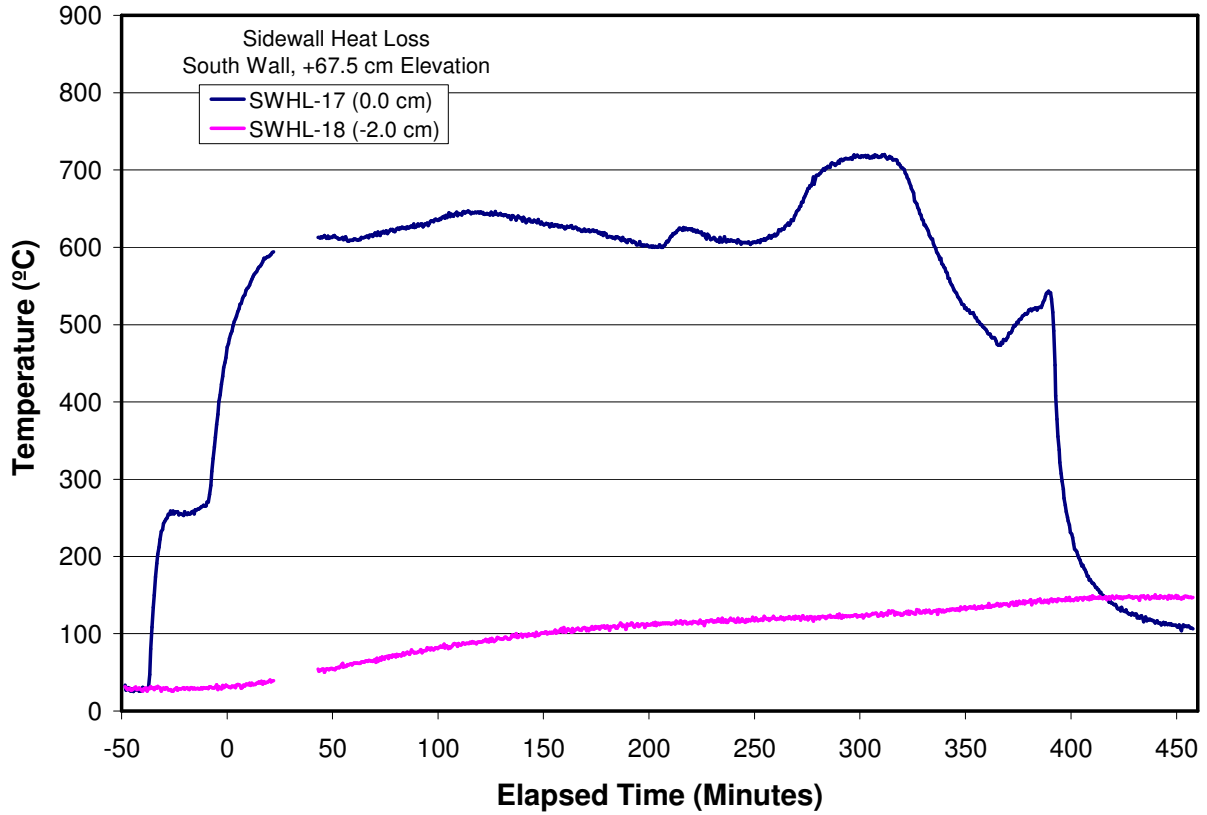


**Figure B-33. Test Section Sidewall Heat Loss Data at the +67.5 cm Elevation.**

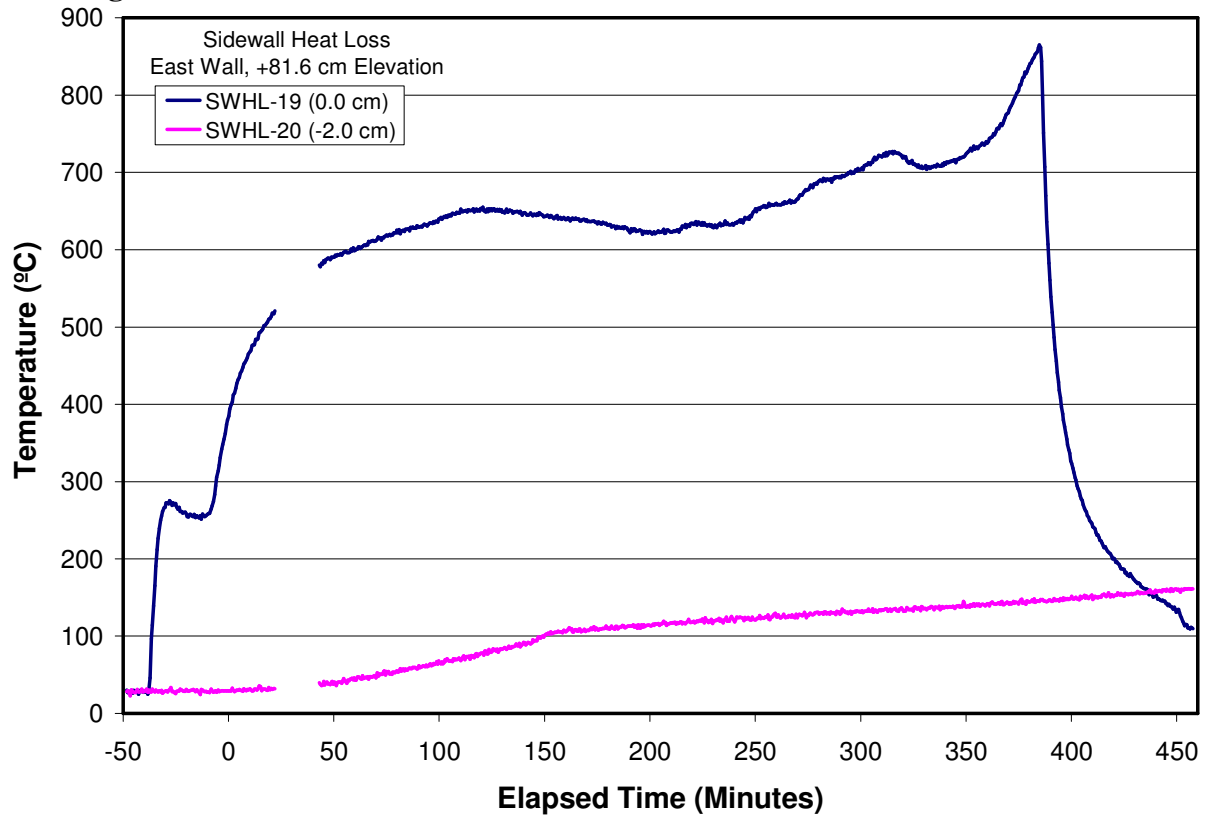


**Figure B-34. Test Section Sidewall Heat Loss Data at the +81.6 cm Elevation.**

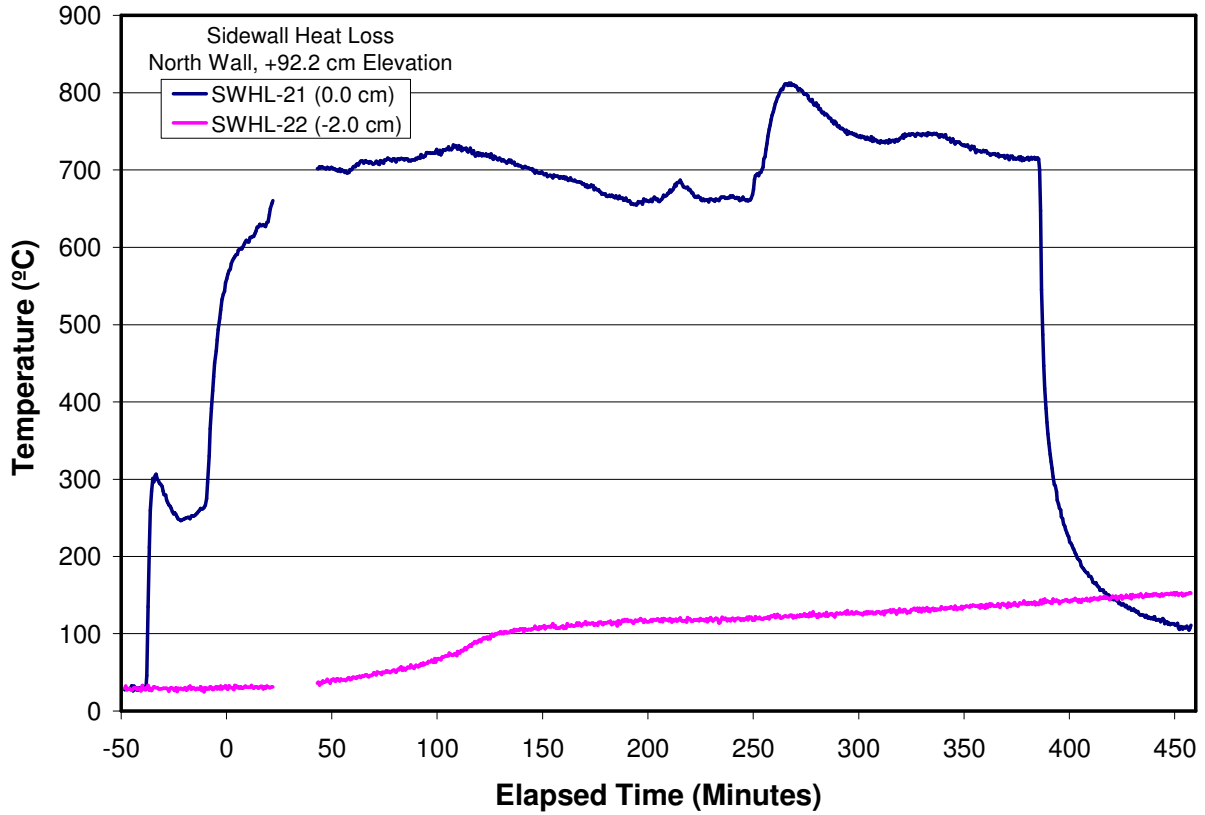


**Figure B-35. Test Section Sidewall Heat Loss Data at the + 92.2 cm Elevation.**

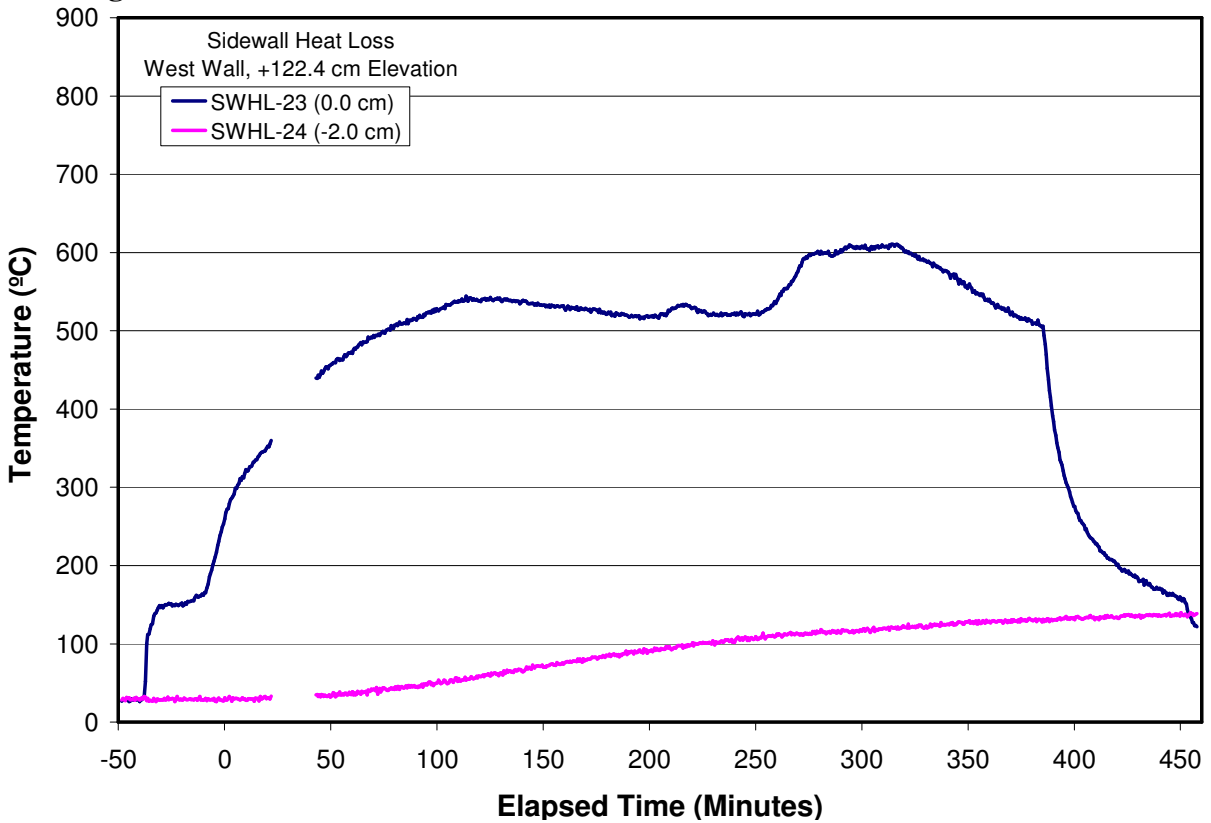


**Figure B-36. Test Section Sidewall Heat Loss Data at the + 122.4 cm Elevation.**

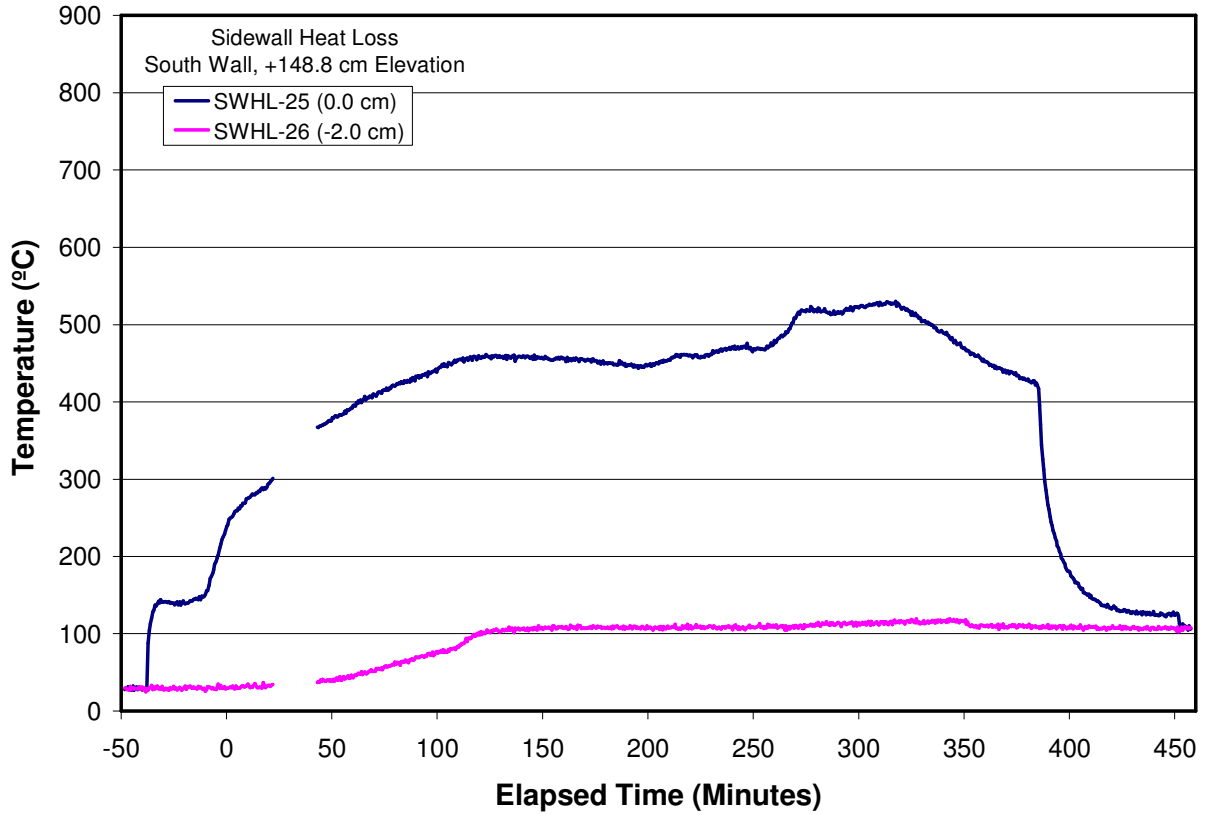


Figure B-37. Test Section Sidewall Heat Loss Data at the + 148.8 cm Elevation.

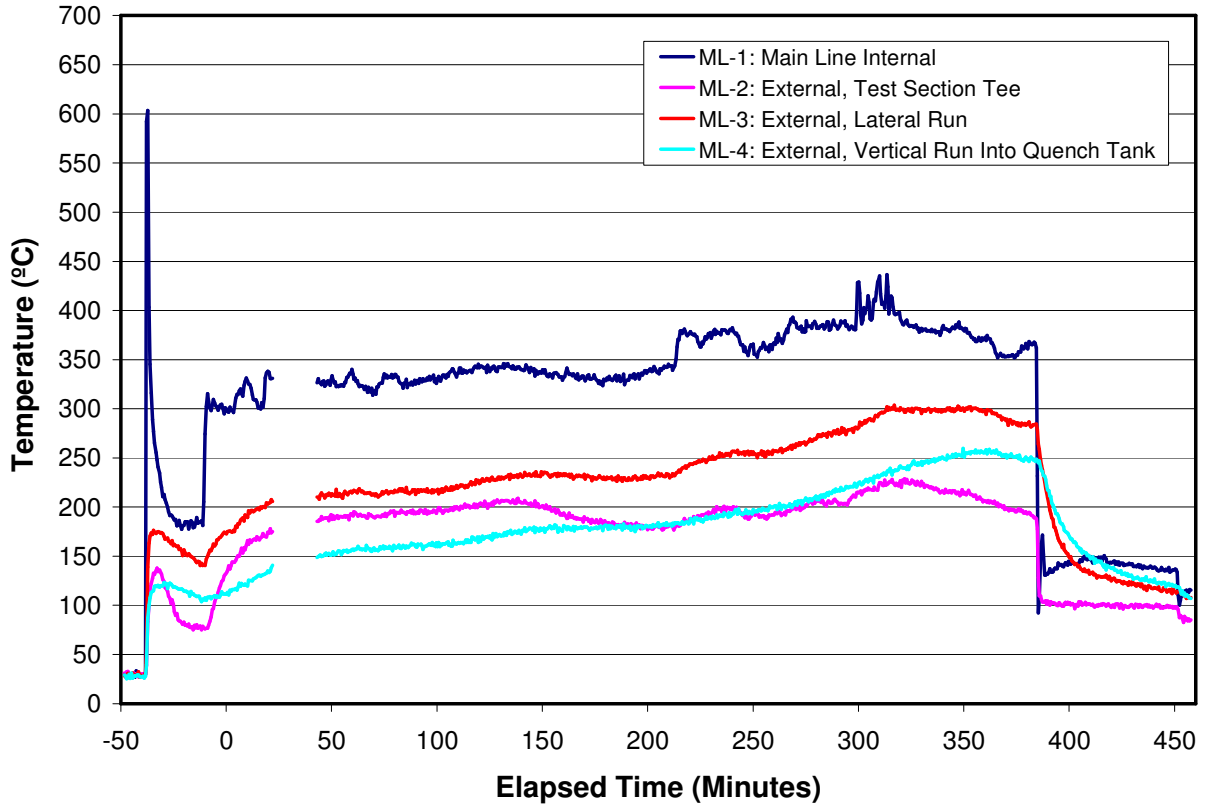


Figure B-38. Test Section Mainline Thermocouple Data.

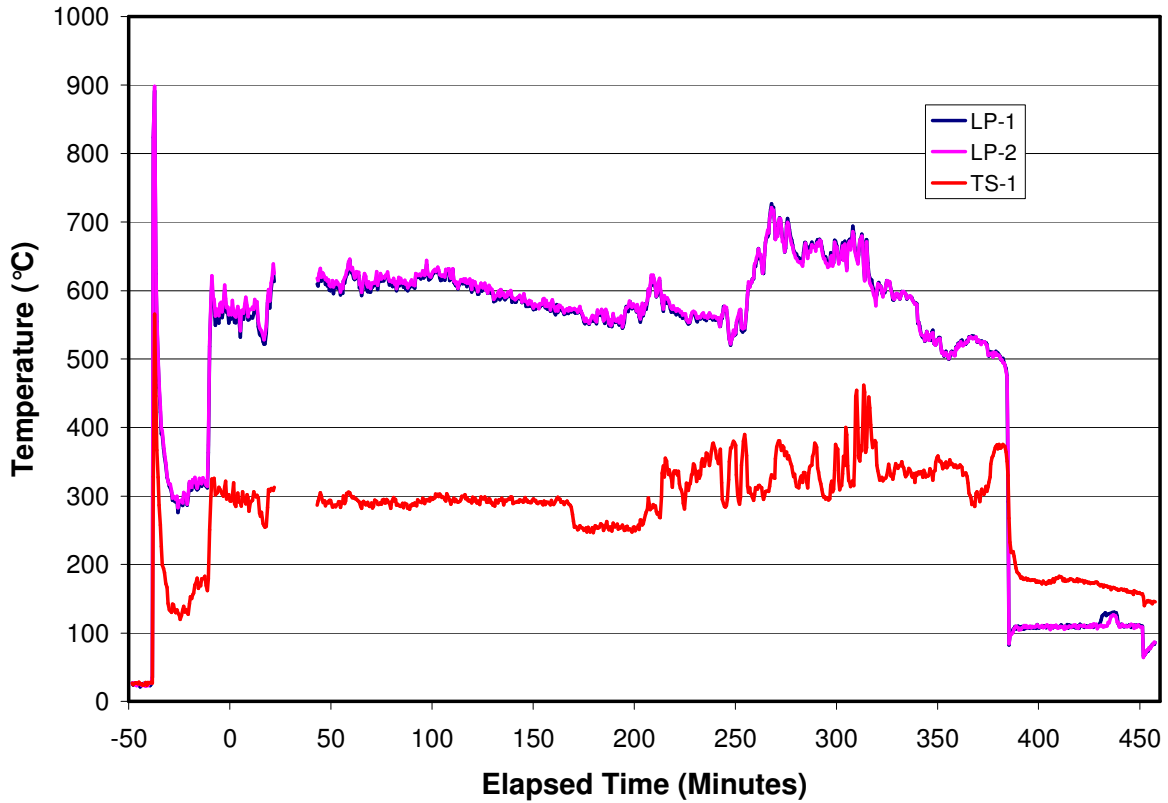


Figure B-39. Test Section Plenum and Insertable Water Level Probe Thermocouple Data.

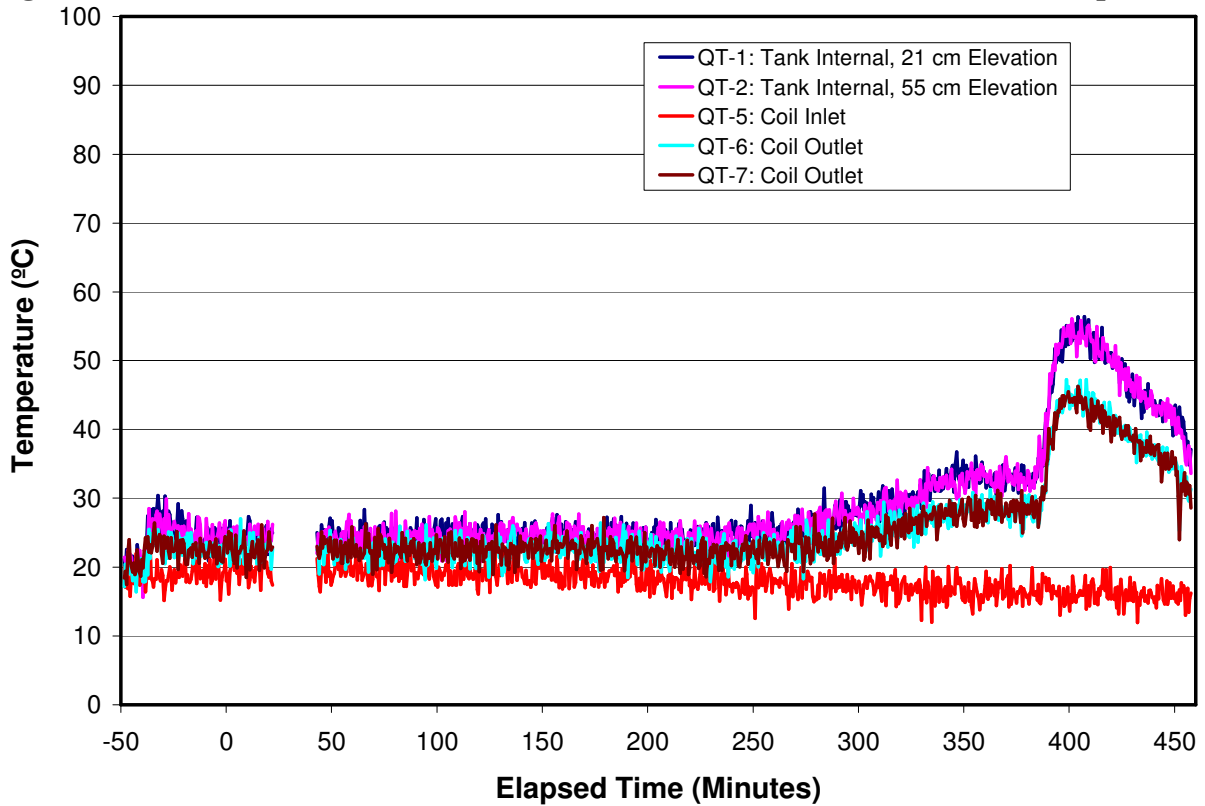
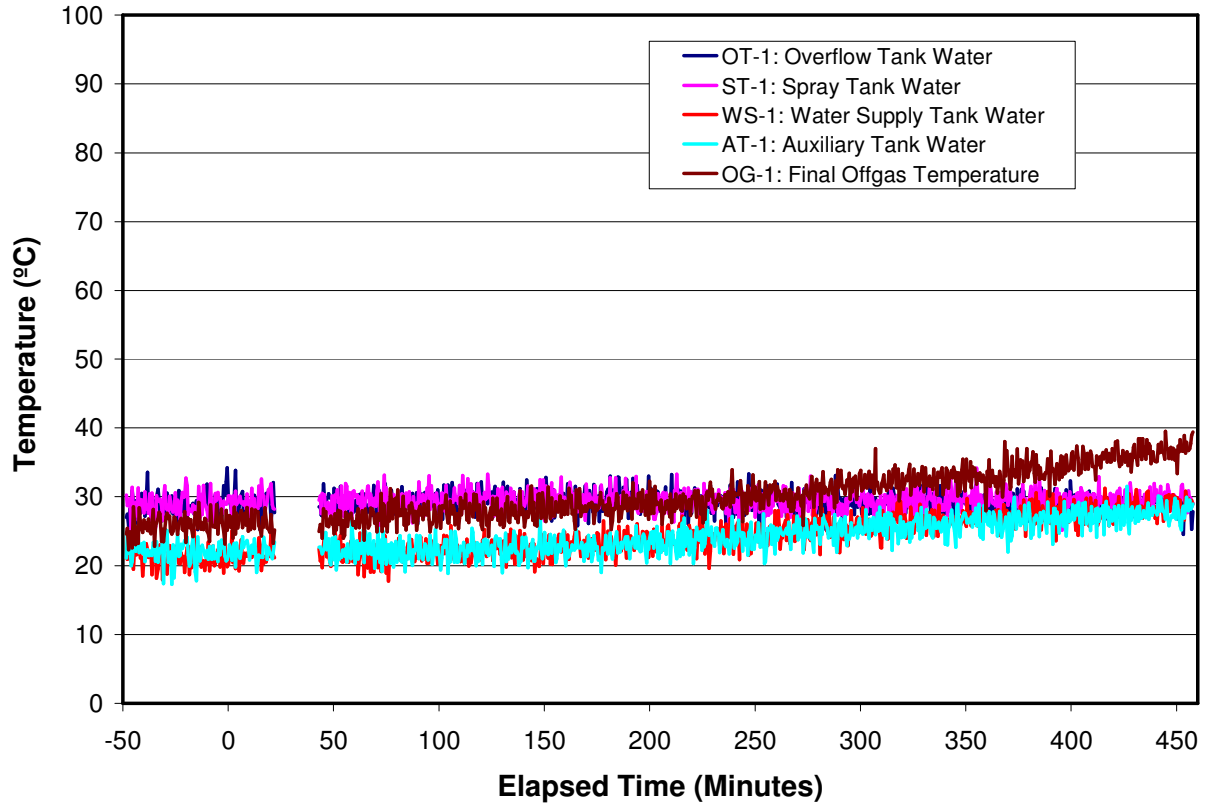
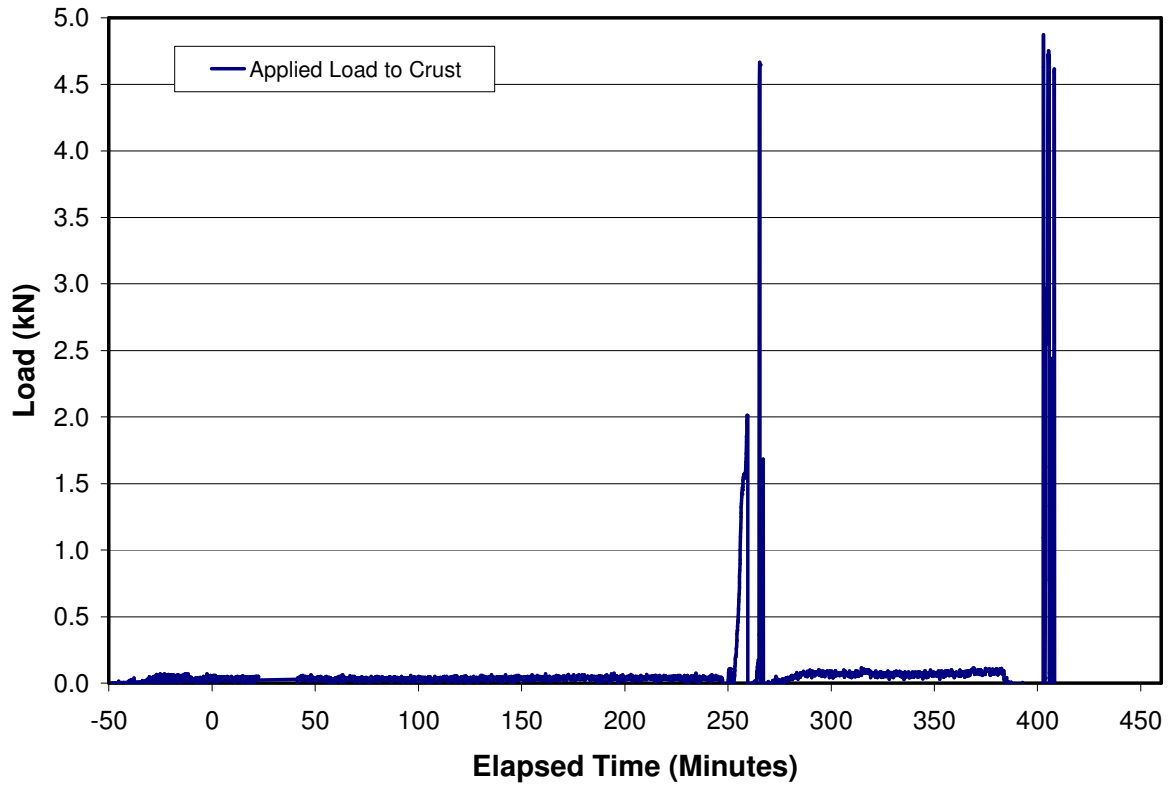


Figure B-40. Quench Tank Water Volume, Coil Inlet, and Coil Outlet Temperature Data.



**Figure B-41. Miscellaneous Temperatures in Water Supply, Quench, and Off Gas Systems.**



**Figure B-42. Crust Lance Load Cell Data.**

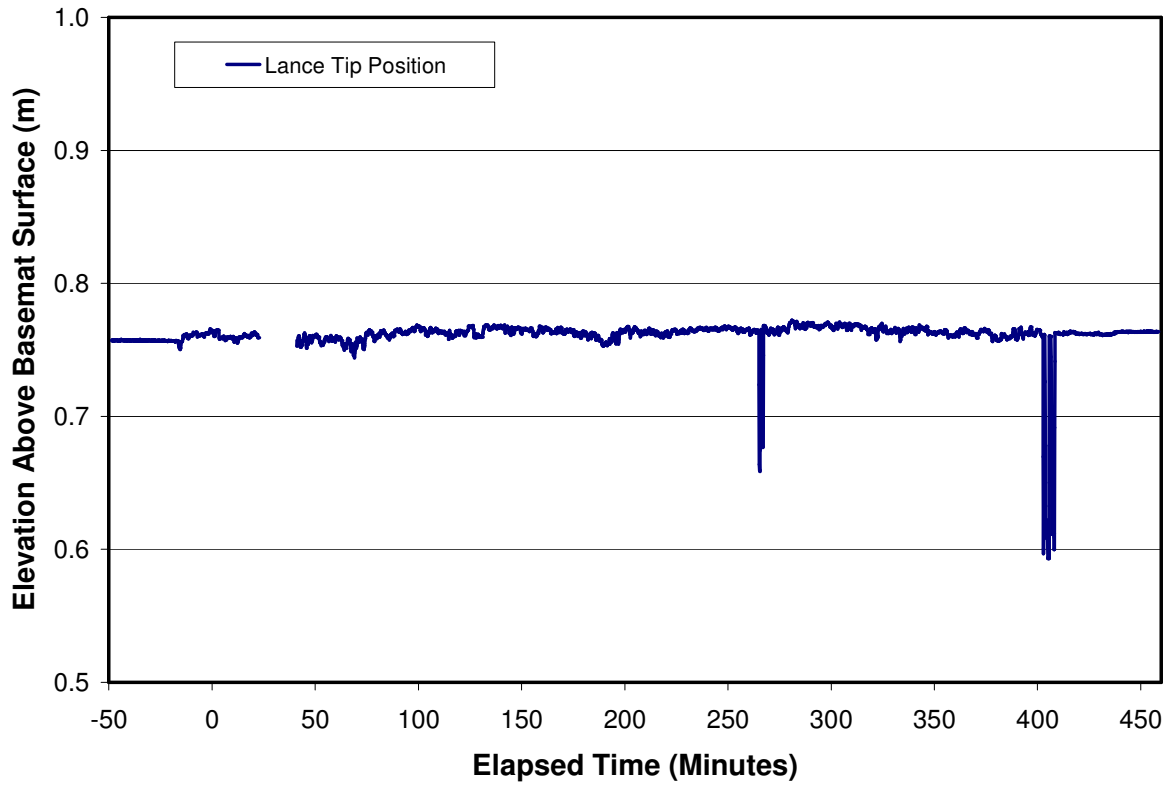


Figure B-43. Lance Position Indicator Data.

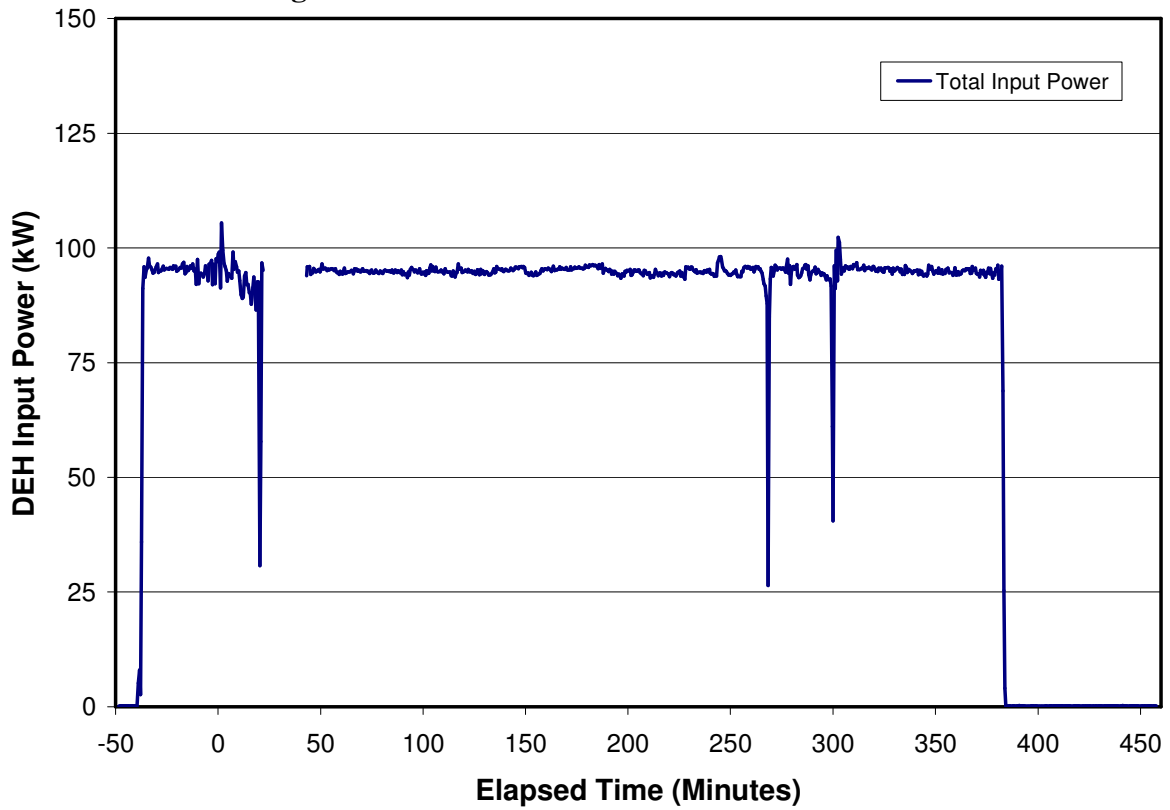
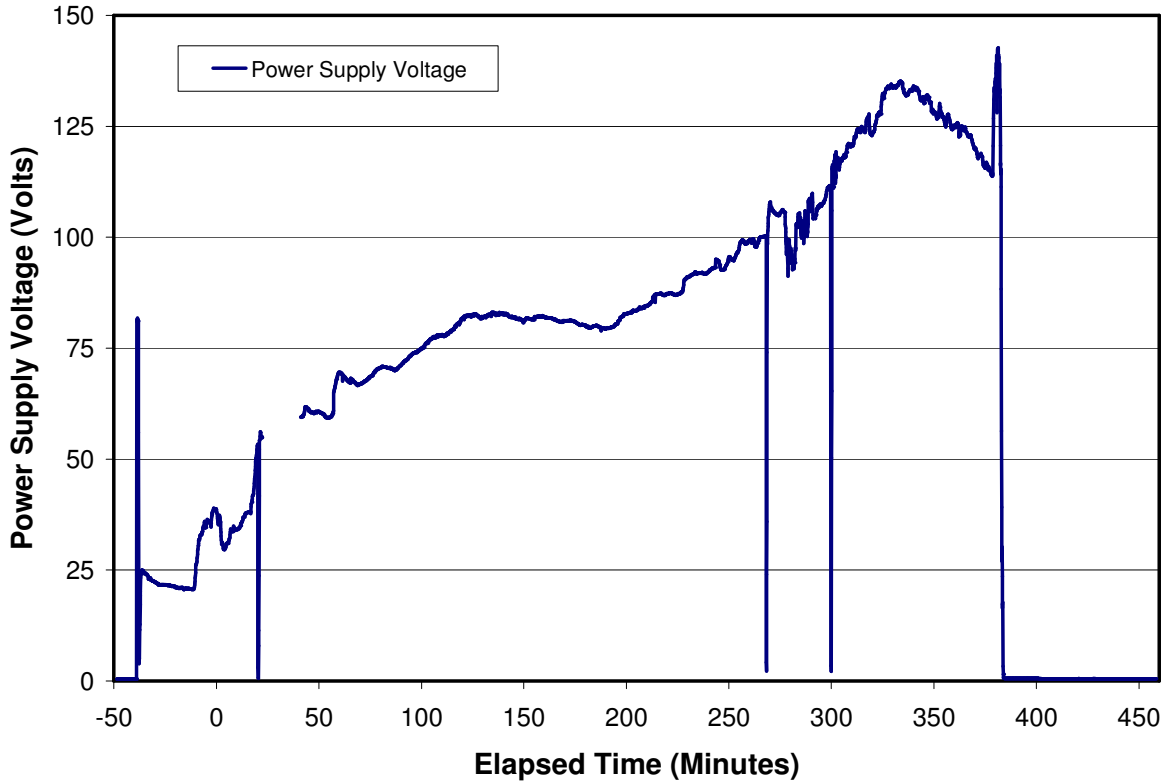
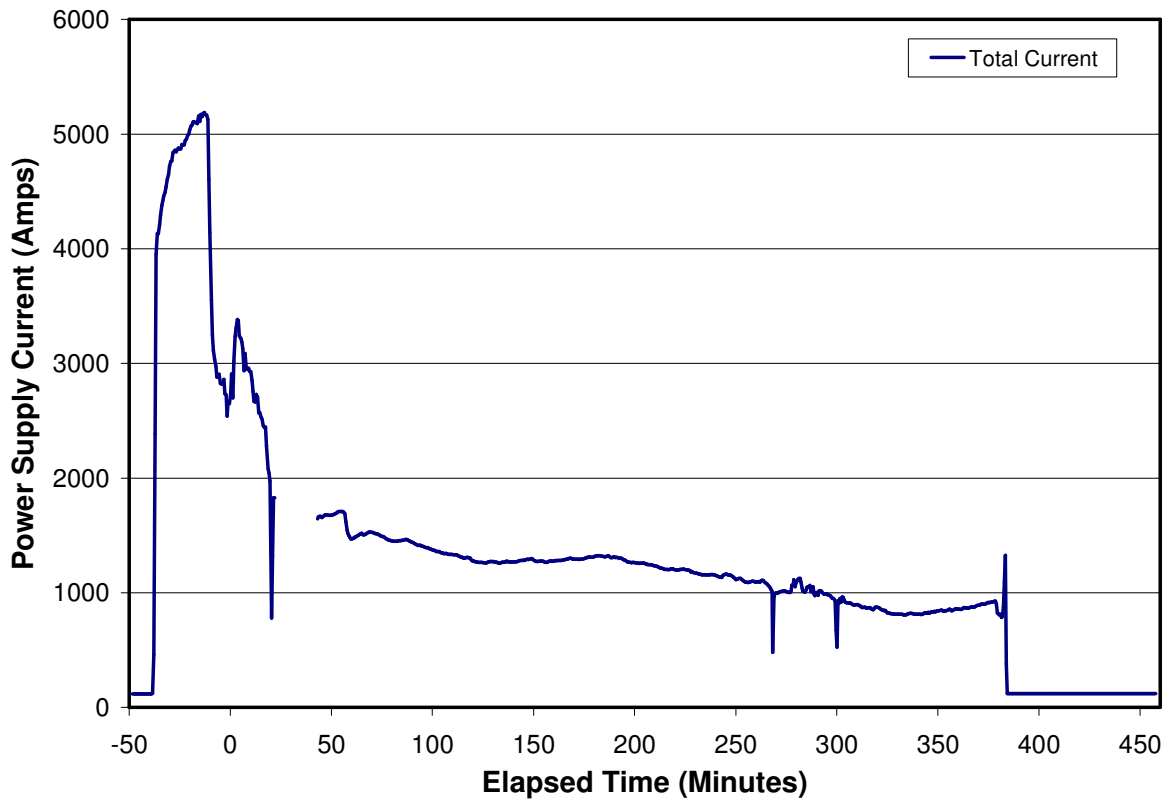


Figure B-44. Total Power Supply Power.



**Figure B-45. Power Supply Voltage Data.**



**Figure B-46. Total Power Supply Current Data.**

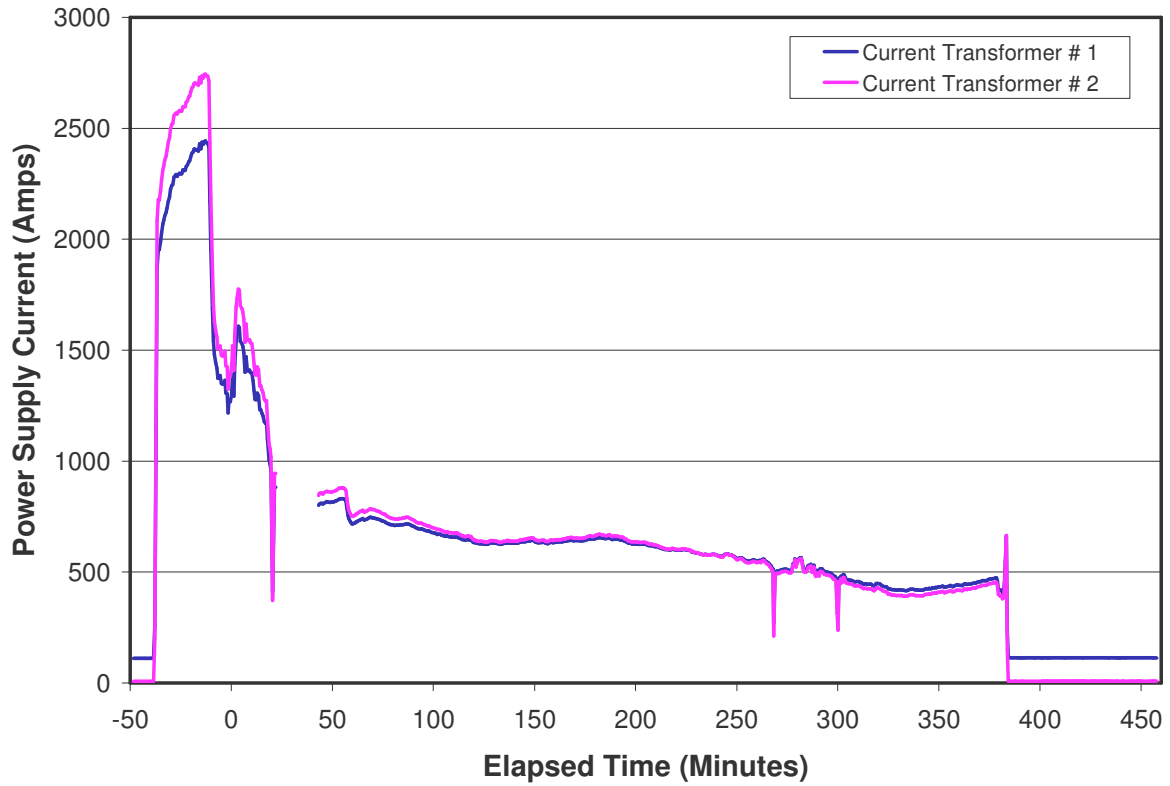


**Figure B-47. Power Supply Current Transformer Data.**

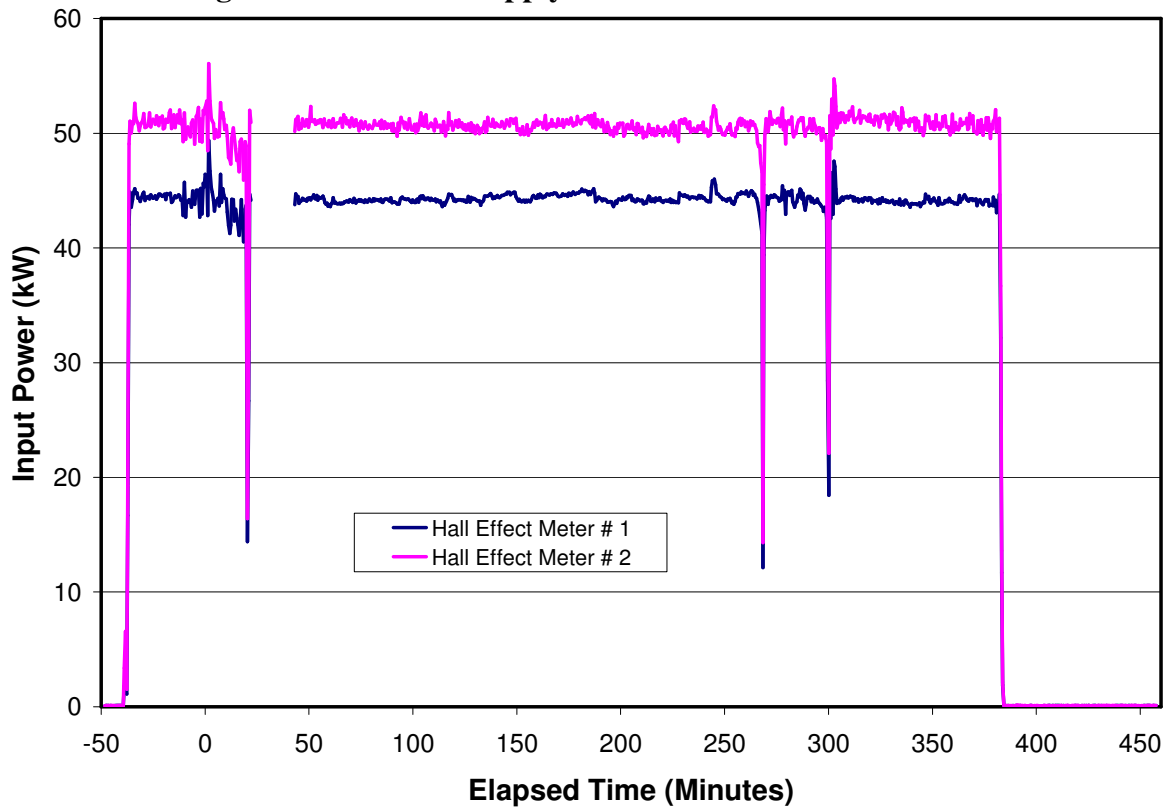


**Figure B-48. Hall Effect Meter Data.**

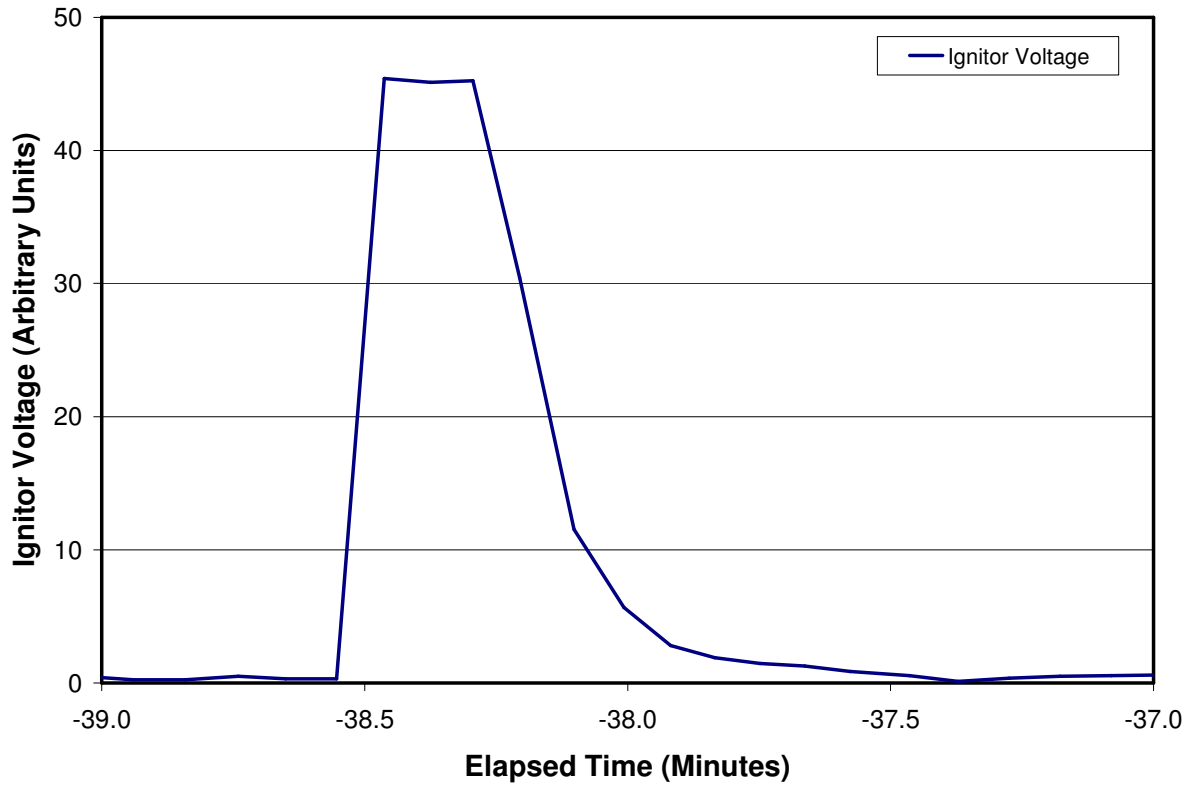


**Figure B-49. Voltage across Igniter Shunt.**

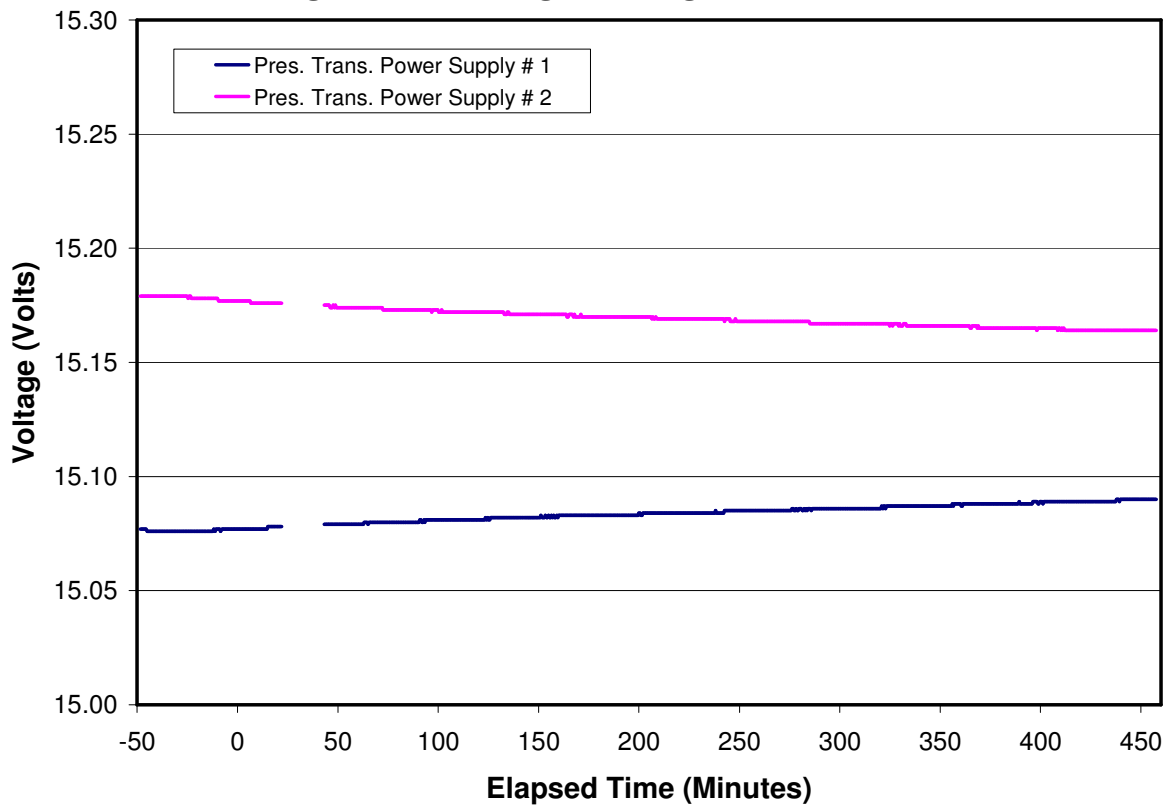


**Figure B-50. Pressure Transducer Power Supply Voltages.**

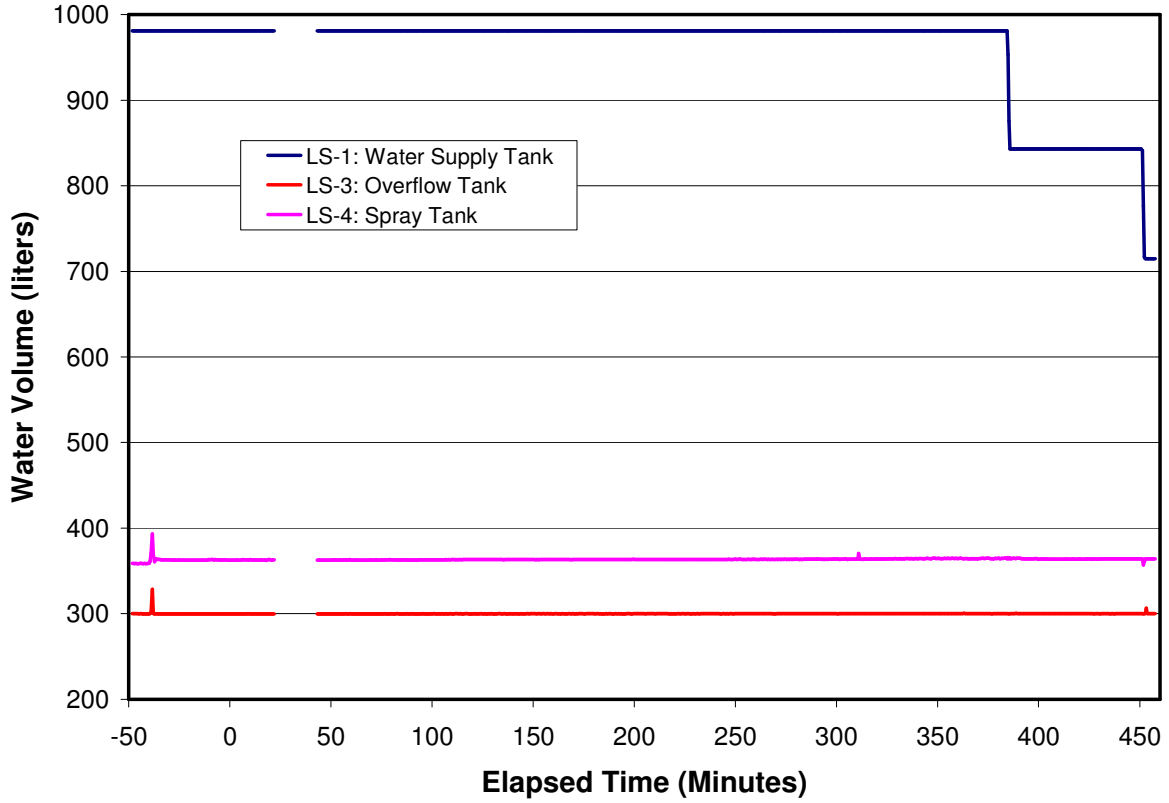


**Figure B-51. Water Supply, Overflow, and Spray Tank Water Volume Data.**

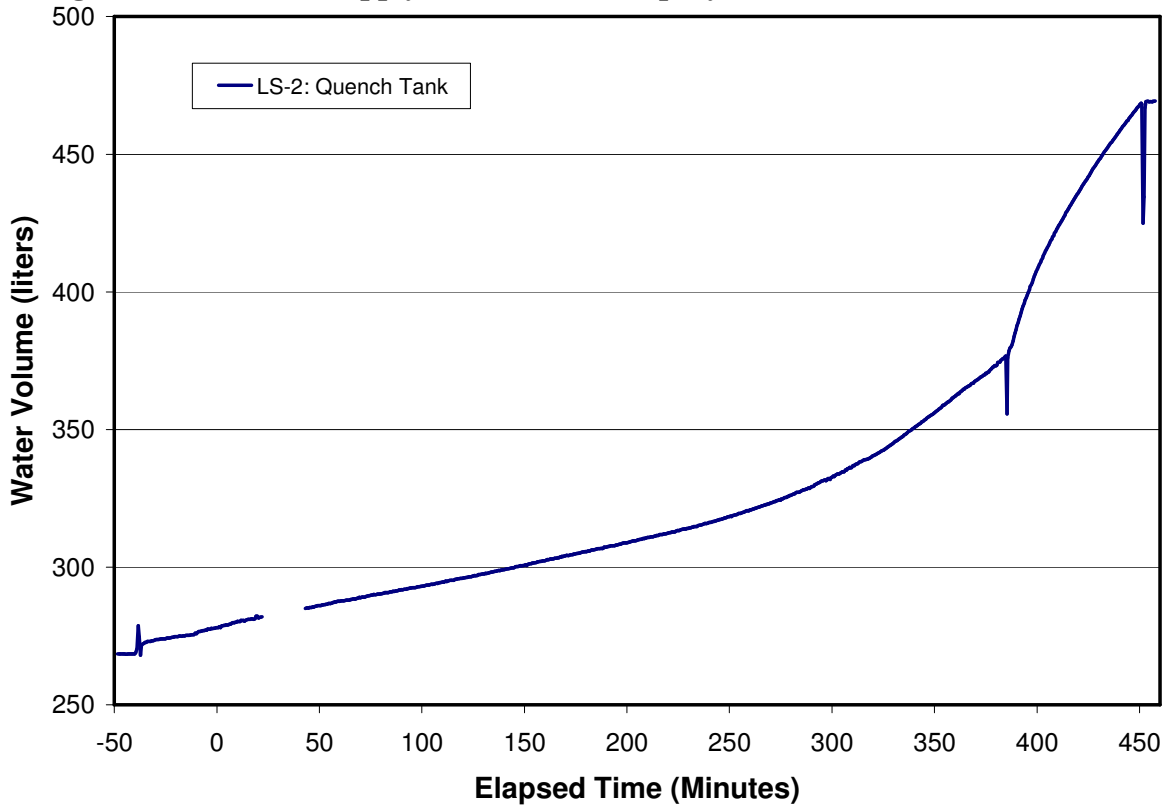


**Figure B-52. Quench Tank Water Volume Data.**

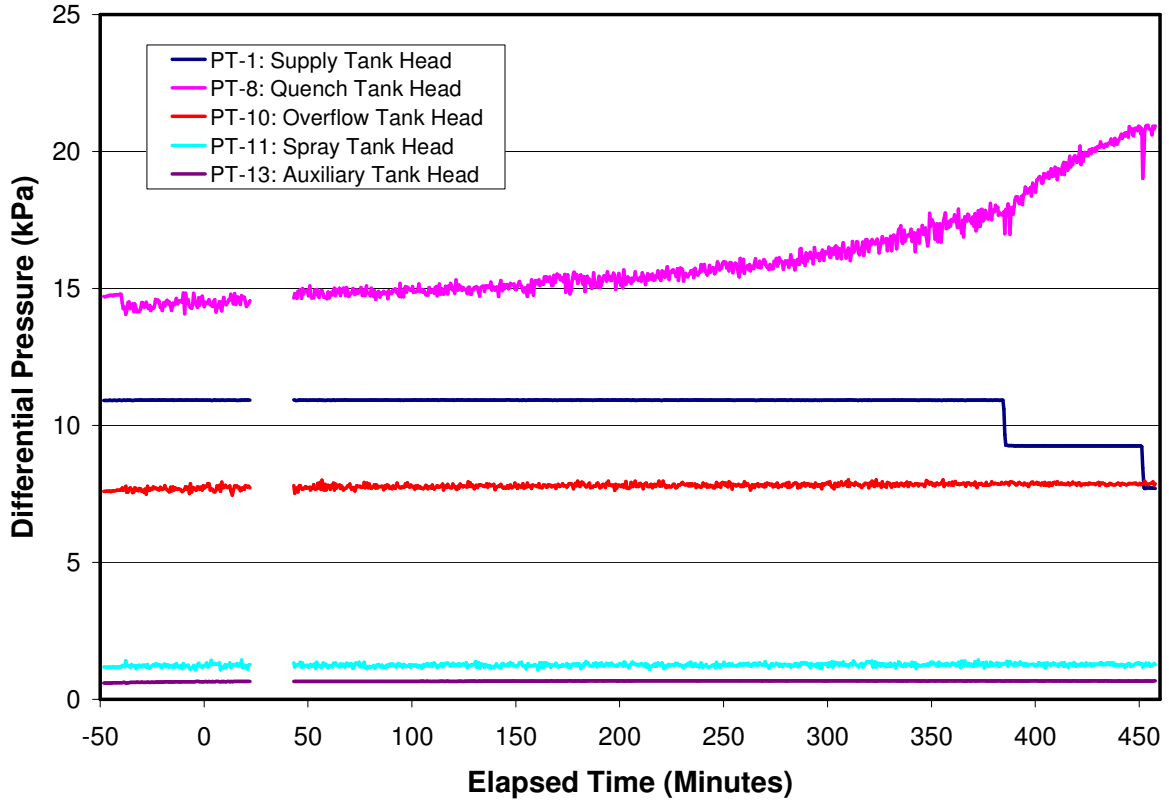


**Figure B-53. Supply and Quench System Tank Head Data (Backup).**

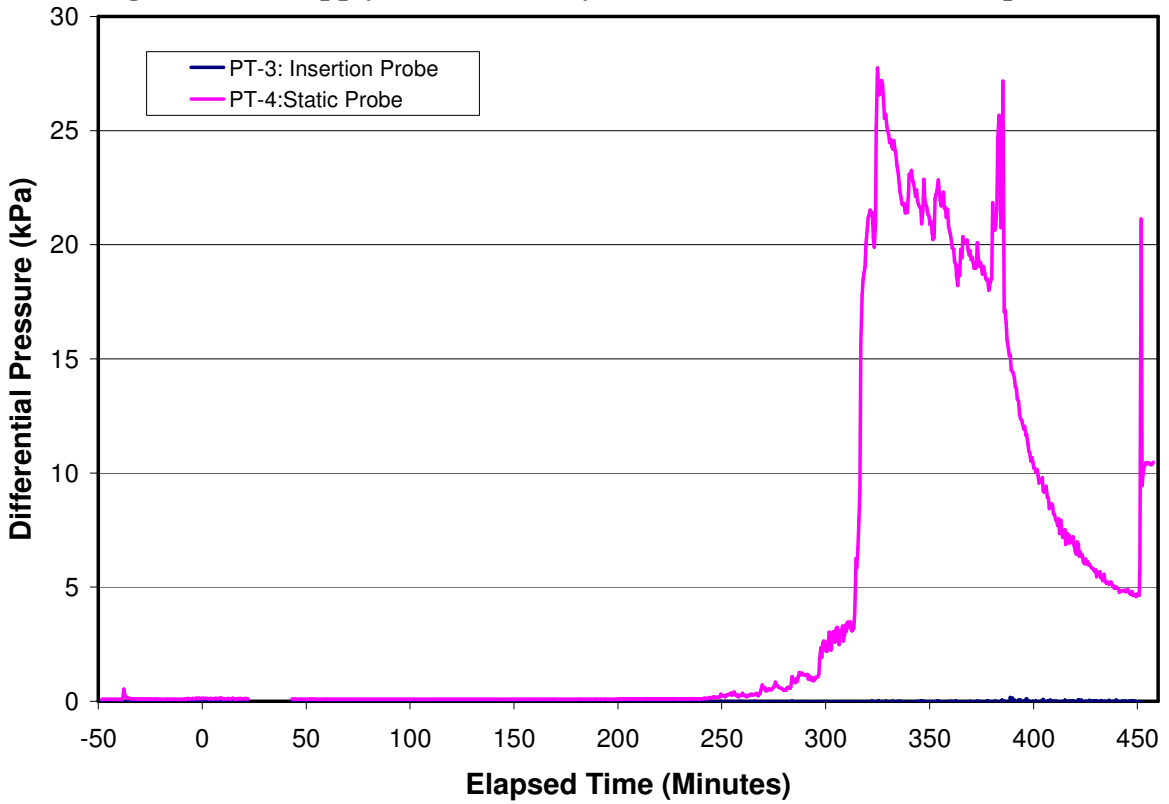


**Figure B-54. Test Section Water Head Transducer Data.**

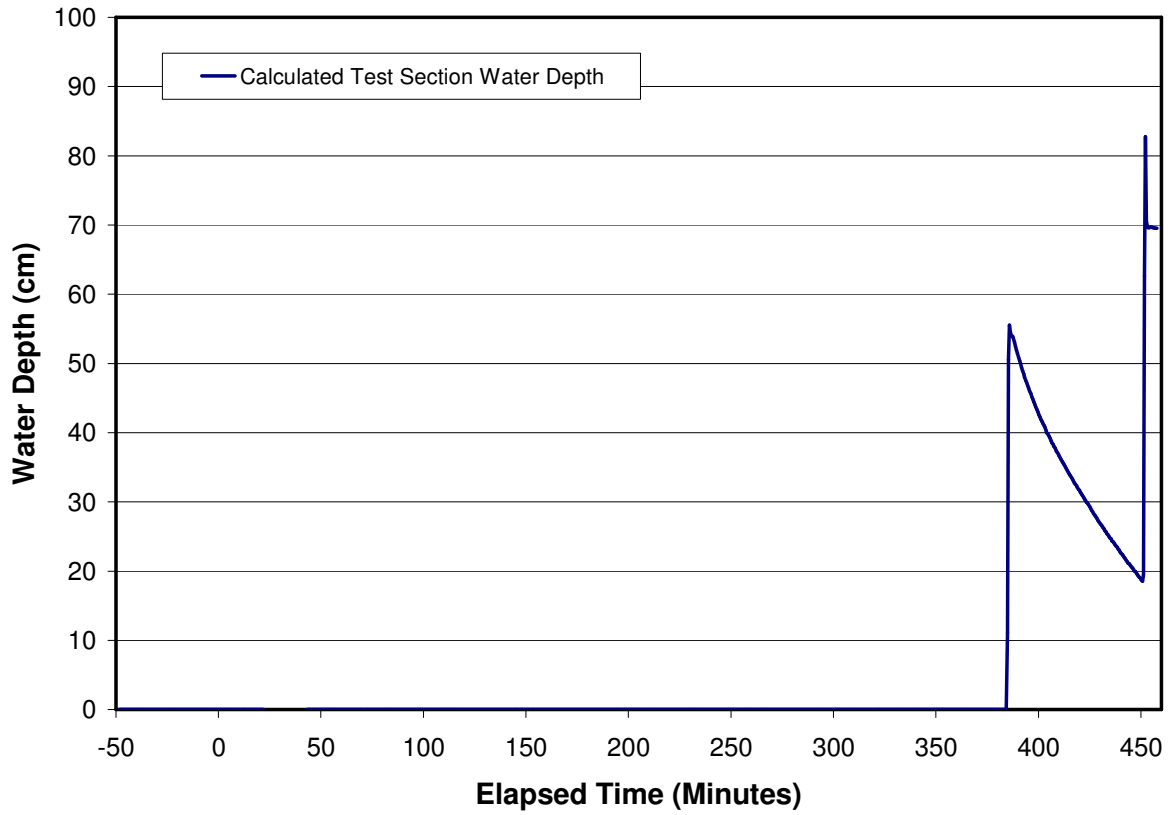


**Figure B-55. Calculated Water Depth in Test Section.**

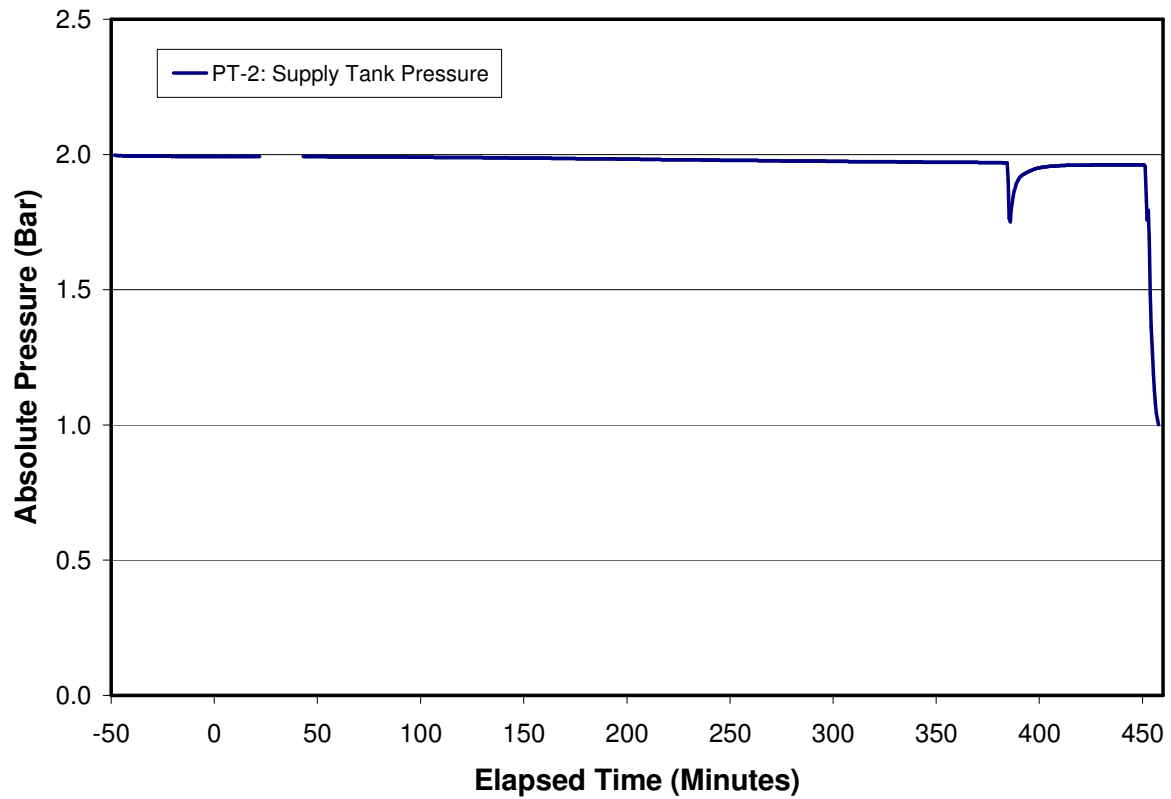


**Figure B-56. Water Supply Tank Pressure.**

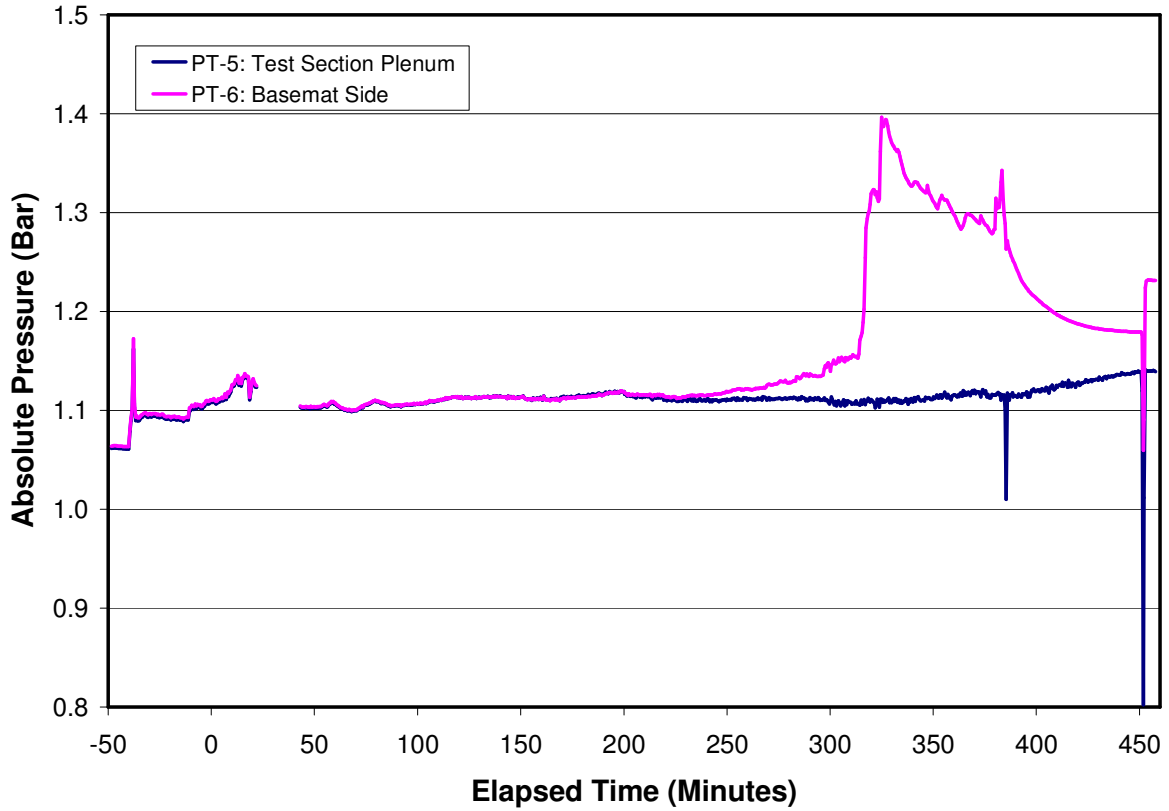


Figure B-57. Test Section Pressure.

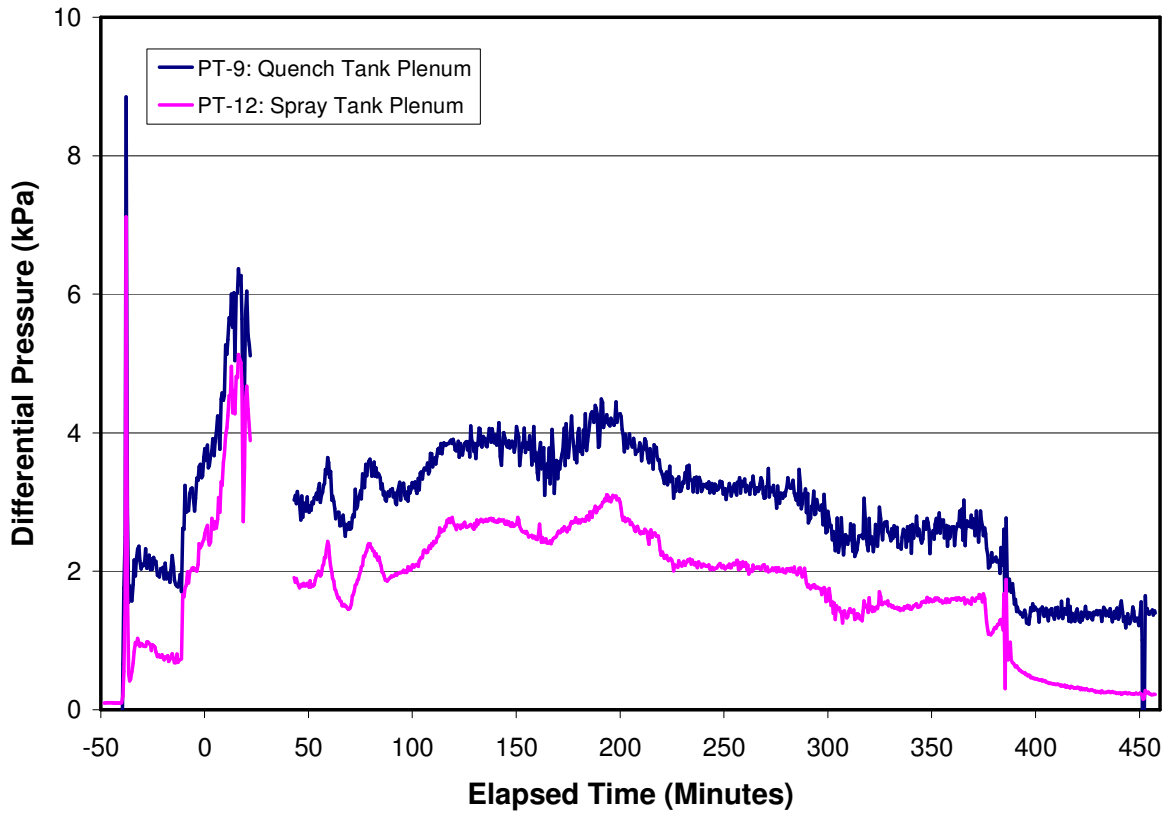


Figure B-58. Quench/Overflow and Spray Tank Plenum Differential Pressures.

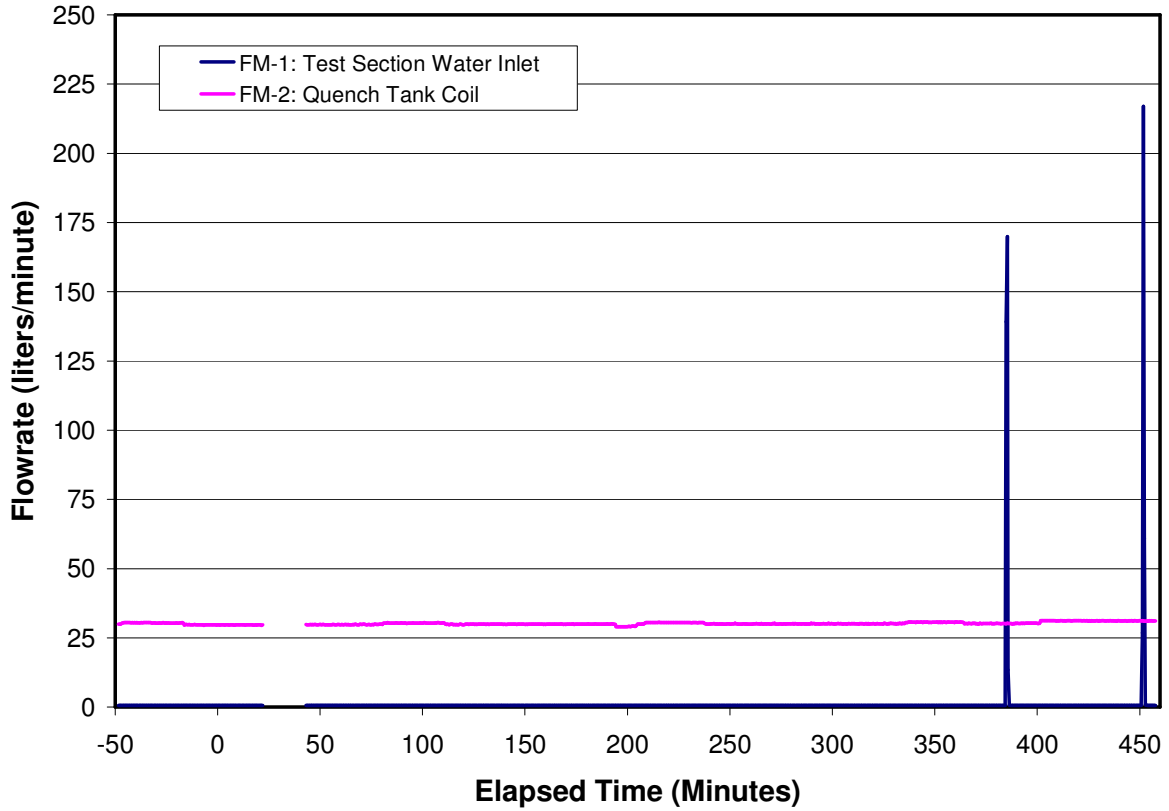


Figure B-59. Water Flow Rates.

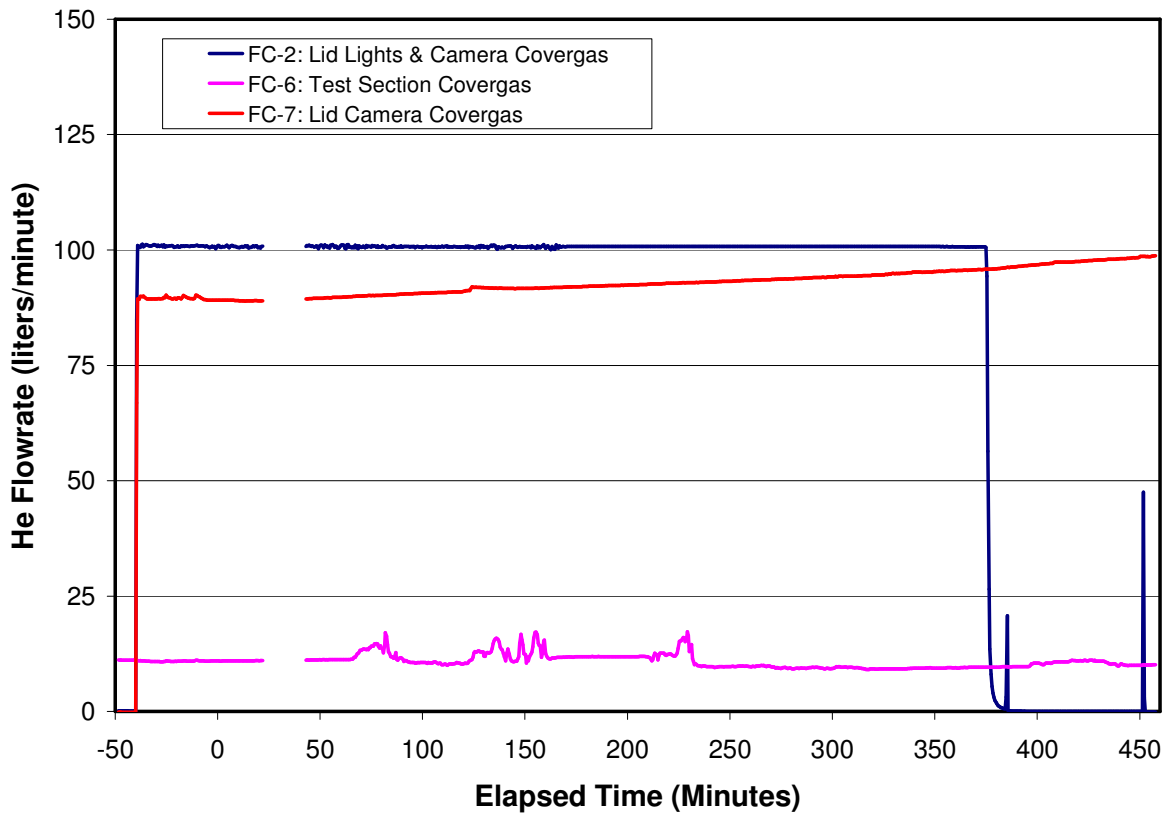
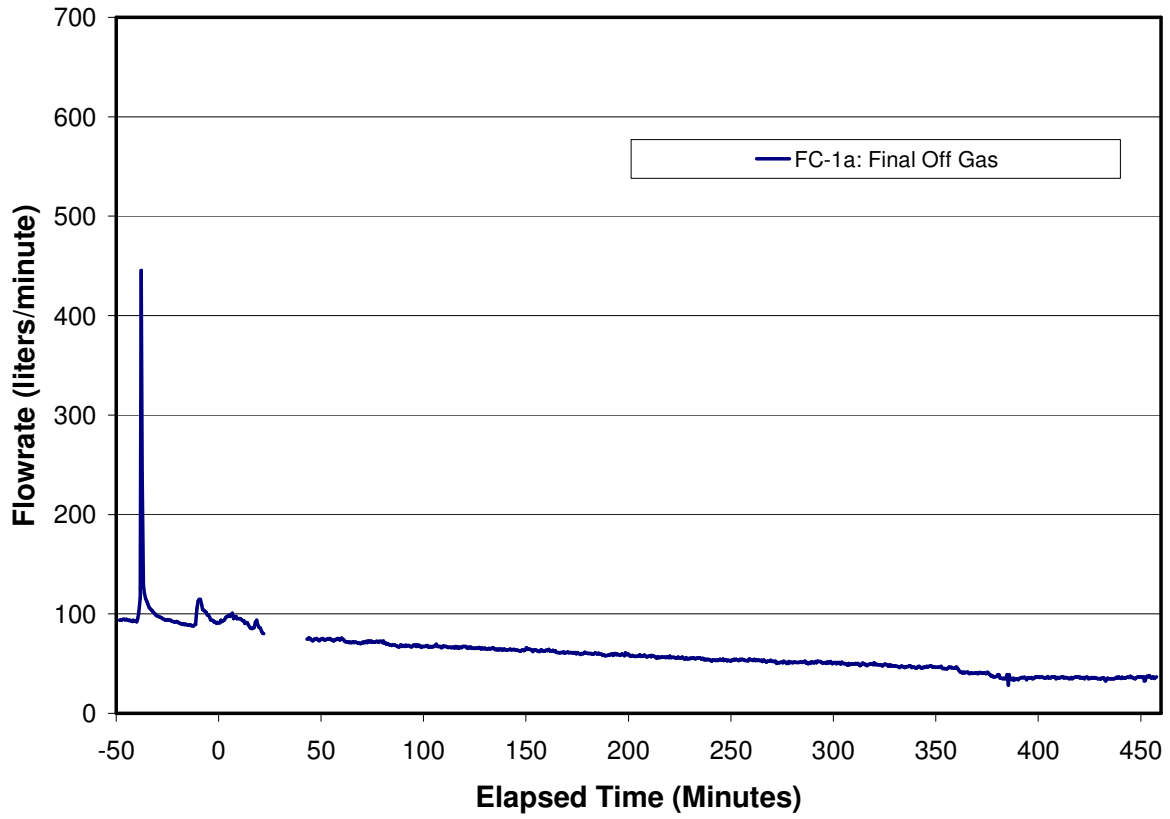


Figure B-60. Test Section Helium Cover Gas Flow Rates.



**Figure B-61. Final Off Gas Flow Rate.**